METAL CARBOXYLATE COMPLEXES RELEVANT TO THE FISCHER-TROPSCH SYNTHESIS

ANDREW PIENAAR
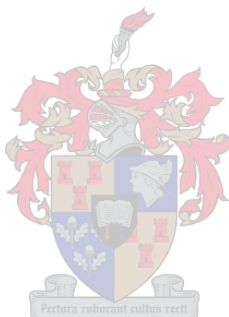
Thesis presented in fulfilment of the requirements for the degree of

MASTER

of

NATURAL SCIENCE

at the

UNIVERSITY OF STELLENBOSCH

Supervisor: Prof H. G. Raubenheimer
Co-supervisor: Dr. S. Cronje

March 2005

Opsomming

Karboksilaatkomplekse is belangrik in 'n Fischer-Tropsch raffinadery-omgewing aangesien die teenwoordigheid van organiese (karboksiel) sure in die produkstrome tot die vorming van karboksilaatsoute lei. Dit word algemeen aanvaar dat die ontbinding van organiese sure, gekataliseer deur metale, beheer word deur die ontbinding van die metaalsoute, óf komplekse, wat gevorm word na 'n reaksie tussen die metaal en hierdie sure. Die bepaling van die struktuur asook die fisiese eienskappe van karboksilaatkomplekse kan 'n belangrike bydrae maak tot die verstand van die meganisme betrokke by die dekarboksilasie van organiese sure.

Die strukture van koper(II)allielasetaat, sink(II)propionaat, sink(II)isopentanoaat, ytrrium(III)asetaat en lantaan(III)propionaat is suksesvol deur die gebruik van X-straal diffraksie bepaal. Sodoende is bevind dat sink 'n tetrahedriese oriëntasie in karboksilaatkomplekse verkies wat verskil van die karboksilate van koper, lantaan en yttrium wat verkieslik in 'n oktahedriese koördinasie voorkom. Die karboksilaat, O-C-O, hoeke het 'n bestek tussen 119˚ en 125˚ en alle koolstof kettings kristalliseer in 'n *anti-* konformasie behalwe in koper(II)allielasetaat waar die koolstofketting voorkom in *gauche-*konformasie.

Termiese gravimetrie, infrarooispektroskopie en X-straal poeierdiffraksie is gekombineer met rekenaar modelering – deur gebruik te maak van DFT berekeninge en B-LYP vlak teorie - om voordelige interne parameters te vind vir yttrium(III)karboksilate. Die gekose model was gegrond op bestaande kennis van yttrium(III)karboksilaat komplekse en stel ons in staat om 'n moontlike struktuur vir yttrium(III)propionaat voor te stel. Die gebruik van infrarooimetings was veral voordelig in die voorspelling van bindingstoestande van die karboksilaatligand deur gebruik te maak van Nakamoto se bevindings en aanbevelings. Slegs vir formiaatsoute van yttrium en sink is dit gevind dat hierdie voorskrifte nie van toepassing is nie.

Deur die organiese, asikliese gedeelte van die mono-karboksilaatligand te varieër met verlenging en vertakking, kon vasgestel word dat die hittekapasiteit van sinkkomplekse baie afhanklik is van die koördinerende ligand, alhoewel die gedrag van die ooreenstemmende yttriumkomplekse baie min daardeur beinvloed word.

Termiese ontbinding van lantaan(III)propionaat het die vorming van simmetriese ketone by 'n spesifieke temperatuur tot gevolg. Dit kontrasteer met 'n vorige studie waarin slegs koolstofdioksied as byproduk gemeld word tydens sodanige termiese ontbinding. Literatuur aangaande lantaan(III)karboksilaate met nie-sikliese organiese kettings aanvaar dat 'n lagie-struktuur slegs deur komplekse met langer organiese kettings aangeneem word. Die pakking van lantaan(III)propionaat toon egter dat hierdie aaname foutief is en dat die kompleks in 'n lagie-struktuur saampak.

ABSTRACT

In a Fischer-Tropsch refinery environment carboxylate complexes are of interest since the carboxylic acids present in product streams lead to formation of carboxylate salts through leaching of process equipment and catalysts. It is widely accepted that decomposition of organic (carboxylic) acids catalysed by metals is controlled by the decomposition of metal salts or complexes previously formed with such an acid. The determination of physical and structural properties of caboxylate complexes could contribute to the explanation of the mechanism involved in the decarboxylation of carboxylic acids.

We have successfully determined the molecular structures of copper(II) allyl acetate, zinc(II) formiate, zinc(II) isovaleroate, yttrium(III) acetate and lanthanum(III) propionate. It has been established that zinc has a preferred tetrahedral coordination in carboxylate complexes compared to the octahedral coordination of copper, lanthanum and yttrium complexes considered. The carboxylate O-C-O angle in these complexes range between 119˚ and 125˚ and the conformation of the carbon chains is *anti* in all cases except for copper(II) allyl acetate, where a *gauche* conformation is adopted.

Using structural methods such as TGA, infrared spectroscopy and X-Ray powder diffraction and combining it with existing knowledge of yttrium carboxylates and the effective use of computational chemistry – to calculate favourable internal parameters, using DFT calculations and B-LYP level theory - a likely structure for yttrium(III) propionate is proposed. The use of infrared measurements were especially valuable towards predictions of possible structures and the postulations of Nakamoto, on the relation between carboxylate carbonyl stretching frequencies and the nature of the carboxylate bond, could be used to accurately identify – except for the formiate salts of zinc(II) and yttrium(III) – the bonding mode present in the relevant compounds.

We systematically tuned the non-cyclic organic part of the mono carboxylate ligand by lengthening and branching of the alkyl chain and determined that thermal decomposition and heat capacity of zinc complexes are a strong function of the ligand, while the behaviour of analogous yttrium complexes is hardly affected.

The thermal investigation of lanthanum(III) propionate yielded a result that is in contrast with a previous study - where only CO_2 was reported as byproduct - and we report an alternative result which indicates formation of symmetric ketones when the compound is heated to a high enough temperature. Earlier general assumptions about the layer-like crystal structure of lanthanum complexes coordinated by alkyl chain carboxylate are contradicted by the crystallographic data we collected for this compound. The crystal packing of lanthanum(III) propionate clearly shows a layered structure which is unexpected for a carboxylate with such a short alkyl.

Acknowledgements

I would like to thank those who assisted me during the course of completing this project:

My friends and family who supported me throughout these two years

Prof. H. G. Raubenheimer, for his patient (and sometimes not so patient) input and guidance

Arno de Klerk, for both his good faith, support and a large number of ideas

Dr. S. Cronje, for her ideas and shared experience

Prof. L. J. Barbour and Dr. C. Esterhuysen, for their invaluable crystallographic advice and assistance

Dr. C. Esterhuysen and Greta Heydenrich, for their help to generate molecular modeling data for yttrium(III) propionate

Sasol, for financial support

Everyone at the Sasol bursary office, as well as Dr. Cathy Dwyer, who have always made themselves available

Everyone else in the research group, for creating a nice work environment.

Declaration

I, the undersigned, hereby declare that the work contained in this thesis is my own original work and that I have not previously in its entirety or in part submitted it at any university for a degree.

Signature: ....

Date: ....

CHAPTER 1

INTRODUCTION

The Fischer-Tropsch process for converting synthesis gas to liquid transport fuels was originally developed in Germany and named after F. Fischer and H. Tropsch, the coal researchers who developed the process. During the second world war, this process was used commercially to produce necessary transport fuels, and later these plants were used for the production of waxes, alcohols and other chemicals.[1] Today more auto-manufacturers are viewing Fischer-Tropsch liquids as a viable alternative for conventional (petro-diesel) fuels without compromising fuel efficiency.[2] South African motor vehicles have benefited from Fischer-Tropsch technology for about 50 years!

Many refinery operations downstream from Fischer-Tropsch synthesis entail some form of hydro-treatment. Since the feed is sulphur free, an unsulphided nickel catalyst would in many cases be the catalyst of choice. The presence of organic acids, however, precludes the use of such a catalyst due to acid leaching of the nickel. It would therefore be desirable to find an unsulphided catalyst to decarboxylate these acids *prior* to hydro-treatment. Organic acids, do not limit their attack to the catalysts though, process equipment is also corroded to form carboxylate deposits.[3]

The search for a commercial catalyst could be narrowed if the interactions between metals and carboxylate salts were known. In principle metals which yield carboxylates that decompose at low temperatures may also decompose the corresponding carboxylic acid at low temperatures.

1.1 Aim of this study

With this study our primary goal is the characterisation – with special attention to thermal properties – of metal carboxylates.

13

Literature, especially pertaining to thermal properties, is surprisingly scant when dealing with aliphatic hydrocarbon carboxylates. We will build on knowledge collected by early pioneers in this field and aim to create an increased understanding of the physical properties of a selected series of carboxylates.

We will report and discuss not only new carboxylate compounds but also discuss features of existing compounds that have earlier been neglected. By systematically varying the length of the organic part of the ligand we bring to light effects exhibited by the non bonding parts of the carboxylate. This is shown to impact both the structure and physical characteristics of the complex.

The scope of this project includes the first five monoorganic acid, C1 to C5, carboxylates of zinc, yttrium and lanthanum as well as a single copper carboxylate complex. Copper was chosen for the vast amount of copper carboxylate reference data available. Lanthanum and yttrium on the far left of the transition table and zinc on the far right, were our other choices. The techniques chosen for characterisation are briefly introduced in the following sections and their application to the prepared complexes will follow in the later chapters.

1.2 Background

In the past, studies of transition metal carboxylate complexes (transition metal carboxylates hereafter) have been conducted to elucidate their physicochemical properties as well as a variety of applications in industry. [4,5,6,7] The most comprehensive reviews pertaining to carboxylates salts of metals are contained in an article published by C. Oldham in 1968 and text published by Mehrotra *et al.*[11,22] In Mehrota's book metal carboxylates are exhaustively discussed. Chapters on their synthesis, physicochemical properties as well as structure and bonding are included. The work focuses on a variety of metals and carboxylate species. A lacking feature in this work

14

is systematic variation of the carboxylate group. In many of the complexes considered, that contain more than a single carboxylate type, Mehrotra has claimed that structures of carboxylate compounds can apparently with great accuracy be predicted by using only their spectral and thermal properties.

After publication of Mehrotra's book, several new carboxylate structures, including heterometallic compounds, have been published but no further systematic studies have been completed.

Organic chemists have long been aware that decarboxylation of metal carboxylates, yield a possible avenue for ketone production.[8]

In many instances carboxylic acids are found in a dimeric form, bonded via hydrogen bonds. After coordination to a metal, metal atoms may act as replacement for the bonding hydrogen of such a dimer and in this way keep the dimeric structure intact.[11]
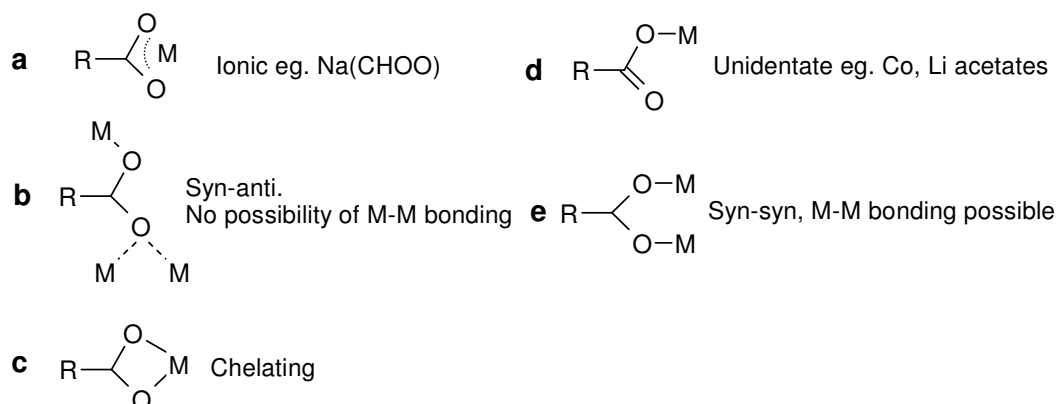
Fig. 1.1 *Bonding modes of carboxylate ligands*

Several possible carboxylate bonding modes are displayed in Fig. 1.1, with charges omitted for simplicity. Ionic bonding (Fig 1.1: **a**) is exemplified in compounds such as acetate salts of potassium and sodium while the other bonding modes (Fig 1.1: **b-e**) are observed for most other metals. Hocking *et al.* [9] has shown that quantifiable structural changes to the carboxylate group, depend on the cationic center it is reacting with. Carboxylate ligands have the

15

interesting feature of being able to bond to metal atoms, in a variety of ways. The RCO_2^- group may act: in a monodentate or bidentate manner and can chelate or bridge metal centers. Bridging ligation, while not the only avenue for polymerization, has been known to give rise to an interesting array of metallo-organic polymers (see Fig. 1.2).[10] Polymers of this type include dimeric units linked to other dimeric units by sharing an oxygen between two metals as well as monomeric units linked by bridging carboxylates
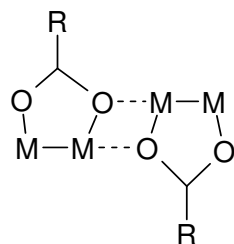
Polymerisation of dimers.   Polymerization of monomers.
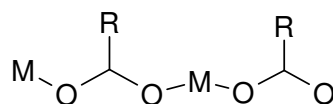
Fig. 1.2 *Polymerization modes of carboxylate units*

Close proximity of the two metal atoms bridged by a carboxylate ion in syn-syn configuration, allows interaction to take place, and indeed, even multiple bonds to form.[12] Carboxylate-bridged metal dimers take the form depicted in Fig. 1.3, and a quick search of a crystallographic database reveals that this behavior is displayed for complexes of osmium, tungsten, rhenium copper and many others.
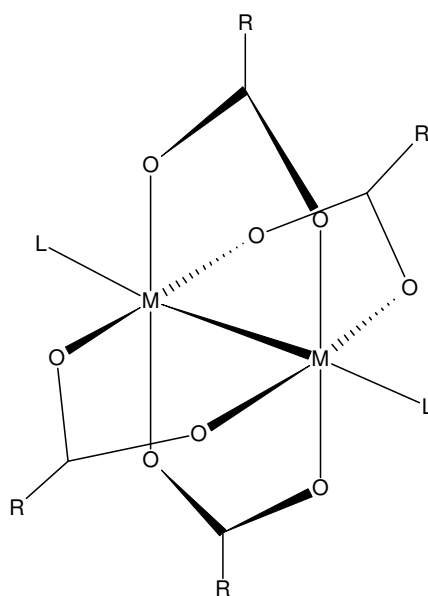
Fig. 1.3 *Common structure for divalent bridged metal carboxylate dimers, with electron delocalization not shown*[12]

Metal-metal interactions occur mostly in lower oxidation states, although it happens readily for the earlier transition metals even in their higher oxidation states.[13]

Due to the variety of bonding modes characteristic of carboxylates, solid phase transitions that entail the shifting of coordinated oxygens to different metallic centers, *i.e.* a change in carboxylate bonding mode (as observed for Cu(II) carboxylates and displayed in figure 1.3),[14] or a shift from a polymeric to a monomeric structure may occur.[15] Certain metal carboxylates (e.g. lead butyrate and hexanoate) are known to form a liquid crystalline phase between the isotropic liquid and crystal phases, especially when longer carbon chains are involved.[16]

While transition metal carboxylates are by no means rare or inaccessible, complete characterization has been, with notable exception of the acetates, largely neglected. Little or no attempts have been made to conduct a systematic study, across periods, down groups or with variation of organic chain length and, thus, deficiencies exist within carboxylate literature.
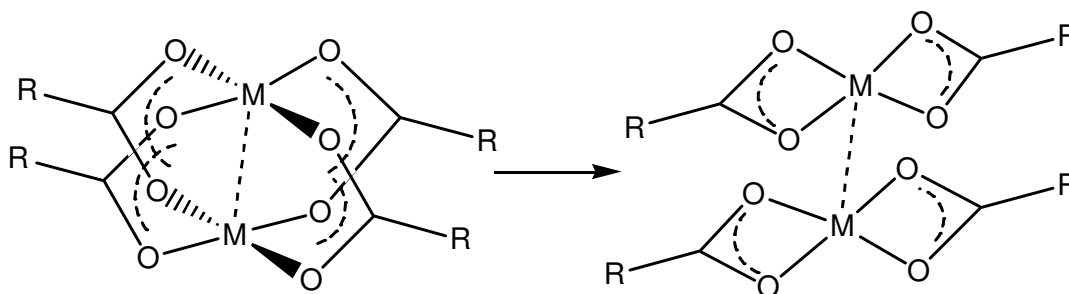
Fig 1.4 *Possible carboxylate phase transitions.*

1.3 Characterisation Techniques

1.31 Thermal Studies

Thermal analyses of metal carboxylates, as well as the interpretation thereof, are in many cases complicated by the richness of their phase behavior. Solid-solid state transitions, as well as smectic-isotropic liquid phase transitions are possible.

Previous work performed on the thermal properties of metal carboxylates is largely limited to the decompositional patterns of some rare earth acetates. Additionally, reports of changes in bonding modes of a carboxylate ion to a metal center as a function of temperature are available.[15]

Anhydrous acetates of rare earth metals are known to exhibit in several situations, a two-stage decomposition ending ultimately with the oxide of the given metal. Gravimetric studies have not shown the formation of the normal carbonate, however, for certain lanthanides (Nd, Sm, La) it is known that the normal carbonate does indeed form prior to decomposition.[8]

In hydrated salts, loss of water precedes the above-mentioned decompositions, in a stepwise, or single-step process. Similar patterns are observed for other transition metals that will be detailed in later sections.

The decomposition of compounds are studied by differential scanning calorimetry (DSC), which indicates changes in heat flow as a function of temperature, and thermal gravimetric analysis (TGA), which in turn shows mass loss as a function of temperature. A combination of the two techniques yield a powerful tool for thermal characterisation.

The calculated decomposition enthalpy for the compound is taken as the sum of enthalphies for thermal events measurable in the regions indicated on

collected thermograms and has been included in the thermal sections of chapters 2 to 6.

1.32 Infrared Spectroscopy

While spectroscopy is not the most powerful technique for studying transition metal carboxylates, its usefulness cannot be ignored. There are no major differences in local symmetry for the low symmetry, free carboxylate ion (RCO_2^-) and its coordinated analogue in a transition metal carboxylates.[11] Therefore, the differing types of carboxylate coordination cannot be distinguished based on the number of infrared or Raman-active vibrations. The free acetate has 15 different infrared active fundamentals but only the symmetric and asymmetric stretching modes of the RCO_2^- group have been investigated in structural analysis.[8] This is a pity, since the carboxylate group lends itself to infrared spectroscopy because of strong absorbances which are not observed in acidic form.[38]

Many chemical species exhibit electron delocalisation. The two carbon-oxygen bonds in a carboxylate group will be degenerate unless there is an external interaction that overrides the delocalisation.[9] Since the degree of interaction between the cationic centre and the coordinated ligand affects the delocalisation and thus the stretching frequencies of the carboxylate ion appreciably, the importance of infrared spectroscopy is clear.

The bonding modes of the carboxylate ligand can to some extent be followed by relating carbon-oxygen stretching frequencies to the nature of the carboxylate coordination.[18] Nakamato and co-workers propose that the differences between the symmetric and asymmetric stretch for the RCO_2^- ion can be used as an indication of its coordination in a carboxylate complex,[19] considering mondentate, chelating, bridging and polymeric situations.[20]

19

For monodentate carboxylate groups, the anti-symmetric RCO_2^- stretch shows an increase, while the symmetric stretch decreases relative to that of the values observed for RCOONa and RCOOK. This happens since the bonding mode of the ligand can affect the carbon-oxygen bond lengths appreciably, even to the extent of assuming a pseudo ester configuration and, therefore, allowing "true" monodentaticity. [18]

Most literature reports which investigated the spectral properties of carboxylates concur that a Δv_{COO} ranging from 150-180 cm^{-1} correspond to bridging bidentate carboxylate ligands, even though differences of up to 200 cm^{-1} have been reported. For chelating bidentate ligands, this energy difference is much closer to 100 cm^{-1}.[21] A study of a series of metal formiate and acetate coordination compounds of known structure, includes investigation of metal-oxygen vibrations using low-frequency infrared.[22]

Studies in this field have revealed that, not only is vibrational spectroscopy a suitable method to study phase transitions in carboxylate complexes, it provides key information in interpreting thermal phase behaviour. Assignments of infrared absorptions for compounds prepared during this project were made by comparison to absorptions of sodium and potassium salts of the relevant carboxylic acid species, as well as using standard infrared absorption tables and charts.[11, 19, 20]

1.33 X-Ray diffractometry

The Bragg father and son team considered crystals as planar layers of atoms that behaved as reflecting planes. Atoms, contained within one of these planes, would scatter incoming X-rays with an intensity proportional to the amount of electrons within it. While not physically correct, this model helped them arrive at their famous equation, also known as Bragg's Law. Bragg's Law applies irrespective of the positions of atoms and is dependant only on

the spacing between the planes in a molecule. W.L Bragg demonstrated that measurements of diffraction patterns give information on the distribution of electrondensity in a unit cell.

Powder Diffraction

In those cases where single crystals of given compounds were not obtained, powder diffraction techniques were employed. While this technique is not the technique of choice, since structure solution is a drawn out and haphazard process, other useful data such as unit cell size, compound purity and positive identification are made available. This technique also enables the user to determine qualitatively the crystallinity of the sample powder and peak symmetry may even be used to determine crystallite shapes. Since, as opposed to single crystal diffraction, data is not collected for a single entity, three dimensional data is much harder to extract. A powder pattern can be used for fingerprinting of a particular compound, since each pattern is unique to each compound.

To extract unit cell data from a powder pattern, the pattern needs to be indexed. Indexing involves finding h, k and l values for interplanar spacings (or *d* spacings), as contained in Bragg's Law ($\lambda = 2\,d\sin\theta$). These *d*-space values correspond to reflections observed (one *d* value for every θ) and are displayed as peaks, with intensities dependant on the intensity of the reflections, on the diffraction pattern. In those cases where preferred orientation plays a role, and orientation of the powdered crystallites is not completely random, the intensity of one or more reflections is inaccurately reported. This does not, however, affect the position of the reflection and thus cannot affect indexing.

Several algorithms have been developed over the years to find a solution to the indexing problem, not all of which always yield similar results. To discriminate between "good" and "bad" solutions a statistical criterion is needed.

De Wolff *et al.*[23] suggested the "figure of merit" (*M*). The quantity *M*, considers the fraction of calculated lines actually observed. A very unusual property of *M*

21

is that it is a statistical criterion that does not include a standard deviation (σ) in its definition. Since indexings with deviations much larger than σ are either discarded or explained as impurities, *M* is allowed as sole arbitrator. This means *M* is only a value that evaluates how well a solution correlates to the successfully indexed peaks in a pattern and is not affected by the amount, or intensity, of unindexed lines.

De Wolff, in defining the figure of merit, suggested using 20 diffraction lines for indexing and comparison of patterns.[23] This approach has been followed by most other researchers of the time and has become standard practice in modern science.

Claiming a particular indexing as correct, can only be verified by single crystal diffraction or structure solution from the powder pattern, but in the same breath it can only be proved *incorrect* by the same methods. It occasionally happens that even incorrect indexings have high figures of merit. While the suggested minimum value for *M* is 6 according to de Wolff, with anything greater than 10 being good, he also states that even a solution with a merit of 1 can only be disproved by structure solution!

Single Crystal Diffraction
The experimental technique which has been most widely employed, and with greatest success, to reveal and investigate the structure of crystalline molecules is undoubtedly single crystal diffraction.

Crystal structure determination is a two part process. First the size and shape of the unit cell (the lattice parameters) need to be determined and this is done by evaluation of the geometry of the diffraction pattern. Secondly the relative intensities of the diffraction spots in a pattern are used to determine the lattice type and distribution of the atoms in the structure.[24]

Using data from several indexed Bragg reflections, unit cell data can be calculated. Once this is done the atoms need to be placed. The two most

popular methods for doing this are direct methods and the Patterson synthesis.

Direct methods uses experimental data and combines observed electron density waves in a statistical manner to arrive at a distribution within the unit cell. This method assumes that no measured densities are negative and that it consists of sharp peaks at atomic positions.

During the Patterson synthesis, a trial structure is generated by using known atomic positions.

Once an approximate structure has been generated, it needs to be refined for which least squares refinement is the method of choice. Refinement of a structure involves improving the parameters of an approximate structure. To separate a good refinement from a not so good refinement, the R index is defined. The R value is a measure of the precision of results of a refinement with values smaller than 0.06 (6%) considered acceptable.

The knowledge of the three dimensional structure of a molecule, is an unparalleled aid in the interpretation of spectroscopic and gravimetric data.

1.34 Synthesis of compounds

Synthesis of transition metal carboxylates may be achieved in a variety of ways, the most simple of which is probably via acid-base reactions. Such a methodology widely employed in literature for acetate compounds, involves dissolving metal oxides in acetic acid.[8] Other methods of preparation which were explored include, the sol-gel method[25] and volatilization of mineral acids in aqueous solution by allowing the carboxylate to precipitate. During this project, these methods were explored as part of this study, and will be discussed in detail in the experimental sections.

1.4 References

1. *McGraw-Hill Dictionary of Scientific and Technical Terms.*, McGraw-Hill. 5th ed., 1994, p761

2. United States Environmental Protection Agency, Transportation and Air Quality division, www.epa.gov

3. A. de Klerk, Sastech R&D, personal communication

4. M.F Ramos Moita, M.T.S. Duarte and R. Fausto, *Spec. Lett.* (1994), **27**, 1421

5. M.A Hasan, M.I. Zaki and L. Pasupulety, *Appl. Cat. A: Gen.* (2003), **243**, 81-92

6. M. Watanabe, H. Inomata, R. L Smith Jr. and K. Arai, *Appl. Cat. A: Gen.*(2001), 149

7. T. Yokoyama and N. Yamagata, *Appl. Cat. A: Gen.* (2001), **221**, 227

8. K.C Patil, G.V Chandrashekhar, M.V George and C.N. R Rao, *Can. J. Chem.*(1968), **46**, 257

9. R.K. Hocking and T.W Humbley, *Inorg. Chem.* (2003), **42**

10. P.C Junk, C.J Kepert, L. Wei-Min, B.W Skelton, A.H White, *Aust. J. Chem.* (1999), **42**, 437

11. R.C Mehrotra and R. Bohra, *Metal Carboxylates,* Academic Press Inc., New York, 1983

12. Hsiao-Yun Weng, Chih-Wei Lee, Yao-Yin Chuang, Maw-Cherng Suen, Jhy-Der Chen and Chen-Hsiung Hung, *Inorg. Chim. Acta* (2003), **351,** 89

13. J.Lewis, *Pure and Applied Chemistry*(1965)*,* **10**, 11

14. M.F Ramos Moita and M.T.S Duarte, *J.Chem. Soc. Faraday Trans.*(1994), **90**, 2953

15. G. Adachi and E.A Secco, *Can. J. Chem.*(1972),**50,** 3100

16. Konkoly-Thege, I. Ruff, S.O Adeosun and S.J Sime, *Thermochim.. Acta* (1978), **24**, 89

17. S.E Cabannis and I. F. McVey, *Spectrochimica Acta Part A* (1995), **51**, 2385

18. G.B Deacon and R.J Phillips, *Coord. Chem. Rev.*(1980)*,***33**,227

19a. K. Nakamoto, F. Fujita, S. Tanaka and M, Kobayashi, *J. Am. Chem. Soc.*(1957), **79**, 4904

19b. K. Nakamoto, *Infrared and Raman Spectra of Inorganic and Coordination Compounds*, Wiley, New York, 1978

20. G. Socrates, *Infrared and Raman Characteristic Group Frequencies: Tables and Charts, 3rd Edition*, Wiley, New York, 1994

21. A. Doyle, J. Felchmanm, N.T do Prado Gambardella, C. Nazari Verani and M.L Braganco Tristao, *Polyhedron* (2000),**19**, 2621

22. C.Oldham, *Prog. Inorg.Chem.* (1968),**10**, 223-258.

23. P. M de Wolff, *J. Appl. Cryst.* (1968), **1**, 108

24. Y.B Koh and G. G. Christoph, *Inorg. Chem. (1979),* **18**, 1122

25. F. Ribot, P. Toledano and C. Sanchez, *Inorg. Chim. Acta* (1991), **185**, 239

CHAPTER 2

COPPER ALLYL ACETATE

By the time the earliest review on transition metal carboxylates was published by Olham in 1968,[1] there were already more than 300 published papers regarding copper(II) carboxylates. The structures that were known at this time included both copper(II) formiate and copper(II) acetate. In Oldham's paper he postulated that a copper-copper distance of 2.64 Å is not close enough to indicate appreciable metal-metal interaction. This was claimed on data collected for other dimeric metal carboxylates.

After this publication the next review uniquely dedicacted to copper(II) carboxylates was published by Robert Doedens in 1976.[2] Here a few specific copper(II) carboxylates were discussed with a lot of attention being drawn to the magnetic properties of the complexes with di-metallic centers. Doedens considered a range of dimeric complexes and showed that the unweighted mean of Cu-Cu distances was 2.62 Å and that carbon-oxygen distances as well as Cu-O-C bonding angles were similar, within their standard deviations.

Studies concerning the thermal behaviour of copper(II) carboxylates have concluded that the breaking of metal-water bonds must not be considered of primary importance when thermal behaviour of hydrated metal compounds are investigated. It was shown that both coordinated and uncoordinated water, when hydrogen bonded to other water molecules, are released simultaneously at low temperatures. When water to water contacts are not present, however, a direct correlation between dehydration and metal water-distance was found.[3]

More recent advances concerning this topic have included the solution of the molecular structure of a vast variety of copper(II) carboxylate complexes. These include carboxylates of longer chain fatty acids ranging from hexanoic

to decanoic acid. Solid-to-liquid crystalline phase transitions were reported for certain copper(II) carboxylates as well as mesophases for some of the longer aliphatic carboxylates.[4]

In this chapter the elucidation of the structure of a newly prepared copper(II) carboxylate (copper allyl acetate) is described. We also report spectral and thermal data pertaining to this compound. To aid in our understanding of this type of compound a series of copper(II) carboxylates of known structure were prepared and used as references. This series consists of the first five organic mono acid carboxylates (formiate to pentanoate) and includes the carboxylate of allyl acetic acid (4-pentenoic acid).

2.1 Results and Discussion

2.11 Synthesis

Basic copper carbonate was added to a hot, vigourously stirred solution of 4-pentenoic acid in water. When effervescence ceased, all excess carbonate was filtered using a Buchner filter and vacuum line. The volume of the filtrate (a dark green solution), was then reduced by rotary evaporation to about 20% of its original volume to aid in crystallisation. The solution was left to evaporate at room temperature in an open atmosphere, and after a week needle-like crystal clusters with crystallites suitable for single crystal diffraction formed. A suitable crystal was selected and used for a single crystal X-ray determination while the bulk was used for additional characterisation.

2.12 Infrared Spectroscopy

Assignments of the relevant absorption peaks are shown in Table 2.1. The first band observed in Fig. 2.1 is the stretching vibration of the sp^2 carbon-hydrogen bond(=C-H) at 3079 cm^{-1} followed by the fermi doublet at 2976 cm^{-1}. This doublet is particular to dimeric copper carboxylates,[5] but is not easily identifiable since it occurs in the same region as strong aliphatic stretches.

27

The difference between the symmetric and asymmetric stretch (163 cm^{-1}) is as expected for bidentate bridging carboxylate ions.[6]
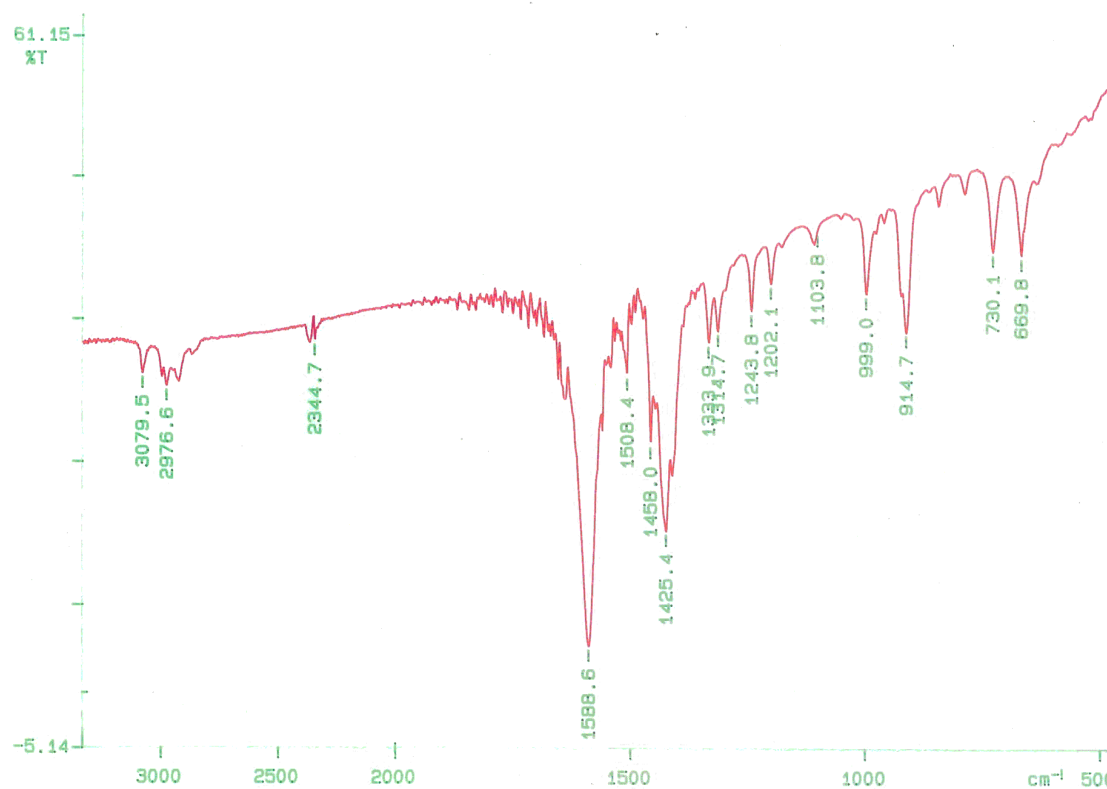
Fig. 2.1 *Infrared spectrum of copper(II) allyl acetate*

Table 2.1 *Infrared absorptions of copper(II) allyl acetate*

Band (cm^{-1})	Assignment
3079	=C-H stretch
1588	Asymmetric carboxylate stretch
1458	CH_3 vibrations
1425	Symmetric carboxylate stretch

2.13 Thermal Studies

The TGA thermogram in figure 2.2 shows that decomposition in this compound occurs in the region between 150 °C and 300 °C with only 31% of the original mass retained after 300 °C. This gravimetric study displays the

single step decomposition of copper(II) allyl acetate to copper oxide when heated above 200 °C.
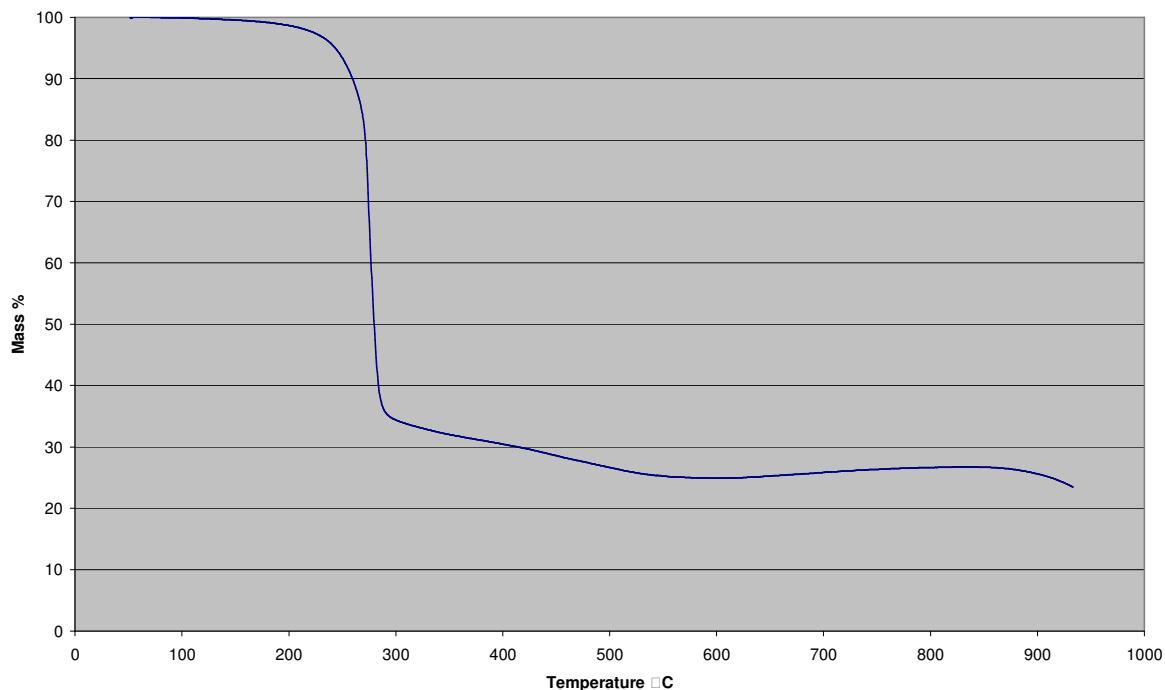
Fig. 2.2 *TGA thermogram for copper(II) allyl acetate*

DSC measurements of the compound shows a thermal peak at 137 °C before decomposition. Melting point measurements show no signs of melting in this region which suggests that this marks the onset of decomposition. With exception of copper(II) propionate, which displays remarkable thermal stability up to 253 °C, all aliphatic copper(II) carboxylates prepared – formiate to pentanoate – start decomposing below 200 °C.

Another interesting observation is that copper(II)allyl acetate starts decomposition at approximately 15 °C higher than copper(II) pentanoate. Since these compounds are isostructural and have equal amounts of carbons in their organic chains, it is clear that the incorporation of unsaturated units leads to greater thermal stability in the complex.

2.14 Crystallography

Copper(II) allyl acetate crystallises in the triclinic space group $P\bar{1}$. From the diagram in figure 2.3 it can be seen that this structure is dimeric linking two crystallographically equivalent copper atoms with four bridging carboxylate ligands. This is the same type of structure that other groups have recorded for the, saturated, pentanoic analogue.
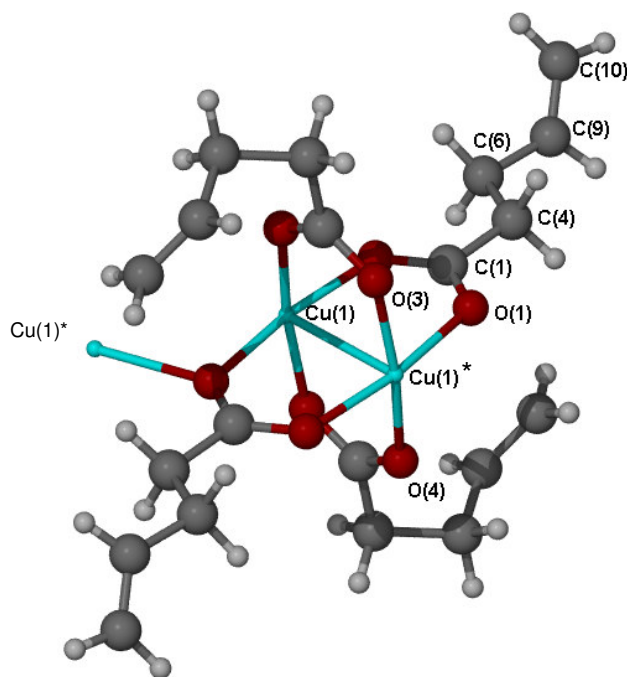
Fig. 2.3 *Crystal structure of copper(II) allyl acetate*

In this structure the copper(II) atom is in an octahedral coordination environment surrounded by 5 oxygen atoms and the adjacent copper atom. Slight angular distortion of the octahedron is observed as a result of the steric requirements of the carboxylate cage. Bond angles around the copper atom on the inside of the carboxylate cage range between 83˚ to 89˚ (Table 2.2). Further polymerization between dimeric units occur via copper-oxygen bonds as displayed in figure 2.4.

30

The copper-copper bond observed in this complex (2.582 Å) is shorter than the one reported in the copper(II) acetate complex (2.64 Å), but similar to that in copper(II) propionate (2.583 Å).[7]

Table 2.2 *Selected bond lengths and angles*

Bond distances (Å)		Bond angles (˚)	
Cu(1)-Cu(1)*	2.582(4)	O(1)-Cu(1)-Cu(1)*	86.21(6)
Cu(1)-O(1)	2.004 (1)	Cu(1)-O(1)-C(1)	123.84(10)
Cu(1)*-O(4)	1.945(1)	Cu(1)-O(1)-C(1)	122.14(11)
C(1)-O(1)	1.275(2)	C(1)-O(1)-C(2)	124.26(2)
C(1)-O(2)	1.253(2)		
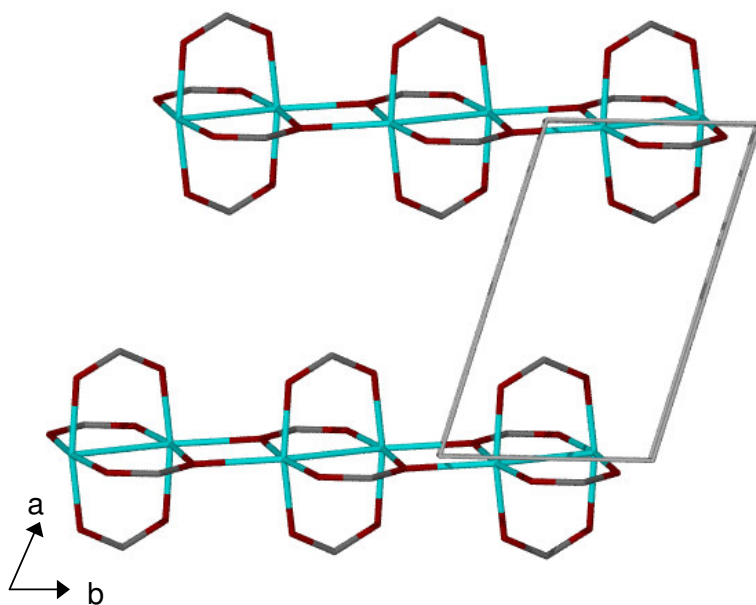
Fig. 2.4 *Linkage of copper(II) allyl acetate dimeric units, with only the carboxylate cage shown, viewed along the c axis.*

Curvature of the carbon chain axial to the plane of polymerization – the plane containing the Cu(1)-O-Cu(1)*-O parallelogram unit (Figures 2.4 and 2.5) – allows for closer packing between polymer layers. The plane of polymerization

31

- defined by Cu, C(1), O(2) , with O(7) having a 0.0039 Å deviation - contains two opposing carboxylate groups. This plane is almost orthogonal (89.12˚) with a plane containing the remaining two carboxylate units (deviation from plane 0.009 Å).
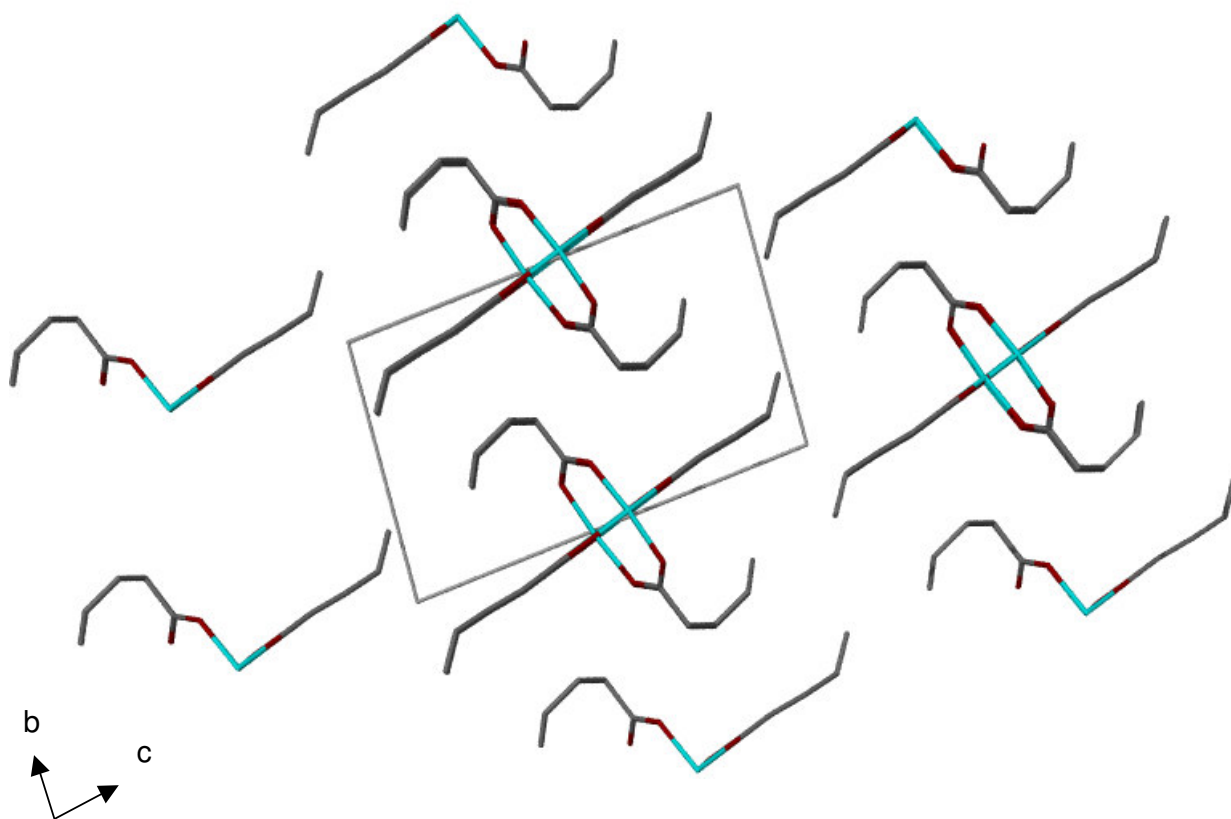
Fig. 2.5 *Packing diagram for copper(II) allyl acetate viewed along the a axis*

According to the IUPAC nomenclature, the name for this compound is catena(tetrakis(:$_2$–pentenoate–O,O'))di-copper(II).

2.2 Experimental

2.21 Preparation

A 1M solution of 4-pentenoic acid (8.4 ml, 8.6 mmol), in water was prepared and heated to just below boiling while stirring vigourously. Basic copper carbonate, $CuCO_3.Cu(OH)_2$, (0.50 g, 2.3 mmol) was then added without

32

cooling the solution. Once the reaction was complete, all excess carbonate was removed from the reaction mixture by filtration on a Buchner filter and vacuum line. The product was obtained by reducing the solvent volume to about 20% of its original value and allowing crystallization in an open atmosphere over several days. A 72% yield was obtained.

2.22 Thermal Analysis

Thermogravimetry and DSC measurements were carried out using a Perkin Elmer TGA 7 Thermogravimetric Analyser. The experiments were performed using a ramp rate of $10\,^{\circ}\text{C.min}^{-1}$ and over temperature ranges as indicated on the graph, with data evaluation performed with Microsoft Excel.

2.23 Infrared Spectroscopy

The infrared spectrum of the compound was recorded on a Perkin Elmer 1600 series FTIR at room temperature. The sample was prepared by dispersion into a KBr pellet and collection was done over the $3000 – 400\ \text{cm}^{-1}$ range at a spectral resolution of $4\ \text{cm}^{-1}$.

2.24 Structure solution

A crystal of this complex was mounted on a glass fibre sample holder and set up on a Nonius Kappa CCD diffractometer. Mo-Kα radiation, wavelength λ(0.17073A) was used and compensated for Lorentz and polarisation effects. Solution of the structure was completed using the X-Seed[8] crystallographic suite as interface, which uses the Shelx-97 program for solution and refinement.[9] The initial solution was obtained using direct methods. All crystallographic data are included in sections devoted to this complex.

Table 2.3 *Crystallographic data for copper(II) allyl acetate*

Empirical formula	$C_{20}H_{28}Cu_2O_8$
Molar mass	523.50
Temperature (K)	173
Wavelength (Å)	0.17107
Crystal system	$P\bar{1}$
Cell dimensions	
a (Å)	5.1746 (10)
b (Å)	8.6881 (2)
c (Å)	13.5484 (3)
α (˚)	93.8540 (10)
β (˚)	97.6130 (10)
γ (˚)	105.469 (1)
Volume ($Å^3$)	578.39
Density ($g.cm^{-3}$)	1.503
F(000)	270
Total Reflections	12141
Unique Reflections	2749
Goodness of fit	1.032
R index	0.031

2.3 Conclusion

The structure of copper(II) pentenoate is reported for the first time and shown to be isomorphous with its saturated carbon chain analogue (copper(III) pentanoate). With its similar structural size to copper(II) pentanoate this compound has an increased thermal stability with onset of decomposition occurring 15 ˚C higher.

2.4 References

1. C. Oldham, *Prog. Inorg. Chem.* (1968), **10**, 223
2. R. J Doedens, *Prog. Inorg. Chem.* (1976), **21**, 209

3. G. Micera, P. Piu, L. Strinna Erre and F. Cariati, *Thermochim. Acta.* (1985), **84,** 175

4. S. Petriček and B. Kozlevčar, *Thermochim. Acta.* (2002), **386**, 59

5. A. Doyle, J. Felchmanm N.T do Prado Gambardella, C. Nazari Verani and M.L Braganco Tristao, *Polyhedron* (2000),**19**, 2621

6. K. Nakamoto, F. Fujita, S. Tanaka and M. Kobayashi, *J. Am. Chem. Soc.* (1957), **79**, 4904

7. Y. H Chung, H. H Wei, Y. H. Liu, G. H Lee and Y. Wang, *Polyhedron* (1998), **17**, 449

8a. L. J. Barbour, *J. Supramol. Chem.* (2001), **1,** 189; 8b. J. L. Atwood and L. J. Barbour, *Cryst. Growth Des.* (2003), **3**, 3

9. G. M. Sheldrick, SHELXL-97, Program for Crystal Structure Analysis, University of Göttingen, Germany, 1997

CHAPTER 3

ZINC(II) CARBOXYLATES

Zinc(II) with a variety of organoligands is considered important in all biological systems and zinc is also important for the activity of metalloenzymes in living organisms.[1,2] In zinc enzymes zinc is coordinated by carboxylate groups which display both bridging and chelating modes as well as bi- and mono-dentacity.[2]

Zinc(II) coordination has been shown to be predominantly tetrahedral in proteins.[4,5] Our work has indicated that this is also true for the carboxylate complexes of zinc(II) prepared here, with the only exception being zinc formiate in which zinc(II) is in an octahedral environment.

Studies of bi metallic thiophene carboxylates of zinc and europium – which display luminescence - has shown that the presence of a zinc center can alter and enhance the luminescent properties of the Eu^{3+} ion.[3]

Spegt[6] has reported, on the basis of X-ray data, that zinc soaps do not exhibit liquid crystal phases and there have been no reports of liquid crystalline phases forming for zinc carboxylates although optical investigation, coupled with DTA measurements, show that a wide array of solid-solid transformations exist. Optical examinations for longer, (C6-C18) zinc carboxylates have shown no liquid-crystalline phases but several solid-solid transitions at temperatures below 400˚C.[7]

For the investigation described in this chapter our goal has been synthesis of a specific series of zinc carboxylates and determination of certain of their physicochemical properties. We have investigated the effect that chain branching and chain length of the carboxylate ligand has on the overall structure and thermal stability of the complex and remark on the effectiveness of certain analytical (i.e. infrared and XRD) methods in the characterization of these complexes.

36

3.1 Results and discussion

3.11 Zinc(II) Formiate

In Baraldi's investigation of metal formiates, he considered the thermal decomposition and infrared spectrum of these compounds. One of the compounds considered was zinc formiate. He concluded that zinc formiate decomposes to zinc oxide when heated above 250 ˚C and that dehydration temperatures are equal for compounds heated under an atmosphere of air or nitrogen.[8]

3.111 Synthesis

Leaching metallic zinc with formic acid and allowing evaporation of the solvent allows the precipitation of zinc formiate (equation 1). This reaction (see equation below) was repeated twice and the second time, instead of rapidly evaporating the solvent, the reaction mixture was left to an open atmosphere at room temperature which allowed the growth of cubic white semi-transparent crystals over a four day period. The product is completely soluble in water as well as in polar organic solvents such as ethanol.

$$Zn \ + \ 2CHOOH \ + \ xH_2O \ \rightarrow \ Zn(CHOO)_2.xH_2O \ + H_2 \qquad \textbf{(1)}$$
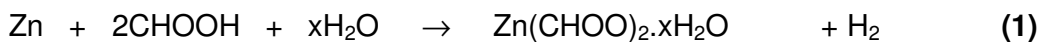
3.112 Infrared Spectroscopy

The difference of 183 cm^{-1} between the symmetric and asymmetric stretching modes of the RCO_2^- ion (Fig. 3.1) is indicative of a bridging carboxylate system according to Nakomoto *et al.*[9] and this is later confirmed by solution of the crystal structure for this compound.

37

A list of infrared assignments is listed in Table 3.1. Several –OH bands are recognised on the spectrum. This suggests that spectroscopically different solvent (water) molecules are present in this complex.

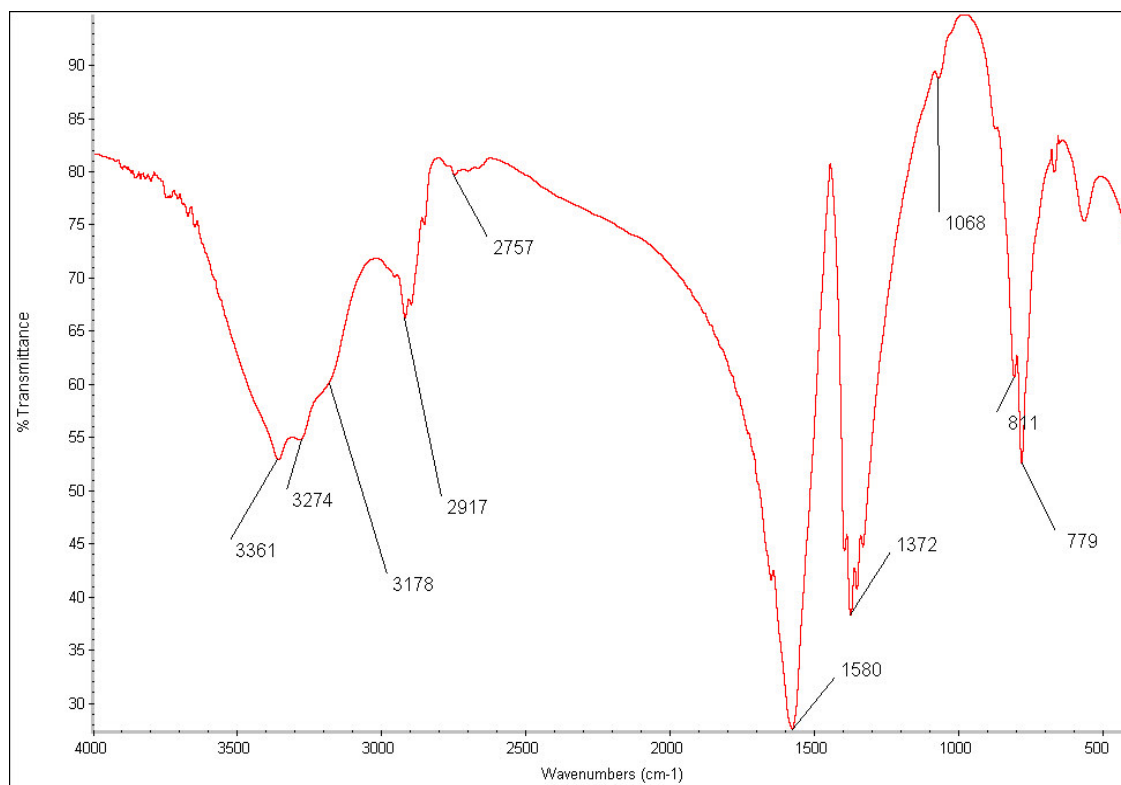**Fig 3.1** *Infrared spectrum of zinc(II) formiate*

Table 3.1 *Stretching frequencies for zinc(II) formiate*

Band (cm^{-1})	Assignment
3361-3178	-OH stretching frequencies
2917	Aliphatic symmetric and asymmetric stretches
1577	RCO_2^- assymmetric stretch
1394	RCO_2^- symmetric stretch
1370, 1346	Aliphatic absorptions

3.113 Thermal Analysis

The TGA graph (Fig. 3.2) of zinc(II) formiate shows that a mass loss of 20 % occurs at 124 ˚C and another of 36 % at 240 ˚C. These values can be seen to relate to endothermic peaks observed on the DSC (Fig. 3.3) profile when taking into consideration that different temperature programs and different instruments were used.

The intense decomposition peak(s) at 300 ˚C on the DSC thermogram (Fig. 3.3) might obscure the peak expected for a thermally induced mass decrease at 230 ˚C, but it is more likely that these are the same thermal event shifted due to the different experimental conditions. The compound retains constant mass after heating above 300 ˚C.
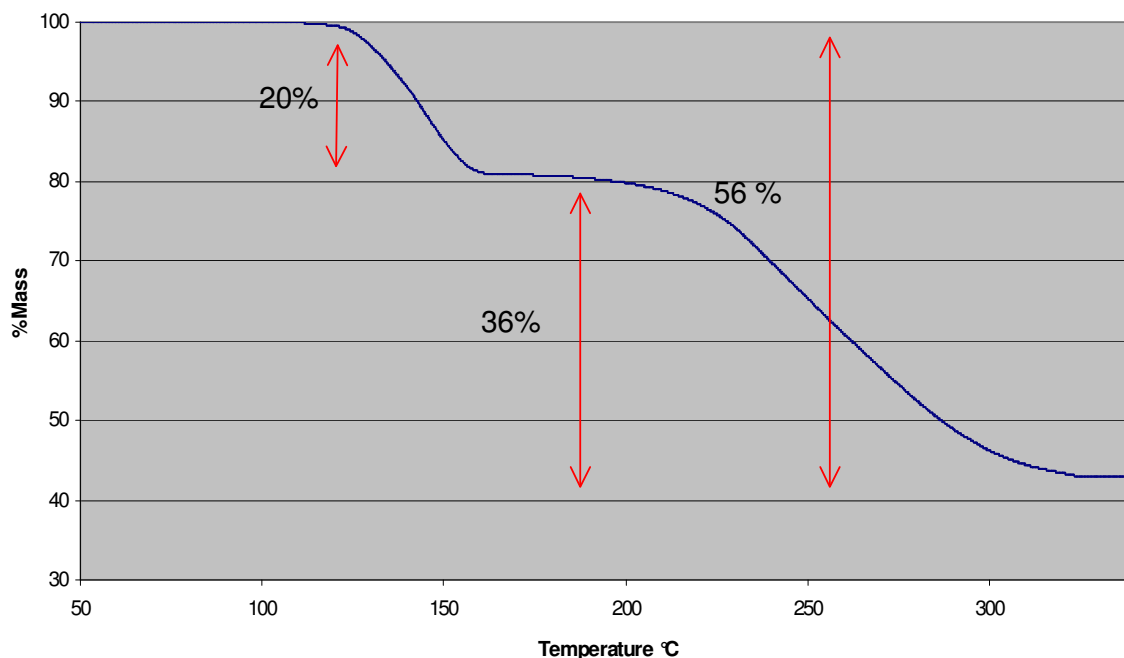

Fig 3.2 *TGA thermogram of zinc(II) formiate*

Calulating a 20 % loss, as indicated by TGA data, on the mass of empirical zinc(II) formiate, $Zn(CHOO)_2.2H_2O$[15], the release of two coordinated water molecules at 100˚C is confirmed. After the 300 ˚C threshold is reached only

39

43 % of the original molecular mass remains, which indicates (within experimental error) the formation of ZnO *via* the loss of two CO units. This thermal decomposition pattern has also been reported by other groups.[11]

^exo

Integral	-5.18 mW°C
Onset	83.29 °C
Peak	93.15 °C
Endset	99.70 °C

Integral	-32.03 mW°C
Onset	285.97 °C
Peak	288.11 °C
Endset	290.39 °C

Integral	-211.8
Onset	294.5
Peak	300.6
Endset	306.1

Integral	4.60 mW°C
Onset	291.28 °C
Peak	294.14 °C
Endset	297.47 °C
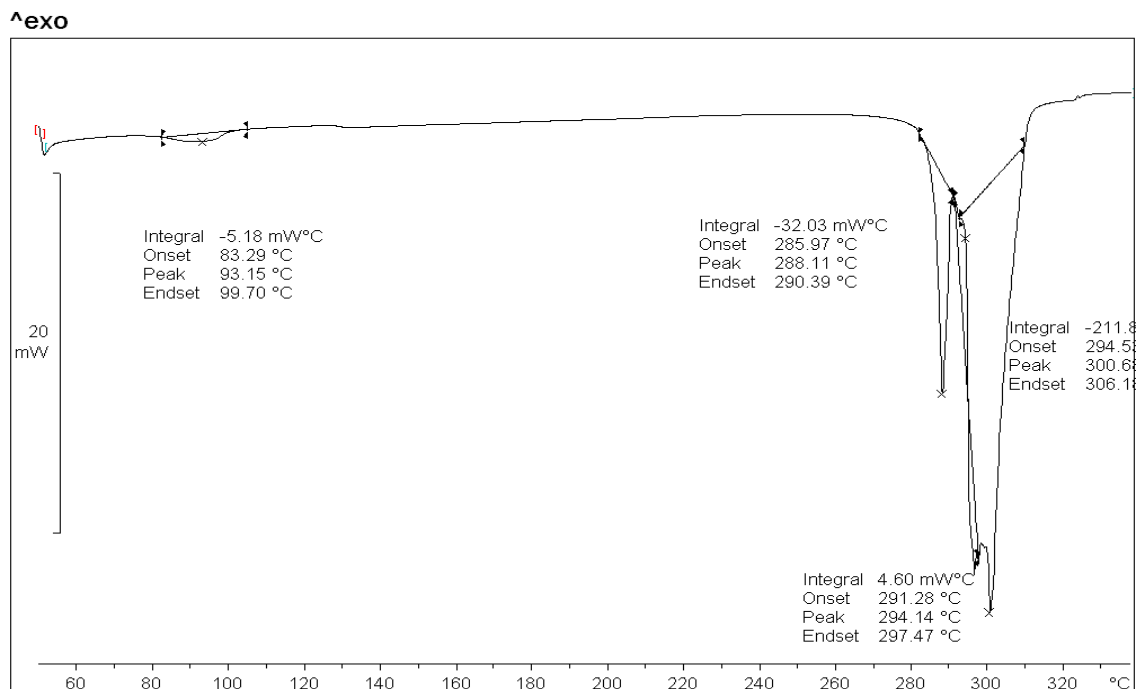
Fig. 3.3 *DSC thermogram of 5.31 mg zinc(II) formiate*

From the integral values on the DSC thermogram the decomposition enthalpy of zinc(II) formiate to zinc oxide is now calculated (equation 2).

$$Zn(CHOO)_2 \quad \rightarrow \quad ZnO \ + \ 2CO_2\uparrow \ + \ H_2O\uparrow \quad \Delta H = \text{-3.5 J.mg}^{-1}$$

(2)

3.114 Powder Diffraction studies

The collected pattern (Fig. 3.4) matches that of zinc(II) formiate (CAS# 14-0761) contained in the database exactly (more than 20 correlating lines) and thus identifying the compound unequivocally. The absence of spurious lines in the diffraction pattern excludes the possibility of any impurities.

40

This pattern has been completely indexed in the relevant region and additional indexing data are not reported here. [12]
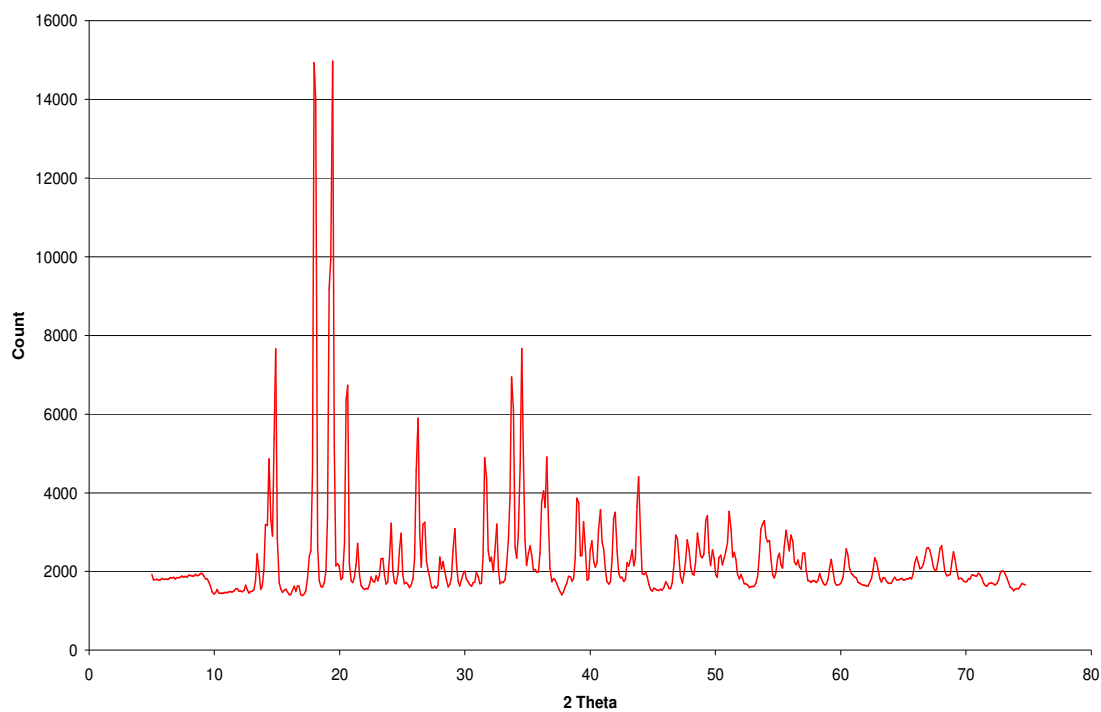
Fig. 3.4 *Powder diffraction pattern of zinc(II) formiate*

3.115 Single Crystal data

While the structure of zinc formiate has been reported by earlier workers it has only been linked to ^{67}Zn NMR and not to thermal or spectroscopic data.[4] Figure 3.5 shows the molecular structure of zinc(II) formiate from the data we collected.

The molecular structure of zinc(II) formiate shows zinc coordinated in an octahedral fashion surrounded by four unidentate carboxylate ions in one plane and two water molecules on the other. The formiate ligand connects neighbouring zinc atoms. The single hydrogen atom on the formiate carbon was not placed but resulted from a calculation during crystal refinement. As can be seen in the packing diagram (Fig. 3.6) the complex crystallises in a

41

network type system, with central zinc systems bonded both horizontally and vertically to neighbouring centers. All angles around the zinc atom are approximately 90˚ which gives it a nearly perfect octahedral geometry.
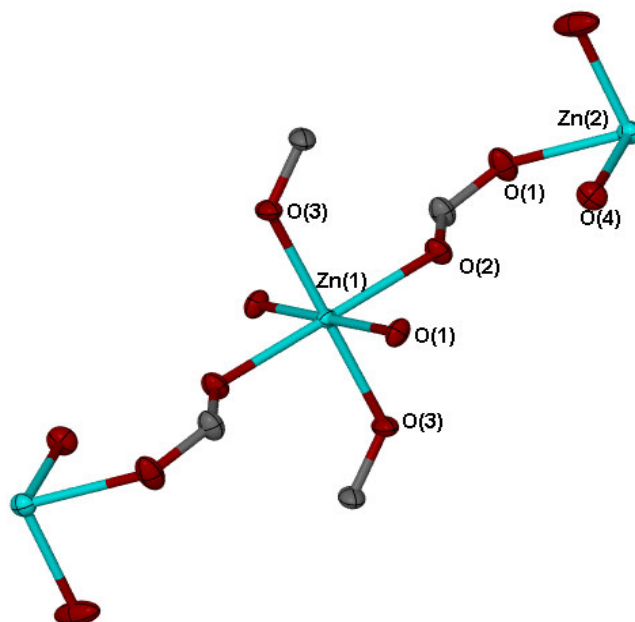
Fig. 3.5 *Molecular structure of zinc(II) formiate, hydrogen atoms omitted for clarity*

Two crystallographically different zinc centers exist. The first one is coordinated by four molecules of water and linked on the apexes of the octahedron to two neighbouring, inequivalent, zinc centers by bridging formiate ligands. The other center has bridging formiate atoms coordinated at each available position and is linked to equivalent zinc atoms in one plane (the plane defined by Zn(1), O(1), O(2)) and inequivalent zinc atoms in the other (defined by Zn(1), O(1), O(3)). The inequivalent atoms share the second plane with no deviation from it.

Table 3.2 *Selected bond lengths and angles for zinc(II) formiate*

Bond lengths (Å)		Bond angles (˚)	
Zn(1)-O(3)	2.099(2)	O(3)-Zn(1)-O(1)	89.50(5)
Zn-O(2)	2.149(2)	O(3)-Zn(1)-O(3)	180.0

| C-O(3) | 1.245(4) | O(4)-Zn(2)-O(4) | 180.0 |
| Zn(2)-O(4) | 2.100(3) | O(1)-C-O(4) | 125.2(4) |
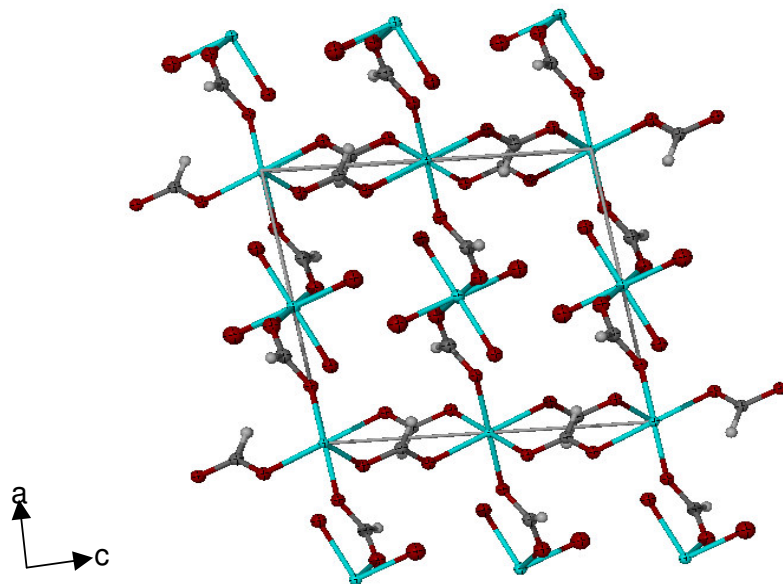
Fig. 3.6 *Packing diagram for zinc(II) formiate viewed along the b* axis

Comparison of zinc-oxygen and carbon-oxygen bonds in this complex shows that bond lengths do not differ appreciably from other zinc carboxylate compounds The carboxylate angle, O(1)-C-O(5) is however 5˚ larger than average carboxylate angles. This is probably due to the slight steric requirements of the hydrogen atom of the formiate group.

3.12 Zinc(II) Acetate

The vibrational spectra of zinc(II) acetate and stearate have been the subject of a paper published by Ishioka and co workers where a relation between the coordination structure of the carboxylate groups around the zinc atom and the vibrational frequencies of the carboxylate rocking mode was found.[13]

3.121 Synthesis

43

Acetic acid was reacted with metallic zinc to prepare this compound. Finely powdered zinc dissolves in an aqueous acetic acid solution over a period of 24 hours and evaporation of the solvent allowed precipitation of the carboxylate complex (see equation 3 below).

$$Zn_{(s)} + 2CH_3COOH_{(aq)} \rightarrow Zn(CH_3COO)_2 + H_{2(g)} \qquad \textbf{(3)}$$
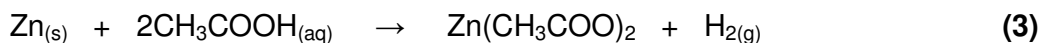
Using water as solvent should prevent polymerisation of the complex, since water takes up coordination sites on the metal, which are usually used to link to neighbouring zinc centers. The acetate ligand also allows water to approach the metal center, which also ensures that the product is soluble in water.

3.122 Infrared Spectroscopy

The frequency difference between the symmetric and asymmetric RCO_2^- stretching frequencies ($\Delta\textbf{\textit{v}}_{\textbf{COO}}$-) is close to the 150 cm^{-1} minimum difference in frequency expected for a bridging carboxylate.[9]

Values of this magnitude, however, are more indicative of a chelating (or bidentate) bonding mode which suggests the presence of the di-hydrated monomeric form of zinc(II) acetate that has been reported for other aqueous medium studies and not catena-bis(μ_2-acetato)-zinc(II), its polymeric analogue.[12]

Strong hydroxide absorptions confirm the presence of crystal water and also suggest that there is water present in the sample that is not coordinated to the metal center. Infrared band assignments for zinc(II) acetate are reported in Table 3.3.
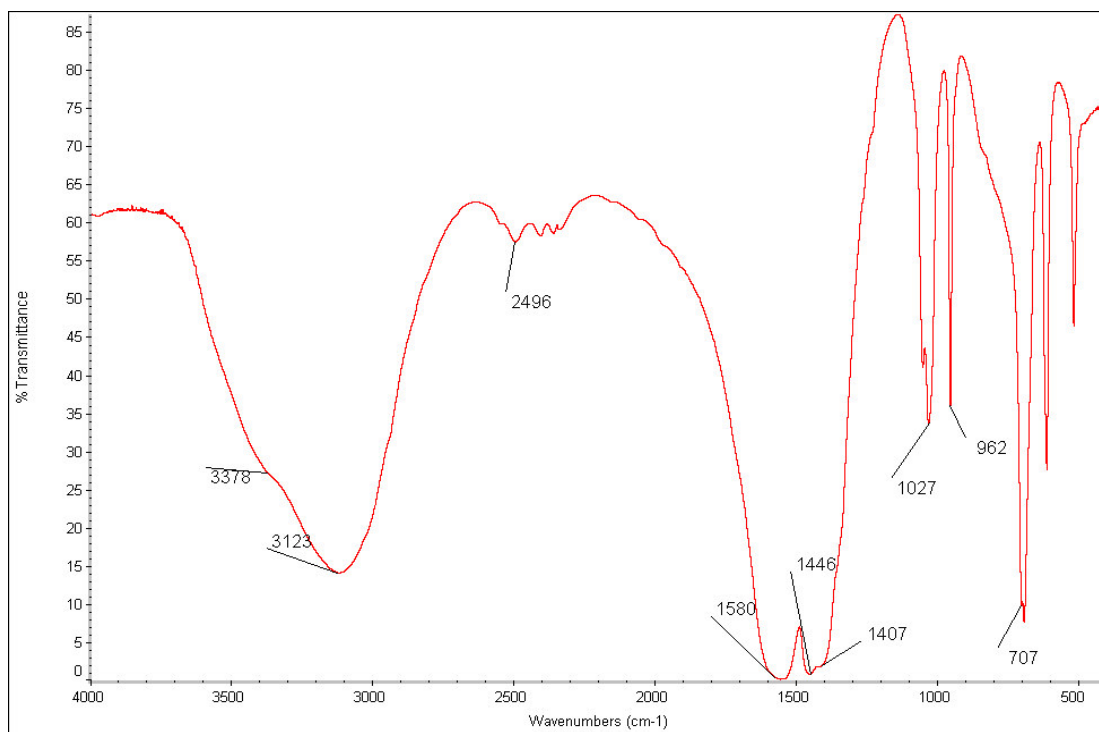
Fig. 3.7 *Infrared spectrum of zinc(II) acetate*

Table 3.3 *Infrared band assignments*

Band (cm^{-1})	Assignment
3378, 3127	-OH stretch
1550	Assymetric RCO_2^- stretch
1450	Aliphatic bending bands
1407	Symmetric RCO_2^- stretch
962-1027	This region contains C-C stretching as well as CH_3 rocking frequencies

3.123 Thermal analysis

The thermogram in Fig. 3.8 shows that, at 75 ˚C a mass loss of 15 % occurs, which indicates that two molecules of water dissociate from the compound, $Mr(Zn(CH_3COOH)_2.2H_2O)$ = 219.3. The compound then appears thermally

45

stable up to 250 ˚C when decomposition sets in (hence the change in the slope of the baseline, Fig. 3.9).

Fig 3.8 *TGA thermogram for zinc(II) acetate*
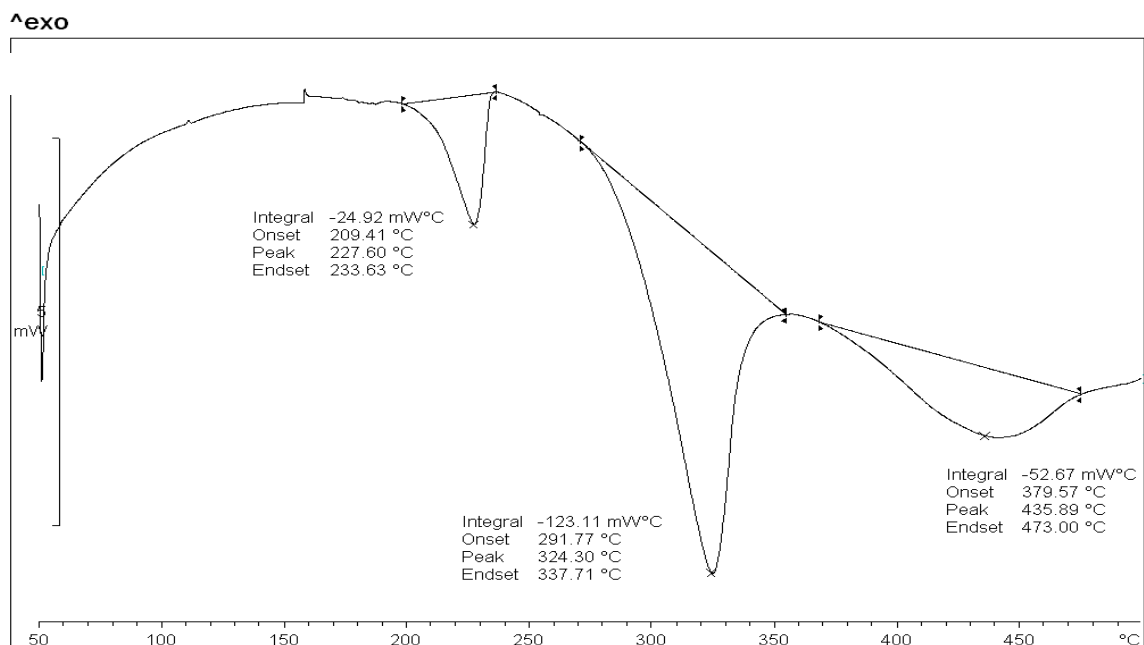
Fig. 3.9 *DSC profile of 2.9 mg zinc(II) acetate*

46

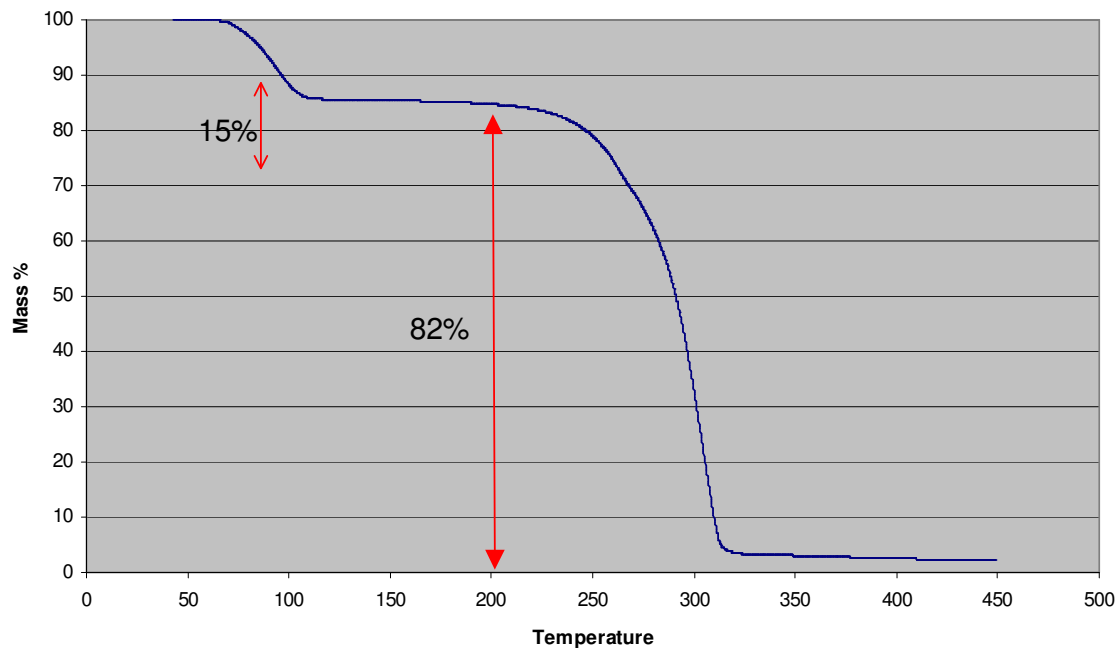Due to physical mass losses during data collection the final TGA value cannot be used. However, weighing the DSC sample pan after measurement leaves a mass equivalent of 120.84. (On an average of 4 measurements with a negligible standard deviation). This mass corresponds to a decomposition product consisting of $Zn(CO_3)$. The endotherm at 228 ˚C has been confirmed as the melting point of the compound using a melting point instrument.

3.124 Powder Diffraction Data

Using powder diffraction the compound could be uniquely identified (correlating more than 20 peaks) as zinc acetate by matching the observed pattern to those contained within the international database.[11] The collected powder diffraction pattern is shown in Fig. 3.10.

Although the pattern has been indexed before,[15] calculated unit cell data has not been accurately calculated. Due to the shape of the crystallites (small flat needles), preferred orientation was evident and extraction of intensity data would be of no value. But since this pattern will not be used for structure solution this was not an obstacle.
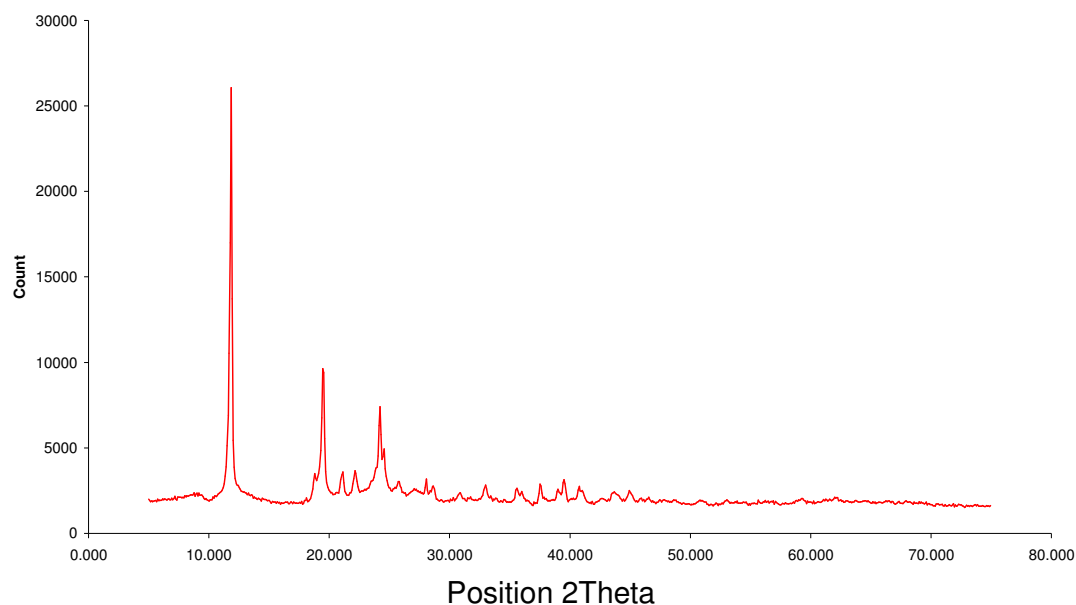
Fig. 3.10 *Powder diffraction pattern of zinc(II) acetate*

The 10 best indexing data sets obtained for zinc acetate using the Crysfire[14] software package and 20 lines sorted according to figure of merit are shown in Table 3.4. Unit cell constants for the most probable set are not in agreement with previously reported powder diffraction values.[12] While the collected powder pattern matches that of zinc acetate in the database, no three dimensional structure data was made available in the reference.
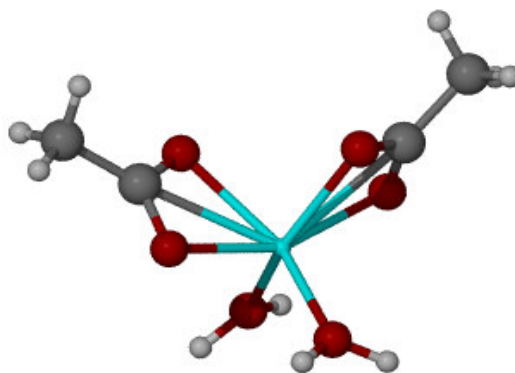
Fig. 3.11 *Structure of zinc(II) acetate[16]*

48

Mining the CCSD for possible structures, the most likely structure on the basis of unit cell data, was found to be the one depicted in Fig. 3.11 as prepared and reported by Ishioka *et al.*[16] Using the cif file for this structure, obtained from the CCSD database and the Powder Cell software package, the powder pattern of this compound was predicted. This predicted pattern matched the observed pattern of our compound and Table 3.5 shows lines that were successfully matched, with a standard deviation of 0.27.

While all predicted peaks were not found on the observed pattern, it is expected that many peaks are obscured by the strong preferred orientation of the crystal. From these results we conclude that the diagram displayed in Fig. 3.11, is indeed the structure of the prepared compound.

Table 3.4 *Indexing data for zinc(II) acetate*

I20	Merit	Volume	Prog	a	b	c	alpha	beta	gamma
19	9.52	689.29	LZ	9.60	9.68	7.95	95.87	96.36	70.27
19	7.00	715.82	TR	11.76	7.80	8.28	90.00	109.51	90.00
19	9.10	724.73	LZ	9.77	9.80	8.35	100.87	101.93	106.25
19	13.95	735.09	LZ	9.74	9.93	8.47	104.33	101.05	105.46
19	10.53	824.24	LZ	11.04	10.19	9.48	109.17	119.80	64.15
19	15.45	848.82	LZ	11.00	10.34	9.77	111.34	119.61	63.38
19	10.00	865.95	LZ	4.96	11.12	15.70	89.25	90.85	90.01
20	8.00	678.19	DV	15.68	5.57	7.76	90.00	90.77	90.00
20	8.00	678.19	DV	17.59	5.57	7.76	90.00	116.95	90.00
20	7.70	678.42	DV	17.40	5.57	7.76	90.00	115.72	90.00
20	10.20	1333.12	LZ	9.70	15.31	9.60	93.93	109.53	82.97

Table 3.5 *Comparison between observed and predicted diffraction values for zinc(II) acetate.*

Observed (° 2θ)	Predicted (° 2θ)	Difference
22.546	22.323	0.223
25.281	25.161	0.120
25.727	25.456	0.271

30.002	29.689	0.313
32.244	31.956	0.288
32.754	32.478	0.276
34.331	34.641	0.310
36.373	35.972	0.401
37.967	37.457	0.510
38.354	38.25	0.104
40.284	40.624	0.340
41.365	40.715	0.650
41.806	41.979	0.173
44.716	44.664	0.052
45.306	45.431	0.125
46.687	46.484	0.203
47.649	47.429	0.220
47.835	47.925	0.090
48.213	48.105	0.108
49.326	50.059	0.733
50.856	50.705	0.151

3.13 Zinc(II) Propionate

The propionate salt of zinc has been proven almost completely insoluble in aqueous media and solutions of propionic acid. This compound was previously prepared by treating zinc oxide with boiling concentrated propionic acid and distillation of the filtered solution *in vacuo* over CaO.[17]

3.131 Synthesis

Zinc propionate was prepared by reacting metallic zinc with propionic acid in aqueous medium. Precipitation of the compound was achieved by evaporation of the solvent. The resultant powder was white, flaky and crystalline with a distinctive smell of propionic acid. ICP analysis confirmed that 29.8 % (30.5 % calculated) of the compound consists of zinc. This is in agreement with the expected value for the anhydrous complex.

$$Zn_{(s)} + 2CH_3CH_2COOH_{(aq)} \rightarrow Zn(CH_3CH_2COO)_2 + H_{2(g)} \quad \textbf{(4)}$$
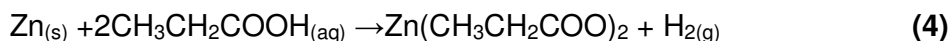
This reaction was also attempted in a dry ethanol medium. Absolute (96%) ethanol was dried and used as solvent and dilutent for the acid. The acid was dried as well, using $MgSO_4$ and fractional distillation. A procedure similar to the one followed for the aqueous reaction was followed, but the reaction yielded an insoluble, non crystalline white product. The apparent need for water to obtain a crystalline product is surprising from analysis results, since no water is eventually incorporated within the crystal structure. During further experiments only the product obtained in aqueous medium was used.

3.132 Infrared Spectroscopy

The separation between the symmetric and asymmetric bands for the carboxylic stretching frequencies (168 cm^{-1}) is large and almost completely excludes the possibility of anything other than a bridging mode of bonding. In all available literature cited, zinc(II) propionate has only been reported in polymeric form. [18] Figure 3.12 shows the IR spectrum of zinc(II) propionate and selcected bands with assignments are collected in Table 3.6.
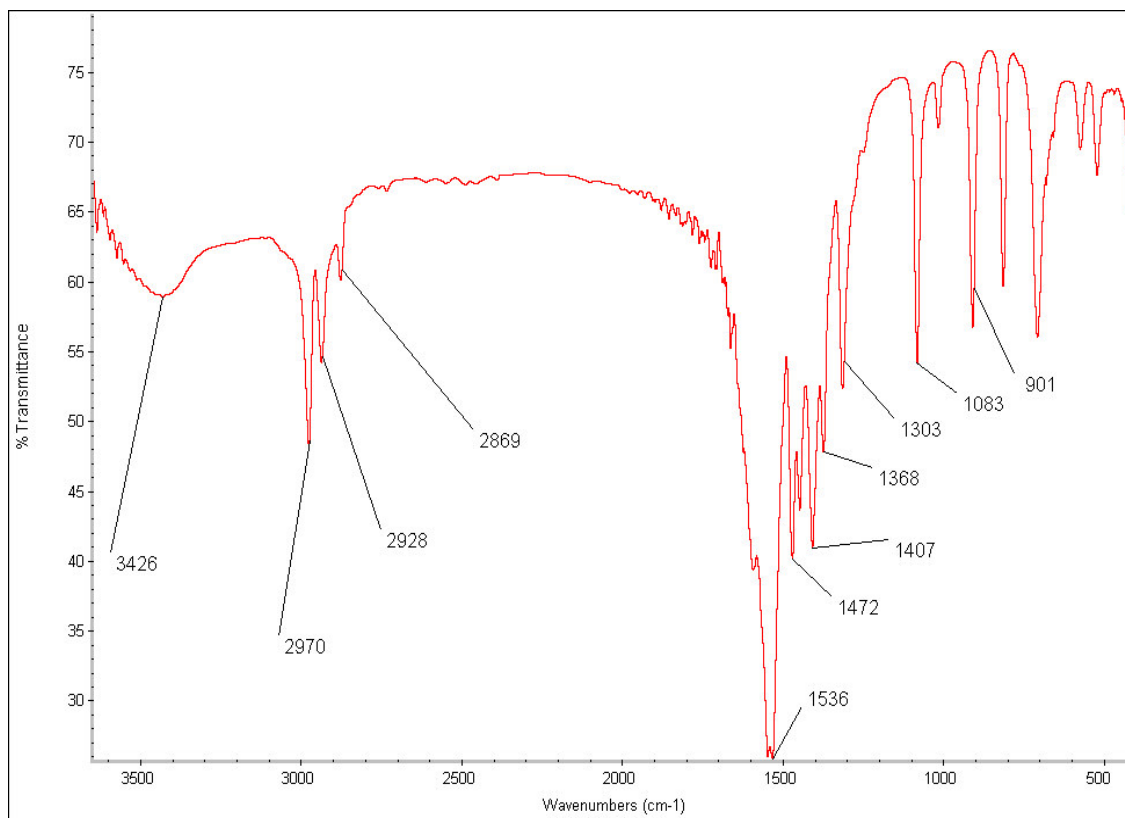
Fig 3.12 *Infrared spectrum of zinc(II) propionate*

Only a slight single hydration band (3426 cm^{-1}) can be seen on the spectrum, this band is broad and most likely a result of incomplete drying of the sample and is not indicative of water of crystallisation since a much stronger absorption (see sections 3.1 and 3.2) would result if that was the case.

Further evidence indicating that no water of crystallisation is present is that coordinated crystal water for the hydrated zinc acetate has its stretch (see Table 3.21) at a much higher value than what is observed here.

Table 3.6 *Infrared bands of zinc(II) propionate*

Band (cm^{-1})	Assignment
3426	-OH stretch
2970-2869	CH_2, CH bands

52

1595-1536	Assymetric RCO_2^- stretch
1468, 1447	Aliphatic bending bands
1368	Symmetric RCO_2^- stretch

3.133 Thermal Analysis

Zinc(II) propionate has a strong melting endotherm (confirmed *via* separate melting point measurements) at 223 ˚C, followed by rapid decomposition starting at about 300 ˚C as shown in the TGA (Fig. 3.13) and DSC (Fig. 3.14) thermograms below.

Once again due to physical mass losses occurring from the sample holder during data collection, the final TGA decompositional mass percentage can not be taken as valid. More careful manual measurements, however, are summarised below.
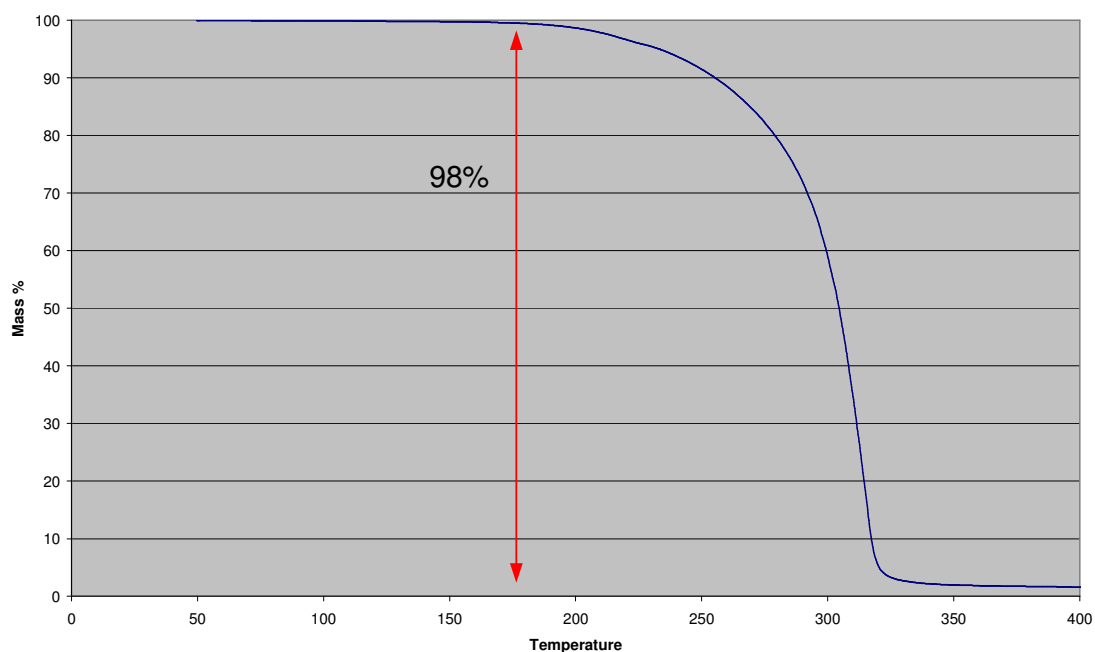

Fig 3.13 *TGA thermogram for zinc(II) propionate*

Mass loss observed for first sample: 1.) 4.94 g - (54.27 g - 50.20 g) =17.6%

second sample: 2.) 2.93 g - (52.59 g - 50.15 g) =16.7%

53

Average: =17.2%
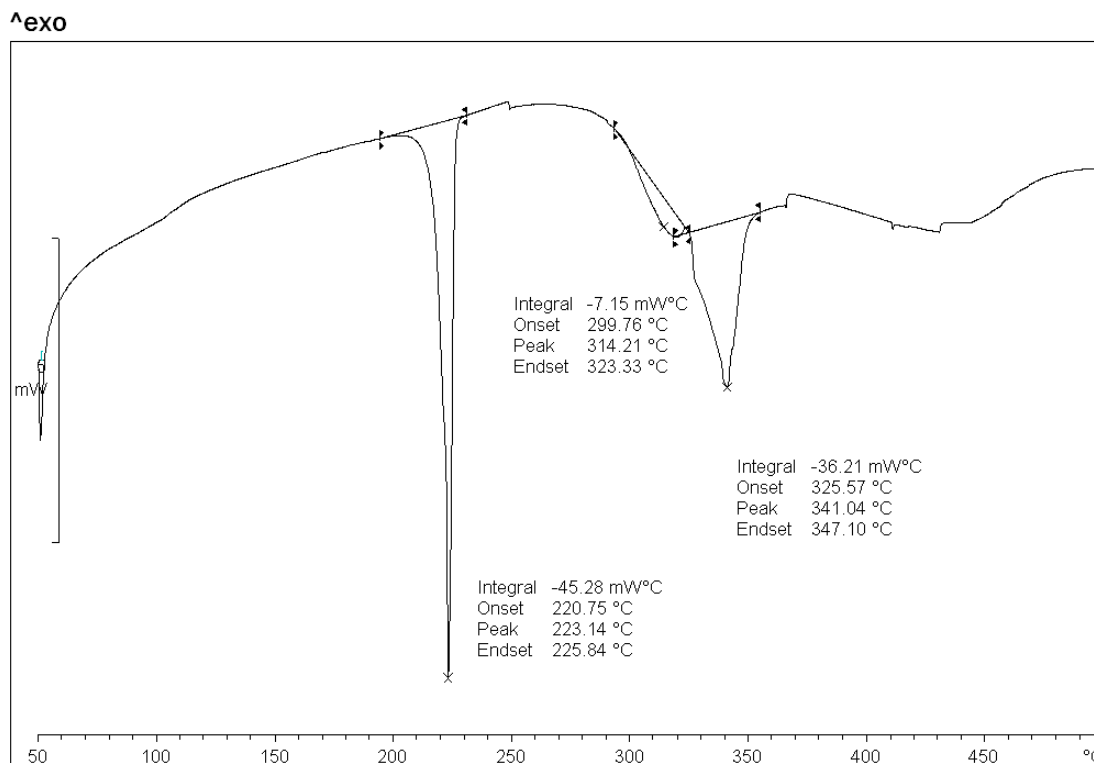
Fig. 3.14 *DSC thermogram for 2.93 mg zinc(II) propionate*

Since the compound has a molecular mass of 211.35, 17.2% equals a mass equivalent of 37 which suggests liberation of carbon monoxide (CO), leaving the zinc atom bonded to two propoxide groups - $Zn(CH_3CH_2CO)_2$ -, as product when heated to 500°C.

3.134 Crystallographic Data

The structure in Fig. 3.45 has been reported within the CCSD, with structure data as indicated in Table 3.7. The tetrahedral zinc atom is surrounded by four monodentate carboxylate ligands, with each carboxylate group bridging two metal centers. This structure is in agreement with spectral and thermal data discussed in this section.

54
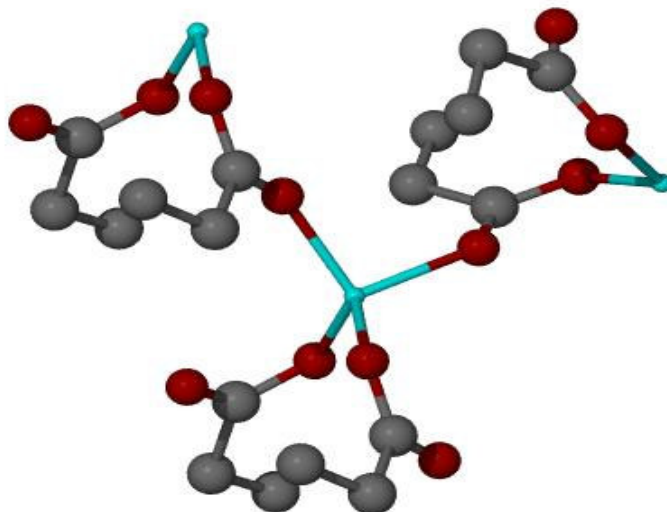
Fig 3.15 *Structure of zinc(II) propionate*[18]

Table 3.7 *Crystallographic data for zinc(II) propionate*[18]

a	9.286
b	4.794
c	19.087
α	90
β	90
γ	90
Volume	849.7

IR data as well as the TGA and DSC thermograms collected confirm that the prepared product has the same anhydrous polymeric structure, as that previously reported for zinc(II) propionate,[18] even though it has been prepared in aqueous medium. It can be seen that the zinc atom is surrounded by organic chains pointing outward in all directions, which keeps away all water from coordinating due to both steric effects of the propionate ligand. This in turn advances the formation of a polymeric structure. Table 3.7 contains data that will be used for comparative purposes in subsequent sections.

3.14 Zinc(II) Butanoate

3.141 Synthesis

Butyric acid was used to dissolve metallic zinc powder into an aqueous medium (equation 5), while butyric acid does not dissolve easily in water at room temperature, slight heating of the reaction mixture allows the formation of a homogenous liquid. A large excess of butyric acid was added to promote the rate of this reaction but heating the reaction mixture to reflux, produces very foul smelling vapours that proved impossible to contain however efficient the water cooler that was used. The mixture was filitered, to remove any unreacted zinc from the mixture and precipitation resulted during evaporation in a rotary evaporator. The yield was a white, flaky crystalline powder. These flaky crystals are smectic in nature and thus unsuitable for single crystal diffraction. The flat, rectangular needles are sandwiched together and inseparable due to their fragility. While this product was not as smelly as the reagent acid, it was still quite pungent.

$$Zn + 2CH_3(CH_2)_2COOH + xH_2O \rightarrow Zn(CH_3(CH_2)_2COO)_2.xH_2O + H_2$$
(5)
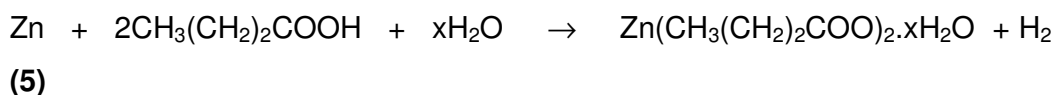
After precipitation of the product it proves insoluble in solvents such as benzene, ethanol, methanol and THF and only marginally soluble in water upon submersion in an ultrasonic bath.

3.142 Infrared Spectroscopy

The infrared spectrum of the prepared compound is shown in Fig. 3.16 and selected band assignments are shown in Table 3.41. The energy gap between the symmetric and asymmetric stretches of the carboxylate group is greater than 150 cm^{-1}, which would mean a bridging carboxylate bonding

56

mode is present if the rules laid down by Nakamoto *et al.*[9] are followed. The spectrum also shows an –OH absorption band, but when compared to the intensity of aliphatic and carboxylate stretches and to –OH absorption frequencies in hydrated compounds, this seems to be only due to residual solvent remaining in the sample.
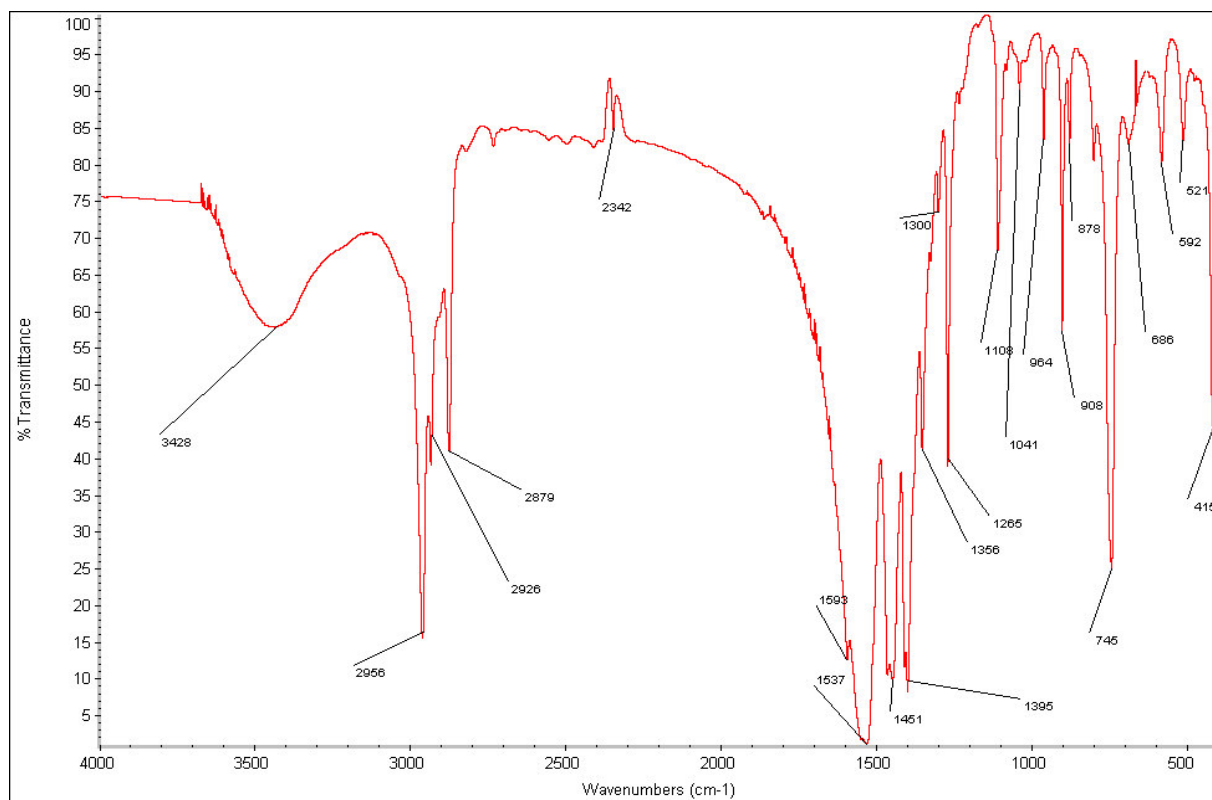
Fig. 3.16 *Infrared spectrum of zinc(II) butanoate*

Table 3.8 *Infrared band assignments*

Band (cm^{-1})	Assignment
3428	-OH stretch
2953-2879	Aliphatic stretching bands
1537	-RCO$_2^-$ assymmetric stretch
1451	Aliphatic bending bands
1394	-RCO$_2^-$ symmetric stretch

As reported previously,[12] the difference of 153 cm^{-1} in the symmetric and asymmetric stretching band of the carboxylate ion indicates that the mode of

57

bonding in this complex is bridging, a shoulder in the asymmetric stretching region which does not seem part of the bridging multiplet, might indicate that another carboxylate bonding mode also occurs in the structure.

3.143 Thermal Analysis

Earlier reports state that thermal decomposition for the monomeric zinc C4-carboxylate starts at 333 K (60 ˚C) accompanied by the endothermic release of two molecules of water.[18] At 593 K (320˚C) an alkylketone and carbon dioxide are released and can be identified by gaseous IR spectroscopy, the final thermal decomposition results in zinc oxide (IR band at 456 cm^{-1}).

In our studies, neither a strong –OH absorption in the infrared spectrum, or a mass decrease in the 100˚C region (Fig. 3.17) are observable, in fact, the first thermal event for this compound is melting that occurs at 175 ˚C (Fig. 3.18). The thermal behaviour and spectral properties of the compound resembles that of the zinc propionate polymer (section 3.3) so closely, that a similar structure (polymeric as opposed to monomeric) can be proposed.
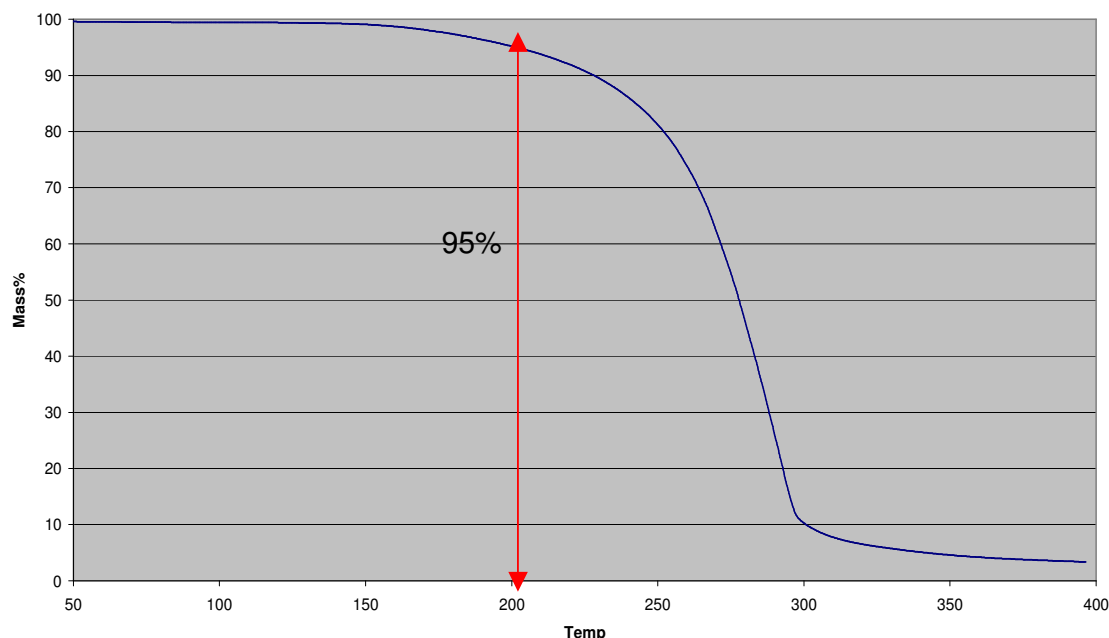
Fig. 3.17 *TGA thermogram for zinc(II) butanoate*

58

The strong endotherm, depicted on the DSC thermogram (Fig. 3.18), at 175 ˚C was confirmed as the melting point for the compound using a melting point instrument. Decomposition starts at 307 ˚C and continues up to 370 ˚C after which the mass remains stable. The melting point of this compound is much lower (50 ˚C) than for zinc propionate (discussed previously), yet decomposition occurs 20 ˚ higher. Using data obtained from the DSC analysis, the decomposition enthalpy of zinc(II) butanoate to zinc oxide can be calculated(equation 6).

$$Zn(CH_3CH_2CH_2COO)_2 \rightarrow ZnO + byproducts \quad \Delta H= -3.281 \ J.mg^{-1} \qquad \textbf{(6)}$$
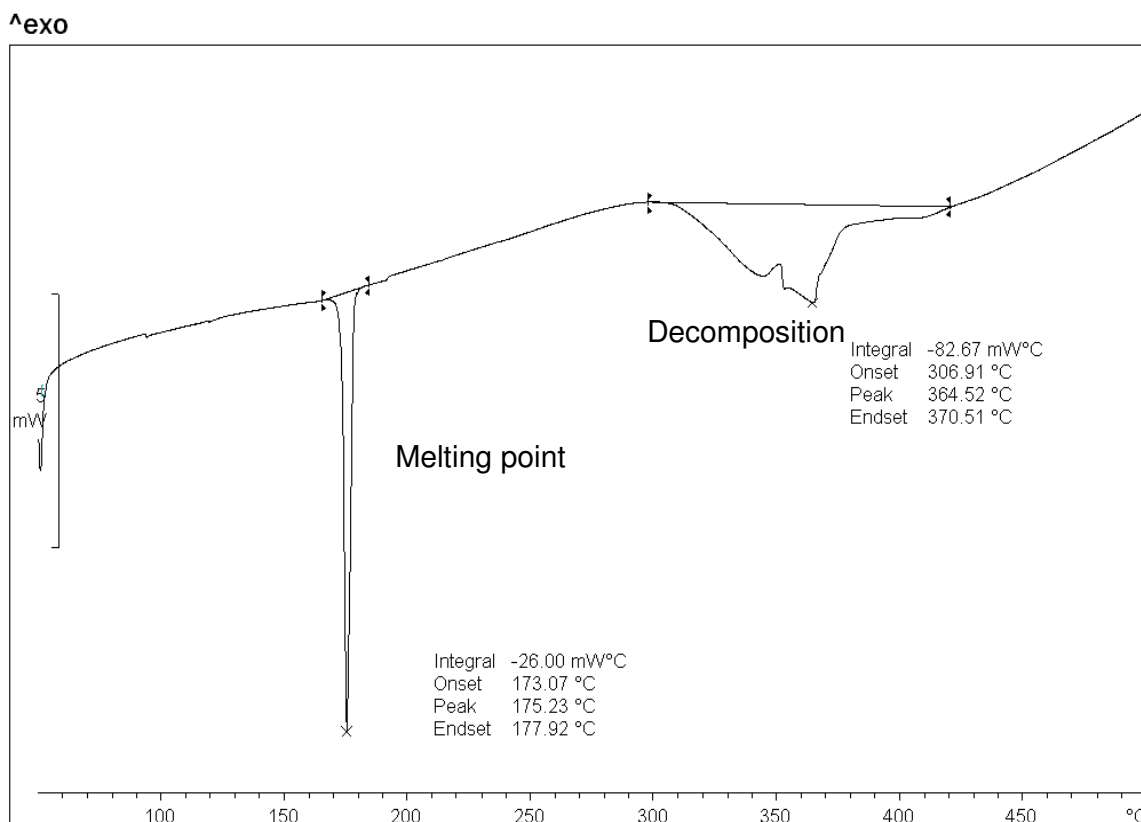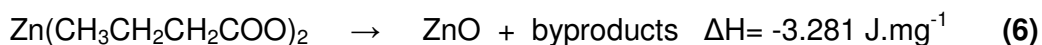
Fig. 3.18 *DSC thermogram for 2.13 mg zinc(II) butanoate*

3.144 Powder Diffraction

The most favourable indexing result for the collected powder pattern of this (prepared) complex has a figure of merit 12 and suggests a unit cell volume of 550.63 $Å^3$ and crystal with triclinic symmetry.

However, when comparing unit cell values and volume to that of zinc(II) propionate (discussed earlier in this chapter), a more likely data set seems to be the one highlighted by italics in Table 3.9. This set reports a volume of 955.93 $Å^3$ with a monoclinic system, this result, like the first, is obtained *via* the TREOR algorithm. This result also has a higher number of successfully indexed lines (18 as opposed to 16) for the result that has the higher figure of merit.

Fig 3.19 *Powder diffraction pattern for zinc(II) butanoate*

When evaluated in combination with spectral and thermal data, these results indicate, a structure similar to that proposed for zinc(II) propionate in section 3.13.

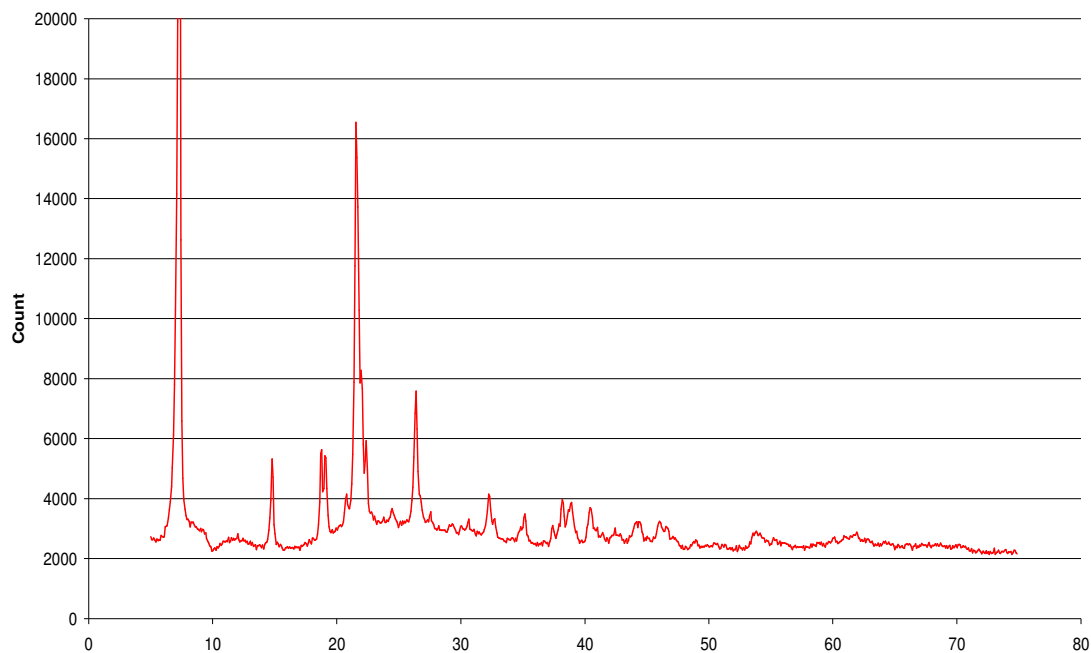**Table 3.9** *Most favourable indexing results for zinc(II) butanoate, sorted according to figures of merit as defined by the indexing programs used*

Merit	Volume	Prog	a	b	c	alpha	beta	gamma
6.1	1179.25	DV	12.13	12.35	7.95	90.00	98.36	90.00
6.2	1165.76	DV	24.74	5.99	7.86	90.00	93.20	90.00
6.6	1093.93	DV	12.41	12.24	7.23	90.00	95.04	90.00
6.6	1093.93	DV	12.41	12.24	7.23	90.00	95.04	90.00
6.9	1165.58	DV	25.54	5.99	7.87	90.00	104.71	90.00
7	*955.93*	*TR*	*13.84*	*6.45*	*11.99*	*90.00*	*116.83*	*90.00*
7	736.04	TR	13.38	11.97	4.98	90.00	112.84	90.00
7	672.57	TR	16.11	9.01	6.04	90.00	130.05	90.00
8	691.56	TR	13.25	4.66	12.04	90.00	111.73	90.00
9	489.92	TR	10.38	7.41	6.50	90.00	101.84	90.00
9	672.79	TR	13.06	9.01	6.05	90.00	109.28	90.00
10	549.63	TR	7.38	7.32	17.77	76.58	115.88	55.925
12	550.64	TR	7.39	7.321	22.05	90.17	133.55	55.871

3.15 Zinc(II) Pentanoate

Panevchik *et al.*[20] used high temperature X-ray diffractometry to show that some organic acid complexes of zinc, including zinc(II) pentanoate, display enantiotropic polymorphism.

3.151 Synthesis

Zinc pentanoate formed when valeric acid was reacted with metallic zinc and hydrogen gas was released as a by product. Even though the reaction was only considered complete when no more observable zinc particles were present, the solution was filtered to prevent contamination due to any unreacted zinc particles remaining. The compound dissolves easily in water or

ethanol, when submersed in an ultrasonic bath, but it's insoluble in all tested organic solvents. As observed for zinc(II) butanoate, even though crystallisation is rather easy, the formed crystals stack together in inseparable layers and are not suitable for single crystal diffraction. A photograph of a cluster of zinc pentanoate crystals is shown in Fig. 3.20.
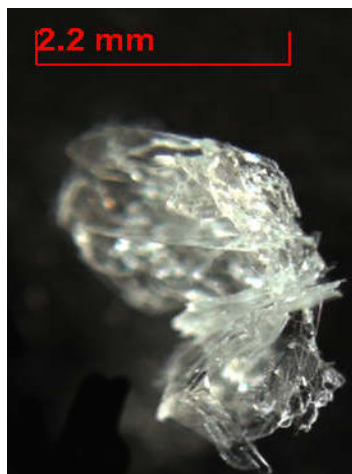
Fig 3.20 *Zinc pentanoate crystals*

3.152 Infrared Spectroscopy

Before the IR spectrum was recorded, the sample was washed with ethanol and dried *in vacuo*. The infrared spectrum in Fig. 3.21 clearly shows that hardly any water is present in the sample and the slight absorption observed is most probably due to residual solvent molecules.

As expected for this longer chain carboxylate, the aliphatic stretching bands at 2959 cm^{-1} are quite predominant and overshadowed only by the carboxylate frequencies. Other bands and their assignments are shown in Table 3.10.

62
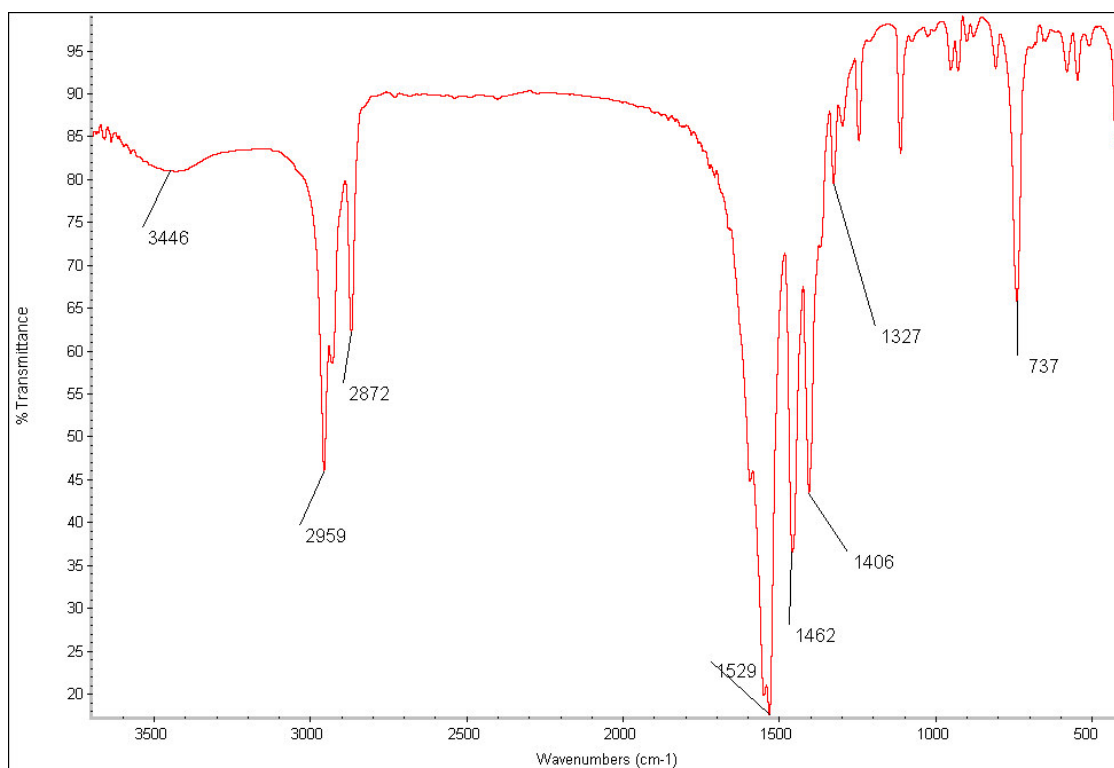
Fig 3.21 *Infrared spectrum for zinc pentanoate*

Carboxylate frequencies, both symmetric and asymmetric, have been known to shift to lower frequencies as the carbon chain length increases.[21] This explains the shift of the asymmetric RCO_2 stretching frequency to 1529 cm^{-1} as opposed to 1580 cm^{-1} for the shorter carboxylate chains.

Table 3.10 *Infrared band assignments*

Band(cm^{-1})	Assignment
3447	-OH stretch
2958-2908	CH, CH_2 symmetric and asymmetric stretches
1529	Assymetric RCO_2^-
1455, 1418	Aliphatic bending bands
1327	Symmetric RCO_2^-
737	-(CH_2) rocking mode

Other changes in the carboxylate stretching frequencies involve an increase in energy for the asymmetric stretch and a slight decrease in the symmetric stretching frequency, when the carboxylate bridges between metal centers.[9]

As a result, the difference in symmetric and asymmetric frequency (202 cm^{-1}) for this compound can be attributed to a monodentate coordination but the result does not completely exclude the possibility of a bridging coordination mode.

3.153 Thermal analysis

The compound shows little or no mass loss before the onset of decomposition at 250 ˚C (Fig. 3.22). Before 200˚C is reached, three sharp endotherms (Fig. 3.23) of increasing intensity occur. Since these endotherms do not correspond to any mass loss (as supported by TGA data and verified by manual measurements) and no melting point is observed in this region, these endotherms result from solid phase transitions. It has to be mentioned however, that when a reversed temperature program is run, which measures thermal events when cooling the sample, these peaks do not recur.
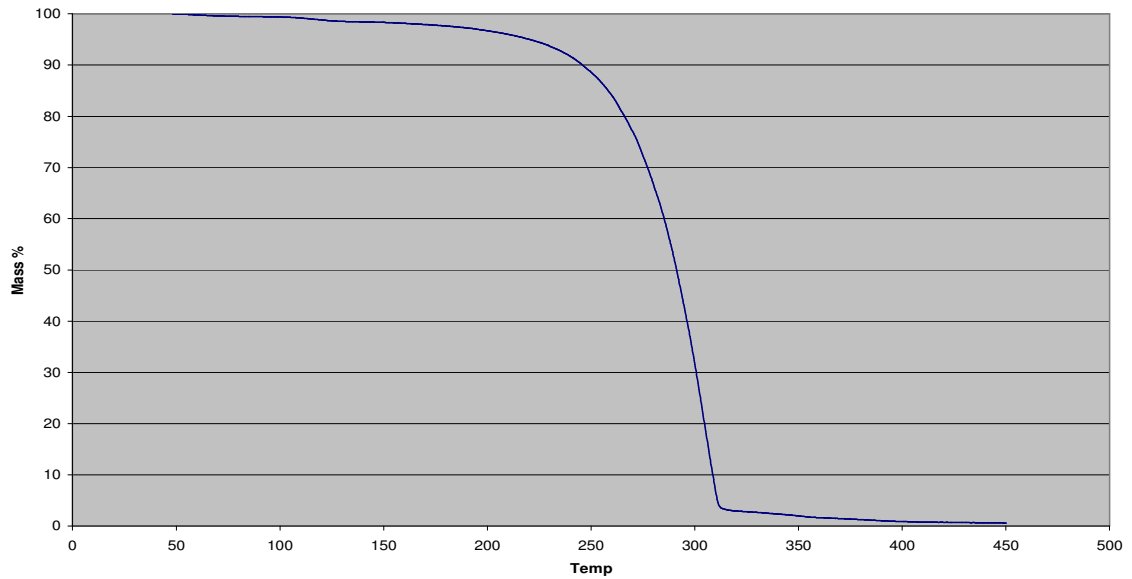
Fig 3.22 *TGA thermogram for zinc(II) pentanoate*
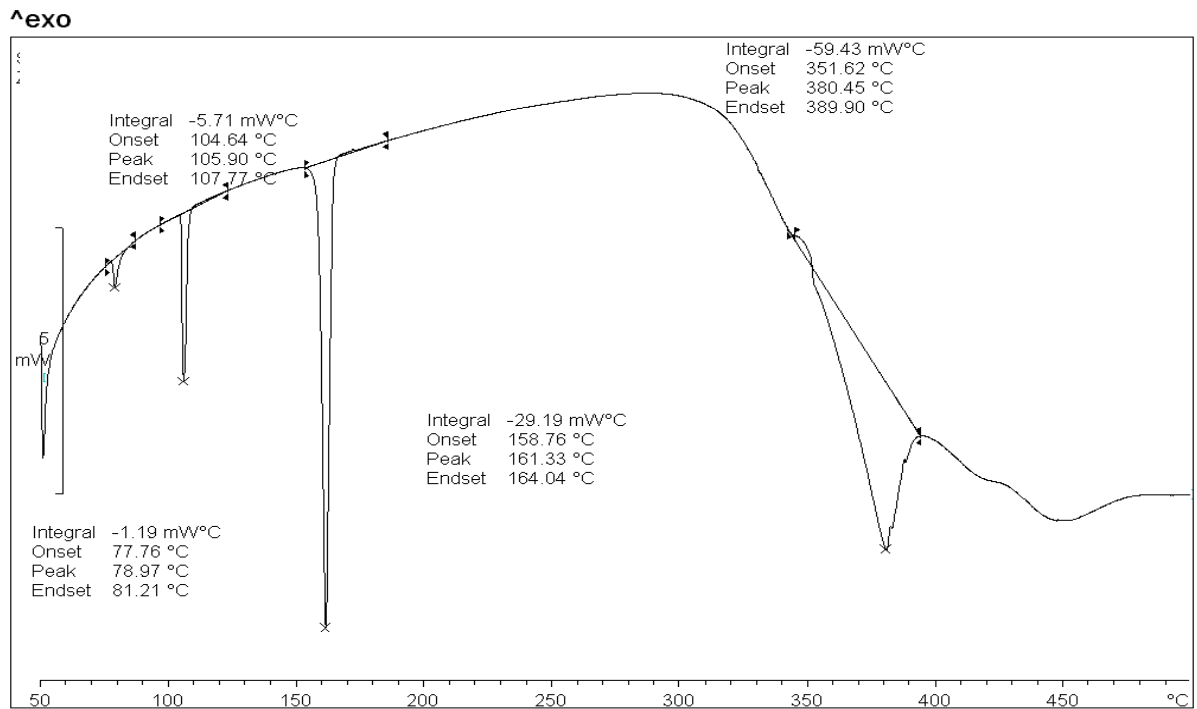
Fig 3.23 *DSC thermogram of 1.93 mg zinc(II) pentanoate*

.

65

3.154 Powder Diffraction

Powder diffraction studies of the collected pattern for the prepared compound (shown in Fig. 3.24 with the peak list and indexes collected in Table 3.11 suggest a unit cell volume of at least 1000 $Å^3$, with DICVOL successfully indexing 19 lines and TREOR indexing 18.

This cell volume is more than twice that of the monomeric acetate complex, but only 25 % larger than the propionate complex and has a less than 6 % volume difference when compared to indexing data obtained for zinc(II) butanoate. When considering these values together and after inspection of thermal and spectral similarities, we propose that all three these zinc(II) carboxylates (propionate, butanoate and pentanoate) have similar polymeric structures.

Fig 3.24 *Powder diffraction pattern for zinc(II) pentanoate*

Table 3.11 *Peak list and indexes*

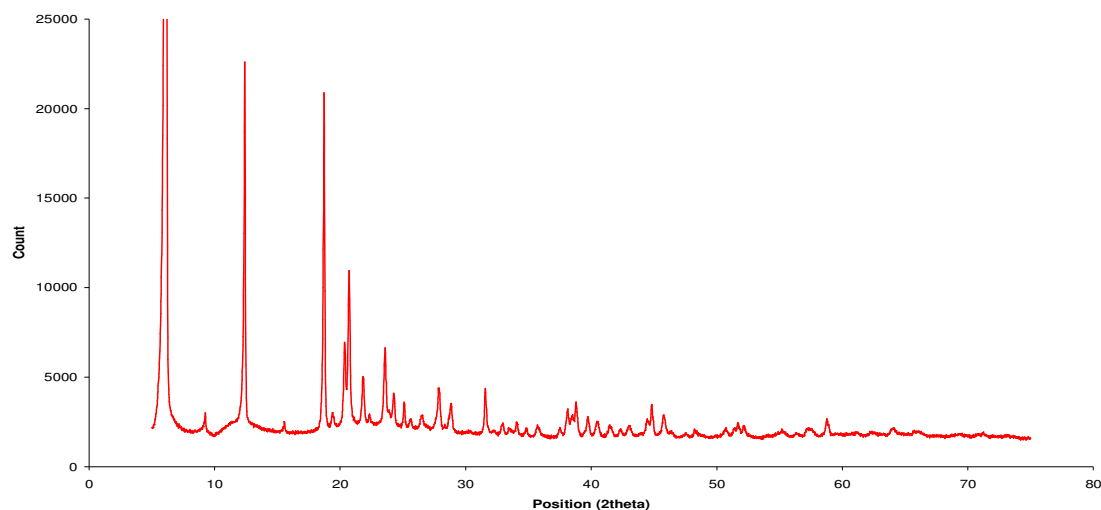| 2Theta	hkl	2Theta	hkl
5.923	001	23.857	50-1
2.282	200	27.899	012
12.407	10-2	28.884	310
15.583	202	31.575	113
18.724	103	38.143	61-1
19.493	20-3	38.824	611
18.724	203	39.814	306
20.730		40.566	612
21.866	30-3	44.844	506

Results, from this study (Table 3.12), show that the compound crystallises with monoclinic symmetry and unit cell values as shown. When scanning through the data files created during indexing for the DICVOL program it appears that the program needs one more line for perfect indexing of this pattern. This expected line, should occur at quite a high two-theta value (2θ= 58.84˚) and is probably contained within our pattern, but a visual inspection of the diffraction pattern shows that background noise starts to obscure peaks in this area and a higher figure of merit should be obtained if the scan step time is increased and, therefore, leading to a better signal to noise ratio.

Table 3.12 *Indexing data for zinc(II) pentanoate*

Merit	Prog	Volume	a	b	c	alpha	beta	gamma
5.1	DV	1010.714	3.537	14.962	19.148	94.151	90	90
5.5	DV	5552.653	4.996	24.880	44.676	90.000	90	90
6	DV	1010.712	3.537	14.963	19.150	94.132	90	90
6	TR	1433.512	9.646	9.983	15.626	106.964	93.404	92.65
6	TR	1433.512	9.646	9.983	15.626	106.964	93.404	92.65
7	TR	1079.786	7.268	10.025	15.846	105.719	100.121	96.064

3.16 Zinc(II) Isovaleroate

Although this branched chain carboxylate is not part of the family of zinc carboxylates discussed in this chapter (formiate to pentanoate), this complex was prepared to not only study the effects of chain branching on the compound properties, but also in an attempt to obtain a monomer of a zinc carboxylate with a aliphatic chain that contains more than two carbons. To our knowledge, no preparative or analytical data about this compound have been published.

3.161 Infrared Spectroscopy

Two types of water can be identified in this spectrum (Fig. 3.25) from the two distinct -OH bands at 3391 cm^{-1} and 3157 cm^{-1}. This can most probably be ascribed to coordinated crystal water and unevaporated solvent still present. The observed bands and assignments are summarised in Table 3.13.
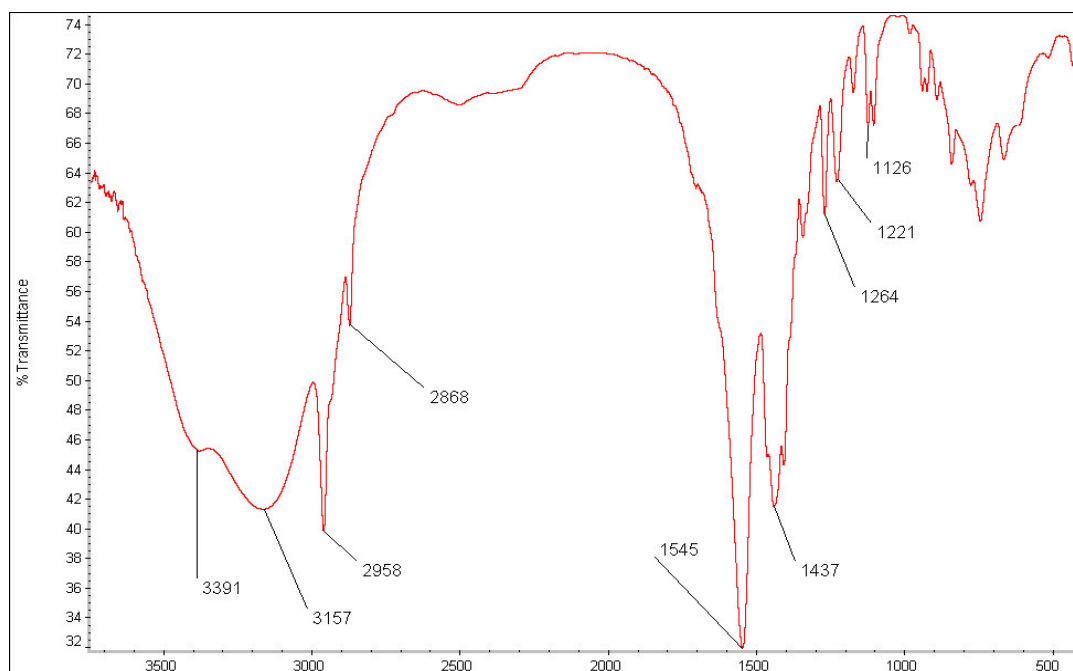

Fig 3.25 *Infrared spectrum of zinc(II) isovaleroate*

These absorptions are followed by the intense aliphatic symmetric stretches at 2958 cm^{-1} and asymmetric aliphatic stretches at 2868 cm^{-1} after which no

further absorptions occur until that of the asymmetric carboxylate. The symmetric RCO_2^- absorption band is obscured and cannot be distinguished from aliphatic absorptions occurring in the same region. The fact that this stretch occurs at a relatively high energy, indicates that a non-bridging or more specifically a bidentate chelating carboxylate is present.

Table 3.13 *Infrared absorption frequencies and assignments*

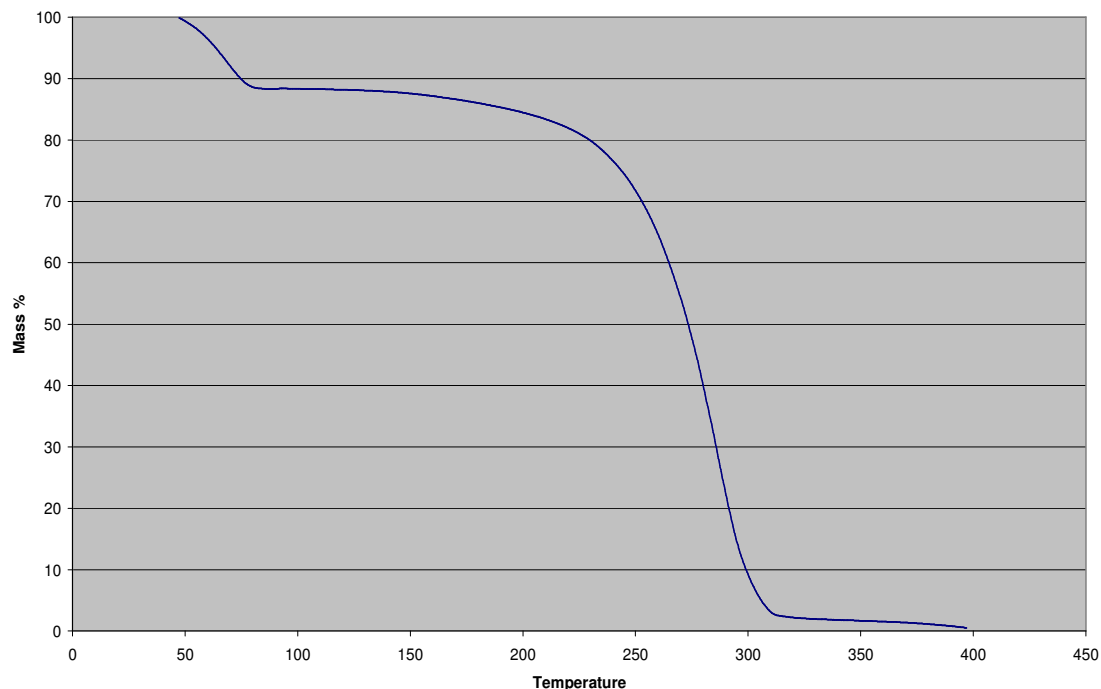| Band (cm^{-1})	Assignment
3391,3157	-OH absorptions
2958,2868	Aliphatic symmetric and asymmetric stretches
1545	Asymmetric carboxylate stretch
1437 region	Aliphatic bend and symmetric carboxylate stretches
1264	Carbon oxygen stretch

3.162 Thermal analysis

Fig 3.26 *TGA thermogram for zinc(II) isovaleroate*

While the decomposition pattern in Fig. 3.26 is inconclusive due to physical sample mass losses (the carboxylate "bubbles" and leaves the sample pan), the loss of water at 95 ˚C is evident. Since this loss accounts for more than 10% of the total mass percentage, it confirms the presence of crystal water in the structure of this complex.

3.163 Crystallographic studies

Crystallographic data for this structure was collected as described in the experimental section. Figure 3.27 shows the structure obtained, followed by Table 3.14 which contains a list of selected bond angles and bond lengths.

Even though the unit cell volume is much greater than expected for a monomeric unit (using the hydrous acetate as reference), it can be seen from the packing diagram (Fig. 3.28) that due to the symmetry of the packing, the unit cell volume is much larger than expected for the size of the molecule.
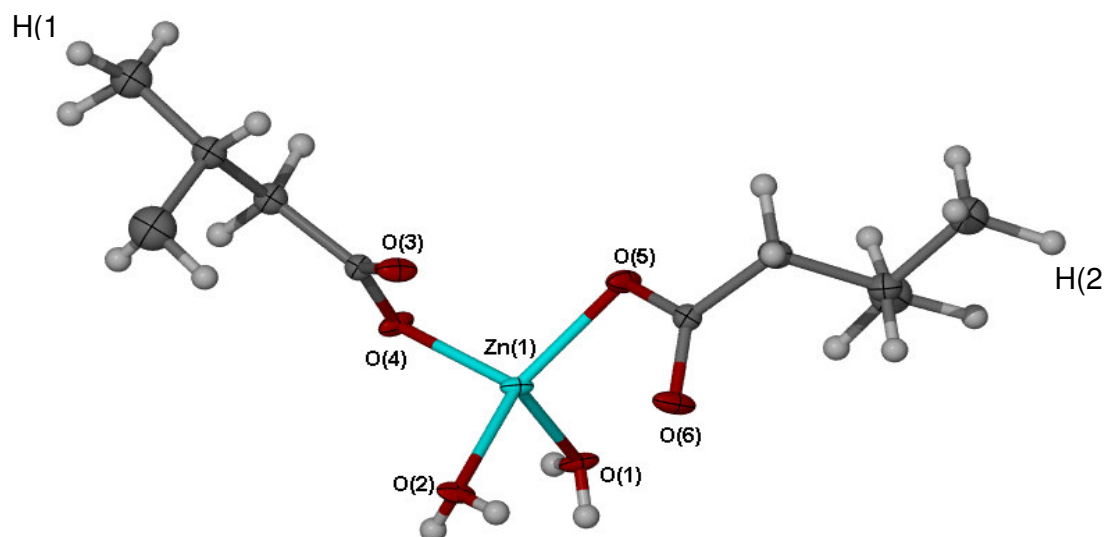
Fig. 3.27 *The molecular structure of zinc(II) isovaleroate*

Table 3.14 Selected bond lengths and angles

Bond Lengths (Å)	
Zn-O(4)	2.040
Zn-O(2)	2.403
Zn-C(1)	2.568
Zn-O(3)	1.989
Zn-O(4)	2.521
Zn-O(5)	1.975
Zn-C(2)	2.621
Bond Angles (°)	
O(1)-C(1)-O(2)	119.86
O(3)-C(2)-O(4)	118.87
C(1)-Zn-O(3)	94.41
O(5)-Zn-O(6)	100.58
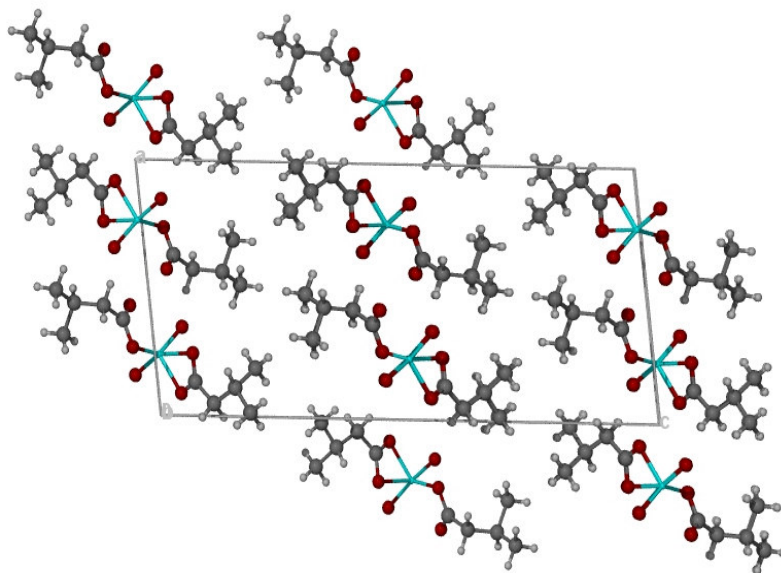
Fig 3.28 *Packing diagram for zinc(II) isovaleroate*

Measuring the absolute molecule length, measured from the two atoms furthest from each other (hydrogens 1 and 2 as on sketch), a value of 12.5 Å is found. This value is about half that of the c-axis length. The absolute "single" molecule volume is thus *much* closer to that of the acetate complex (that has an "absolute" length of 7.6 Å), than for the longer chained polymeric complexes.

3.2 Experimental

Organic acids were purchased from Sigma Aldrich with a minimum purity of 98% and used without further purification unless stated otherwise. All liquid reagents, were weighed directly into the reaction vessels.

3.21 Preparation of Zinc(II) Formiate

72

Zinc(II) formiate was prepared by adding a stoichiometric amount of formic acid (1.14 g, 30.6 mmol) to metallic zinc powder (1 g, 15.3 mmol) in an aqueous medium. The reaction mixture was heated and allowed to reflux until no traces of zinc powder remained (approximately 12 hours) after which the solution was filtered on a Buchner filter and concentrated on a rotary evaporator. The reaction mixture was completely stripped of solvent and dried to obtain a shiny white powder. The reaction produced a yield of 94%.

3.22 Preparation of Zinc(II) Acetate

Metallic zinc (0.91 g, 13.84mmol) was dissolved in a 2M mixture of acetic acid (1.07 g, 27.7 mmol) and water. The reaction was completed by adding a 0.3 ml excess of the acid and allowing overnight reflux. Upon evaporation, a coarse crystalline white powder formed, which proved soluble in water. A yield of 95% was afforded in this preparation.

3.23 Preparation of Zinc(II) Propionate

Metallic zinc powder (1.01 g, 15.44 mmol) was reacted with propionic acid (2.5 ml, 33.2 mmol). Addition the acid to the water (10 ml) and heating to 40˚C created the reaction mixture. Metallic zinc powder was then added and allowed to dissolve with the release of hydrogen gas, this took approximately 16 hours after the reaction mixture was brought to reflux.

3.24 Preparation of Zinc(II) Butanoate

Zinc powder (0.5 g, 7.65 mmol) was reacted with butyric acid (1.14 g, 15.29 mmol). A large excess of butyric acid (2ml) was added to promote the rate of this reaction. The reaction was completed at a temperature of 70˚C, in aqueous medium and it took nearly two days before all metallic zinc was

dissolved. Using an oven at 60 ˚C the powder was then dried overnight. An 82 % yield was obtained.

3.25 Preparation of Zinc(II) Pentanoate

Stoichiometric amounts of metallic zinc powder (0.50 g, 7.7 mmol) and valeric acid (1.66 g, 15.3 mmol) were reacted and allowed to reflux overnight. An excess of 0.5 ml acid was also added. The synthesis was achieved in aqueous medium and precipitation resulted when the solution was concentrated by evaporating the solvent. The resultant product was a white flaky micro crystalline powder.

3.26 Preparation of Zinc(II) Isovaleroate

A acid-water solution was prepared using 2.1 ml of acid and 16 ml of water. The solution was heated to 50 ˚C to promote formation of a homogenous solution and 0.67 grams [10.24 mmol] of fine zinc powder was added. The reaction proceeded very slowly after reaching reflux, and a lot of unreacted zinc was left even after 16 hours. A 2.25 ml excess of iso-valeric acid was then added and the reaction proceeded at a more rapid pace.

Upon completion of the reaction, the solution was filtered and the acid-water solvent evaporated using a Schlenk line. The reaction afforded a 94% yield and half the resulting powder was redissolved and left to slowly crystallise at room temperature.

3.27 Thermal Analysis

Thermogravimetry was carried out using a Perkin Elmer TGA 7 Thermogravimetric Analyser. The experiments were performed using a step

74

size of 10˚C.min^{-1} and over temperature ranges as indicated on the respective graphs, with data evaluation performed using Microsoft Excel.

Differential scanning calorimetry, was completed on a Mettler DSC 822^{e}, using the STARe software package to interpret and examine the data. Aluminium (40 µml) sample pans, pressed and vented by piercing the sample pan lid, were used during collection.

3.28 Infrared Spectroscopy

Infrared spectra were recorded on a Nicolet Thermstar IR spectrophotometer, with the samples dispersed in KBr discs and using continuous dry nitrogen gas to purge the collection chamber. The collection range was 4000 cm^{-1} to 450 cm^{-1} at a resolution of 2 cm^{-1}.

3.29 Powder Diffraction

A powder diffraction pattern was collected on a, Phillips PW 1710 diffractometer, with collection commencing at 5 ˚2θ through to 75 ˚2θ with a step size of 0.0170 ˚2θ and step time of 12 sec. To index the collected powder patterns, the Crysfire[14] software package was used.

Using the TAUP and DICVOL1 algorithms any high symmetry solutions were eliminated and indexed. The TREOR algorithm, which is tolerant of some impurity lines took care of orthorhombic and monoclinic solutions. LZON, is a semi exhaustive algorithm that explores a large number of possible low symmetry solutions and can exclude (or ignore) up to 5 spurious lines. Figures of merit, as described in the introductory chapter, were used to rank the possible solutions in order of a most likely solution.

3.210 Structure solution

Zinc(II) formiate

A crystal of this complex was mounted on a glass fibre sample holder and set up on a Nonius Kappa CCD diffractometer. Mo-Kα radiation, wavelength λ(0.17073 Å) was used and compensated for Lorentz and polarisation effects. Solution of the structure was completed using the WinGX crystallographic suite as interface, which calls the Shelx-97[23] program for solution and refinement. The initial solution was obtained by direct methods. All other crystallographic data are included in sections devoted to this complex.

Table 3.15 *Crystallographic data for zinc formiate*

Empirical formula	$C_2H_2O_6Zn$
Molar mass	83.29
Temperature (K)	173
Wavelength (Å)	0.171073
Crystal system, Space group	Monoclinic, $P2_1/c$
Cell Dimensions	
a/Å	8.69 (1)
b/Å	7.15(1)
c/Å	9.31(1)
α/˚	90.00
β/˚	97.52(3)
γ/˚	90.00
Volume/Å^3	573.01
Density/g.cm^{-3}	2.172
F(000)	368
Total Reflections	4705
Unique Reflections	1418
Goodness of fit	0.698
R index	0.027

Zinc(II) Isovaleroate

A crystal of this complex was cut to size and mounted on a glass fibre sample holder and set up on a Bruker SMART Apex diffractometer. Mo-Kα radiation, wavelength λ(0.17073 Å) was used and compensation made for Lorentz and polarisation effects. Solution of the structure was completed using the X-Seed[22] crystallographic suite as interface, which uses the Shelx-97[23] program for solution and refinement. The initial solution was obtained using direct methods. All crystallographic data are included in sections devoted to this complex.

Table 3.16 *Crystallographic data for zinc(II) isovaleroate*

Empirical formula	$C_{10}H_{18}O_6Zn$
Molar mass	299.61
Temperature (K)	173
Wavelength (Å)	0.171073
Crystal system, Space group	Monoclinic, $P2_1/c$
Cell Dimensions	
a/Å	10.908(2)
b/Å	5.268(11)
c/Å	24.212(5)
α/˚	90.000˚
β/˚	97.52(3)°
γ/˚	90.000
Volume/Å^3	1379.4
Density/g.cm^{-3}	1.443
F(000)	624
Total Reflections	14679
Unique Reflections	3244
Goodness of fit	0.797
R index	0.0466

3.3 Conclusion

From data collected in this chapter, in particular sections 3.11, 3.12 and 3.16 it can be seen that thermal and spectral data can be used as a powerful tool in predicting the structure of aliphatic zinc carboxylates. Additionally it can be seen that preparation of a linear zinc carboxylate in aqueous medium does not guarantee inhibition of polymer formation and that even a little steric hindrance (*i.e.* zinc(II) isovaleroate) has a much larger impact on the final structure.

The structures of the carboxylates in this chapter show that zinc has a preference, like in proteins, to be coordinated in a tetrahedral environment with the only exception being zinc(II) formiate. This tetrahedral coordination is adopted by both polymeric (e.g. zinc(II) propionate) and monomeric (e.g. zinc(II) acetate and zinc(II) isovaleroate) carboxylate complexes.

The zinc carboxylates considered in this chapter enter a thermally stable phase prior to reaching the decomposition threshold and formation of zinc oxide. This stable area is larger for longer chain carboxylates with its onset earlier and the endpoint at a higher temperature as the carboxylate chain length increases. This is most easily visible when DSC thermograms of zinc(II) propionate, butanoate and pentanoate are inspected.

By use of powder diffraction accurate results for unit cell parameters of this series of compounds were obtained and a successful peak to peak match between a predicted powder diffraction pattern of a known structure (zinc(II) acetate) and a collected powder diffraction pattern brings to light the usefulness and effectiveness of this technique.

3.4 References

1. K. Györyova, V. Balek and K. Kovárová, *Thermochim. Acta* (1995), 425
2. B Ye, X Li, I. D Williams and X. Chen, *Inorg. Chem* (2002), **41,** 6426

3. L. Yuan, Z. Li, J. Sun and K. Zhang, *Spectrochim. Acta Part A* (2003), **59**, 2949

4. A. S. Lipton, M.D Smith, R.D Adams and P.D Ellis, *J. Am. Chem. Soc.* (2002),**124**, 410

5. T. Yokoyama and N. Yamagata, *Applied Catalysis A: General* (2001), **221**, 227

6. P. A. Spegt and A.E Skoulios, *Acta Crystallogr.*(1963), **16**, 301

7. Konkoly-Thege, I. Ruff, S.O Adeosun and S.J Sime, *Thermochim. Acta* (1978), **24**, 89

8. P. Baraldi, *Spectrochimica Acta* (1979), **35A**, 1003

9. K. Nakamoto, F. Fujita, S. Tanaka and M, Kobayashi, *J. Am. Chem. Soc.* (1957), **79**, 4904

10. A. S. Lipton, M.D Smith, R.D Adams and P.D Ellis, *J. Am. Chem. Soc.* (2002),**124**, 410

11. International Center for Powder Diffraction Data (ICDD)

12. E. Goldfish, Union Oil Company of California, *Private Communication*. (As reported in 2002 JCPDS data base)

13. T. Ishioka, Y. Shibata, M. Takahashi, I. Kanesaka, *Spectrochim. Acta, Part A: Mol. And Biomol. Spec.* (1998), **54A**, 1811

14. R. Shirley, *The CRYSFIRE System for Automatic Powder Indexing:* User's Manual (2000), The Lattice Press, 41 Guildford Park Avenue, Guildford, Surrey GU2 7NL, England.

15. D. M. Kerloub, *C. R Seances Acad. Sci.*(1967), **264**, 1753

16. T. Ishioka, A. Murata, Y.Kitagawa and K.T Nakamura, *Acta Crystallogr., Sect.C: Cryst Struct. Commun.* (1997), **53**,1029

17. K. N. Semenenko, *Khimiya i Kimicheskaya Teknologiya* (1958)*, **2**, 283

18. W. Clegg, I. R. Little and B. P. Straughan , *Acta Crystallogr., Sect.C: Cryst.Struct.Commun.* (1987) *,**43,**456

19. K. Györyova, V. Balek and K. Kovárová, *Thermochim. Acta* (1995), 425

20. V. V. Panevchik, V. M. Goryaev, *Khimiya i Khimicheskaya Teknologiya* (1980), **23**, 115

21. M. F Ramos Moita, M. T. S. Duarte and R. Fausto, *Spec. Lett.* (1994), **27**, 1421

22a. L. J. Barbour, *J. Supramol. Chem.* (2001), **1,** 189

22b. J. L. Atwood and L. J. Barbour, *Cryst. Growth Des.* (2003), **3**, 3

23. G. M. Sheldrick, SHELXL-97, Program for Crystal Structure Analysis, University of Göttingen, Germany, 1997

CHAPTER 4

YTTRIUM CARBOXYLATES

Yttria, an earth containing yttrium was discovered in 1794 by Gadolin. Yttrium can be found in nearly all rare earth minerals and lunar rocks brought back by the Apollo missions were also found to have very high concentrations of yttrium.

As a metal, yttrium has been used as a deoxidizer for non-ferrous metals such as vanadium and it has also been used as a catalyst for ethylene polymerisation. Yttrium can be added to alluminium and magnesium to form strong alloys.[1]

Recent uses of yttrium carboxylates include using yttrium acetate as well as yttrium isobutyrate in tetrahydrofuran as metalloorganic precursors in the process of creating aluminium garnet fibers.[2]

In many cases, yttrium complexes have been found to have structures isomorphous to similar complexes of dysprosium, erbium and lutetium.[3]

Two possible structures for yttrium(III) formiate were found in a search of the CCSD, one in its hydrated form and the other anhydrous. In both cases the structure contains a central yttrium atom with bridging formiate groups coordinated around it. For the hydrated compound, two water molecules coordinate to the metal center and six formiate units coordinate monodentately.[4,5]

The anhydrous form of yttrium formiate crystallises surrounded by 6 coordinated formiate units, but in this case the bridging carboxylate allows yttrium-yttrium bonds to form between the metal centers which they connect. These metal-metal bonds take up the coordination positions that were occupied by water molecules in the hydrated form.

When exploring known structures of yttrium carboxylates one of the first features noticed is the large amount of them that contain a Y-O-Y-O inner core. This core takes the shape of a parallelogram which brings two neighbouring yttrium atoms to within 4.2 Å of each other which is only 0.7 Å larger than the inter atomic distance in elemental yttrium. This metal-oxygen core seems to be favourable – or at least common - regardless of the organic part of the carboxylate ligand. In Fig. 4.1 two very different yttrium carboxylate complexes prepared by independent groups are presented to illustrate this fact.
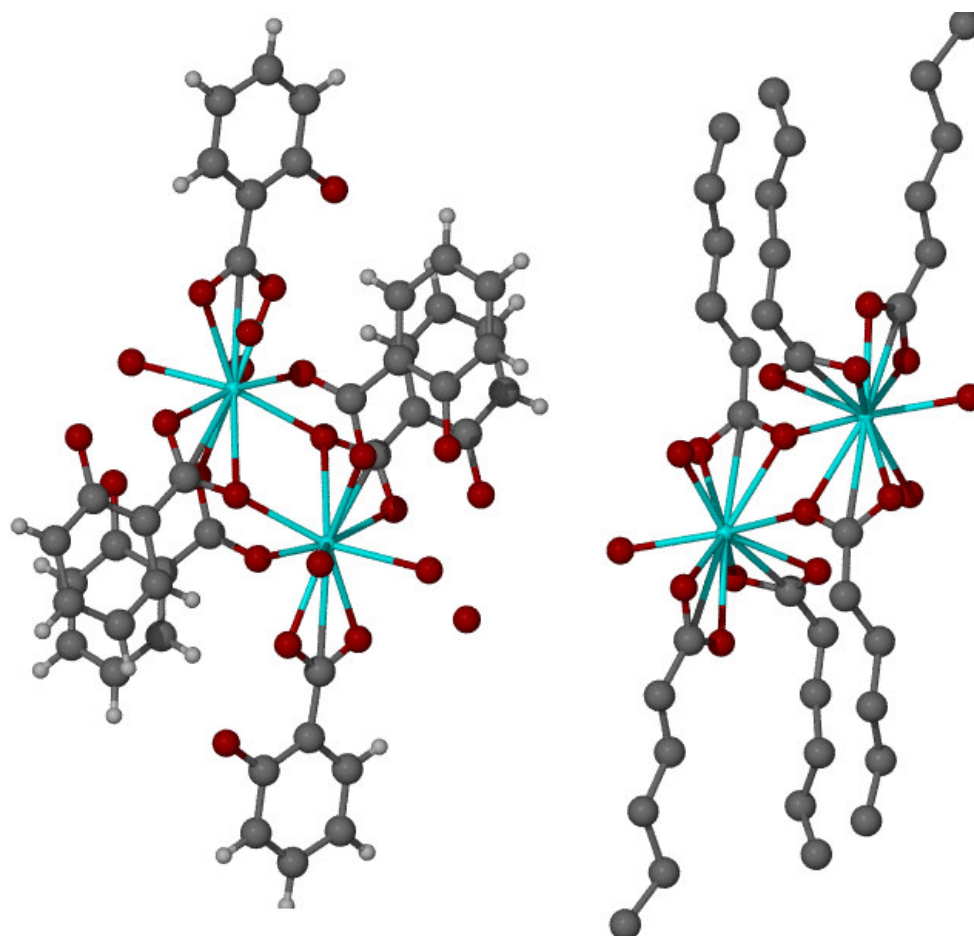

Fig. 4.1 *Yttrium salicylate and hexanoate, prepared by Ma* et al.[6] *and Delong* et al.[7] *respectively.*

In this chapter we devote ourselves to documenting the physical properties of the selected series of yttrium(III) carboxylates. We also propose a structure for a previously unknown yttrium complex using computational chemistry and confirm the energetically favoured dimensions of the internal Y-O-Y-O core. In addition to this, discrepancies and similarities that exist between the prepared compounds of differing carbon chain length are discussed.

4.1 Results and Discussion

4.11 Yttrium(III) Formiate

The anhydrous rare earth triformate, $Ln(CHOO)_3$, of yttrium has previously been prepared by direct reaction of the sesquioxides with aqueous formic acid. Its thermal decomposition was followed using thermogravimetry, high temperature X-ray diffraction and MS gas analysis. It was determined that the oxy carbonate, $Y_2O_2CO_3$ forms prior to decomposition to yttrium oxide.[8,9]

In the field of mineralogy, a review reporting the rhombohedral formiates of Y, Ho, Er showed that these formiates are isostructural. Other structures of formiate complexes included in this study were those of Gd and Tm.[10]

4.111 Synthesis

Carbon dioxide was released when yttrium(III) carbonate was dissolved in formic acid (equation 1) and when the solvent (water) had evaporated cubic yttrium(III) formiate crystals were formed. These crystals are very hygroscopic and undergo visible changes if left outside a dessicator.

$$Y_2(CO_3)_3.xH_2O \ + \ CHOOH \ \rightarrow \ Y(CHOO)_3 \ + \ CO_2 \ + \ H_2O \qquad \textbf{(1)}$$

83
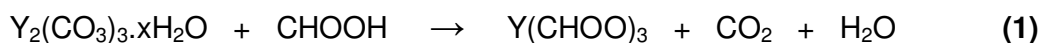
4.112 Infrared Spectroscopy

Inspection of the infrared spectrum (Fig. 4.1) of this compound shows the energy separation between the symmetric and asymmetric carboxylate stretching bands is 233 cm^{-1}. This value seems quite large where a bridging carboxylate mode is expected and is more indicative of the presence of monodentate carboxylate ligands. Previous reports of Cd-Ca and Cu-Sr formiates have, however, shown that a separation value of a similar size is observed even when the ligand bridges two metal centers.[11,12] Broad hydroxide bands at 3369 cm^{-1} and 3291 cm^{-1} due to coordinated and uncoordinated water in the molecule, are present.
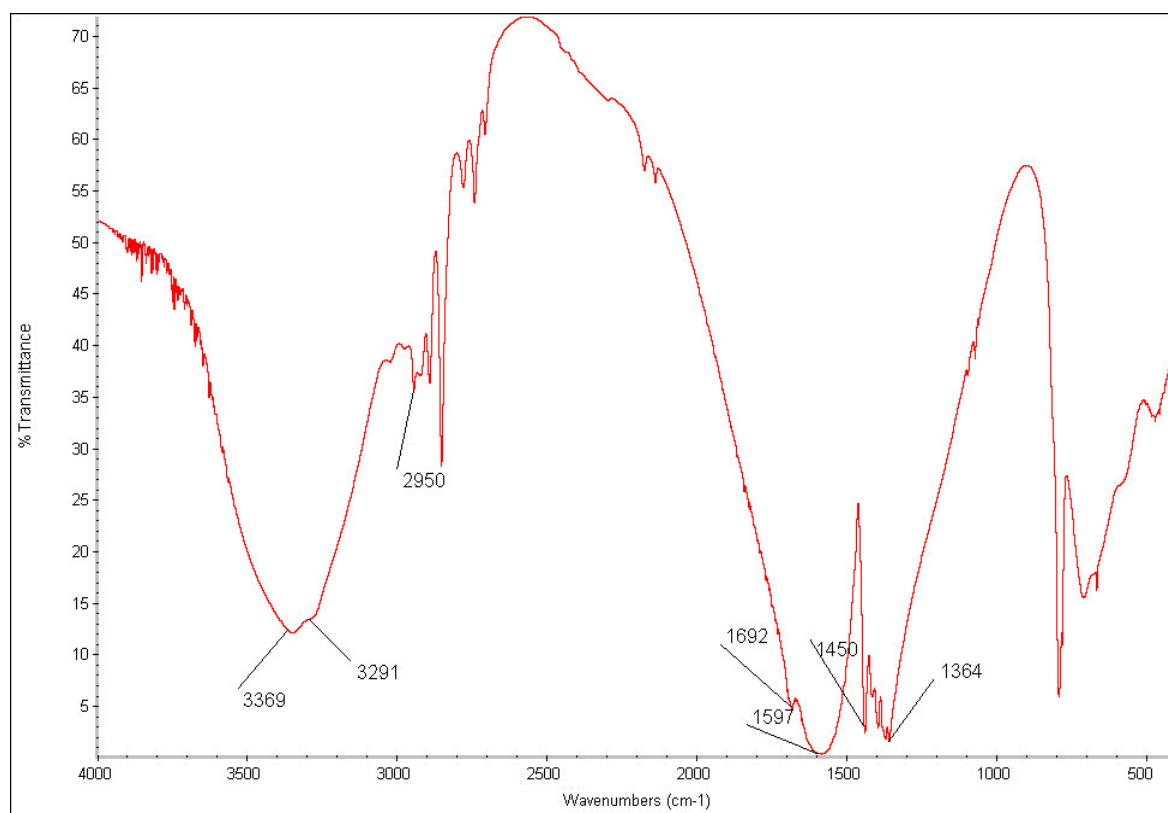

**Fig. 4.1** *Infrared spectrum of yttrium(III) formiate*

The spectrum shows a shoulder at 1692 cm^{-1}. This occurs at a high enough frequency to be excluded as the carbonyl stretch of a formic acid unit and is most probably due to some unreacted acid remaining in the structure. Table 4.1 contains a summary of infrared bands and their assignments.

84

Table 4.1 *Infrared assignments*

Band (cm^{-1})	Assignment
3356, 3291	-OH stretch
2945-2742	C-H stretching modes
1597	Assymetric CO_2^- stretch
1445	C-H bending modes
1364	Symmetric CO_2^- stretch

4.113 Thermal analysis

Analyses of the TGA (Fig. 4.2) and the DSC (Fig. 4.3) thermograms show a 10% mass decrease in the 118-137 °C range which is expected for the release of two water molecules from a dihydrated yttrium(III) formiate system.
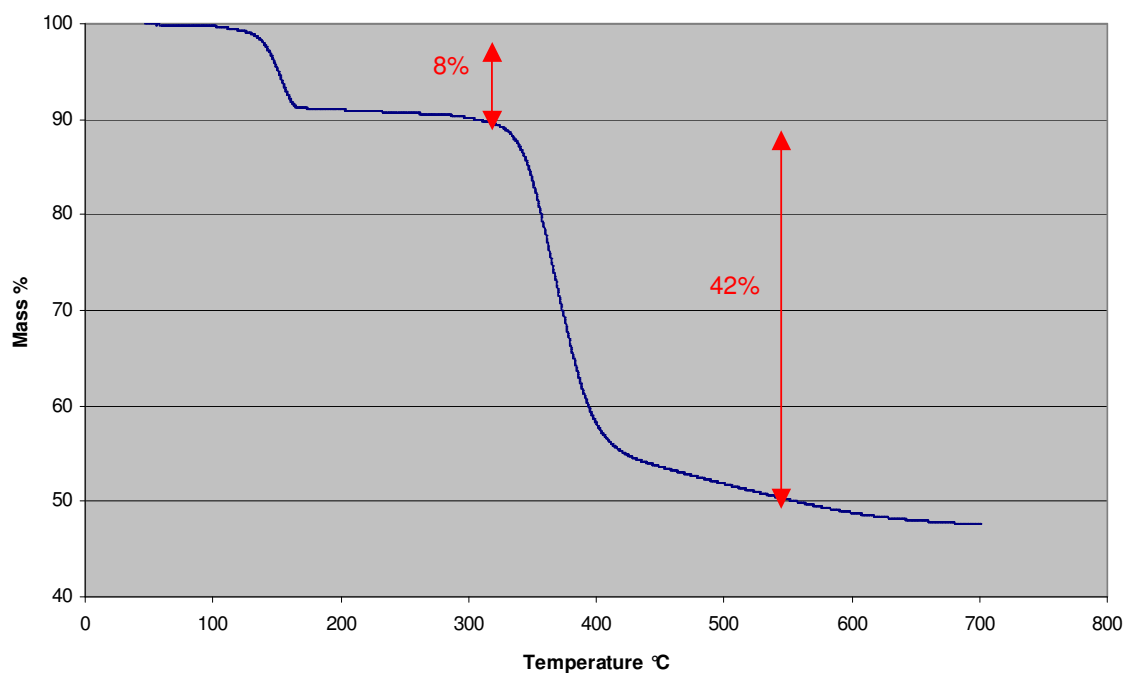
Fig 4.2 *TGA thermogram for yttrium(III) formiate*

85

Decomposition starts at 324 °C and three endothermal peaks are displayed even though only a single change of mass is observable; other mass losses may be obscured by the rapid formation of yttrium(III) oxide.

A stable mass remains after 500 °C, though the sloping line leaves the observer unsure of the mass percentage at decomposition. The DSC profile shows a constant slope throughout the heating run even after the formation of Y_2O_3, which could indicate that the change in heat capacity in this compound is only a function of temperature and not the ligating species.

Only 50% of the original mass is retained and this has been confirmed by ICP analysis to be Y_2O_3, according to the yttrium content. Back extrapolation reaffirms the empirical formula of $Y(CHOO)_3 \cdot 2H_2O$. Equation 2 summarises the thermal decomposition observed:
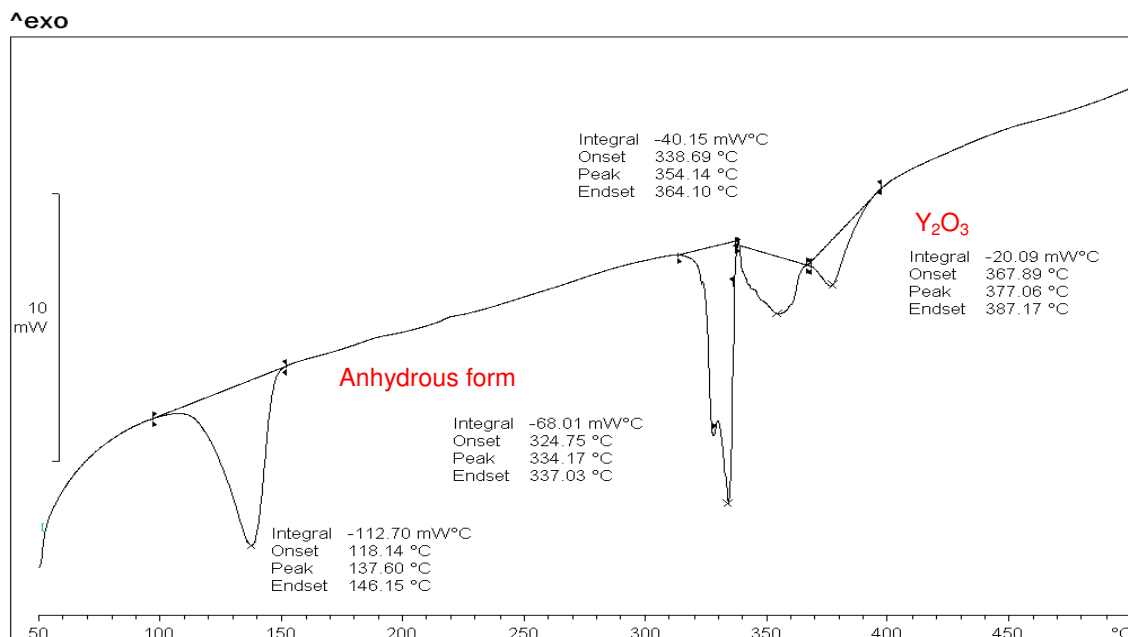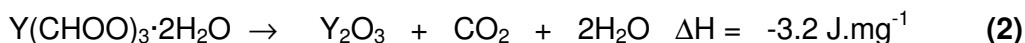
$$Y(CHOO)_3 \cdot 2H_2O \rightarrow Y_2O_3 + CO_2 + 2H_2O \quad \Delta H = -3.2 \text{ J.mg}^{-1} \qquad \textbf{(2)}$$

Fig 4.3 *DSC thermogram for 4.3 mg yttrium(III) formiate*

86

4.114 Crystallographic Data

Thermal and spectral analyses of our compound suggest a structure analogous to the structure - introduced in the introductory passages of this section - displayed in Fig. 4.14 and not the anhydrous form, also known for this compound, that Fig. 4.5 depicts.[4,5] This structure is also similar to the one described for *zinc(II)* formiate in chapter 3 (section 3.11), since both these compounds form network type polymers with metal centers bridged by carboxylate ions and some coordination sites taken up by water molecules.
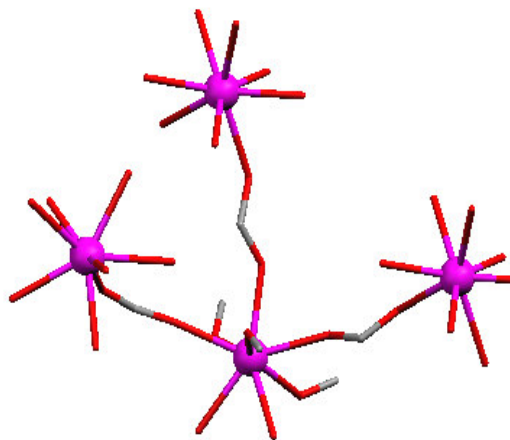

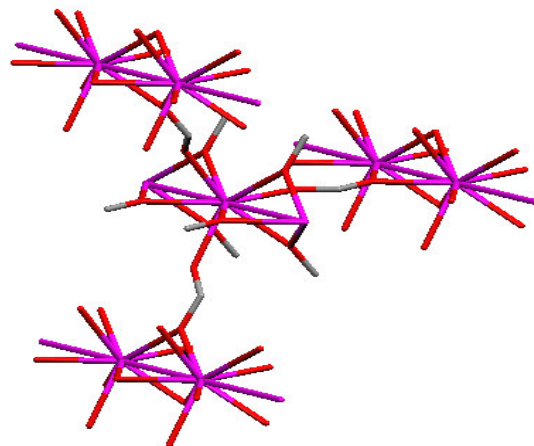**Fig. 4.4** *Hydrated yttrium(III) formiate[4]*

Fig 4.5 *Anhydrous yttrium(III) formiate[5]*

4.12 Yttrium(III) Acetate

4.121 Synthesis

Stoichiometric amounts of acetic acid and yttrium carbonate were used to facilitate this preparation (equation 3). Carbon dioxide was released as the carbonate came into contact with the acetic acid and was driven off by refluxing the reaction mixture. Crystals suitable for a single crystal structure

determination were obtained by evaporation of the acetic acid-water mixture over several days in an open atmosphere.

$$Y_2CO_3.xH_2O + 6CH_3COOH \rightarrow 2Y(CH_3COO)_3 + CO_2 + (x+1)H_2O \quad \textbf{(3)}$$
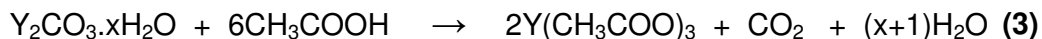
4.122 Infrared Spectroscopy

This spectrum (Fig. 4.6) clearly indicates the presence of hydrated solvent (water) molecules (3295 cm^{-1}) and also uncoordinated water (3175 cm^{-1}), as well as two different modes of carboxylate coordination (1698 cm^{-1}, 1549 cm^{-1}). However, it has been reported that some carboxylate complexes show a carbonyl satellite band around 1688 cm^{-1} due to overtones and combination bands.[14]
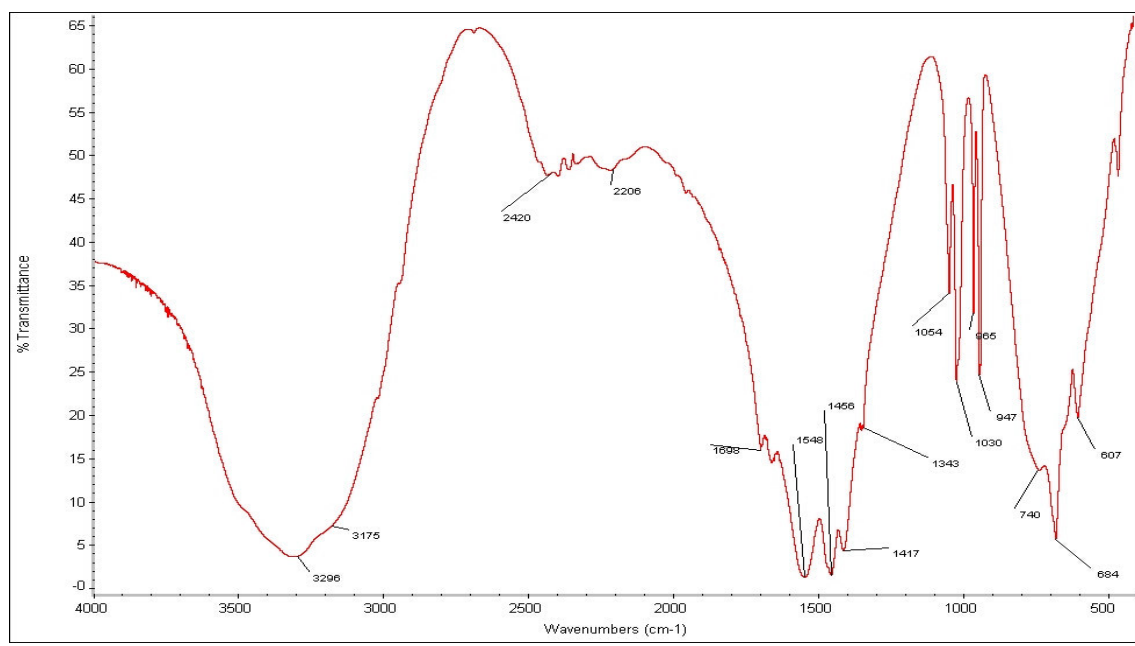

Fig. 4.6 *Infrared spectrum of yttrium(III) acetate*

It has been shown that the mode of coordination of a carboxylate unit can accurately be identified using the energy difference between its symmetric and asymmetric stretching vibrations.[11]

When calculating the energy separation between the symmetric and asymmetric stretching vibrations of this compound, only the bridging mode can be identified (with an energy difference of 206 cm^{-1}) taking into consideration that the symmetric RCO_2^- stretching frequency is not easily identifiable. Table 4.2 consists of a list of infrared absorptions and their assignments, observed for this compound.

Table 4.2 *Infrared stretching frequencies for yttrium(III) acetate*

Band (cm^{-1})	Assignment
3295, 3175	–OH stretches
2428	CO_2 remaining after purging
1698	Carboxylic acid carbonyl stretch
1549	Asymmetric RCO_2^- stretch
1455	Aliphatic bending bands
1343	Symmetric RCO_2^- stretch
1054	Carbon oxygen stretching bands, as well as C-C deformation bands are found in this region

4.123 Thermal Analysis

Thermogravimetric studies show only a marginal mass loss at 100 ˚C (Fig. 4.7) even though a series of broad endothermic events take place in this region (Fig. 4.8). By changing the temperature program to reverse after each observed peak, it was concluded that these endotherms are irreversible processes. Only 65.8% of the original mass remains after the endotherm at 373 ˚C (verified by manual measurements), which is a strong indication of yttrium oxide as decompositional product.

Hussein[15] suggested that upon decomposition a mixture of yttrium oxide and yttrium carbonate remains present below 500 ˚C and only above 600 ˚C all carbonate is converted to oxide. Our gravimetric studies show no evidence of

a carbonate intermediate and only the oxide seems present after yttrium acetate is heated beyond 450 ˚C. Physical mass losses prevent the final value available from the TGA thermogram to be used for interpretation and the value we used was calculated from weighing the DSC sample holder after a thermal sequence was completed.
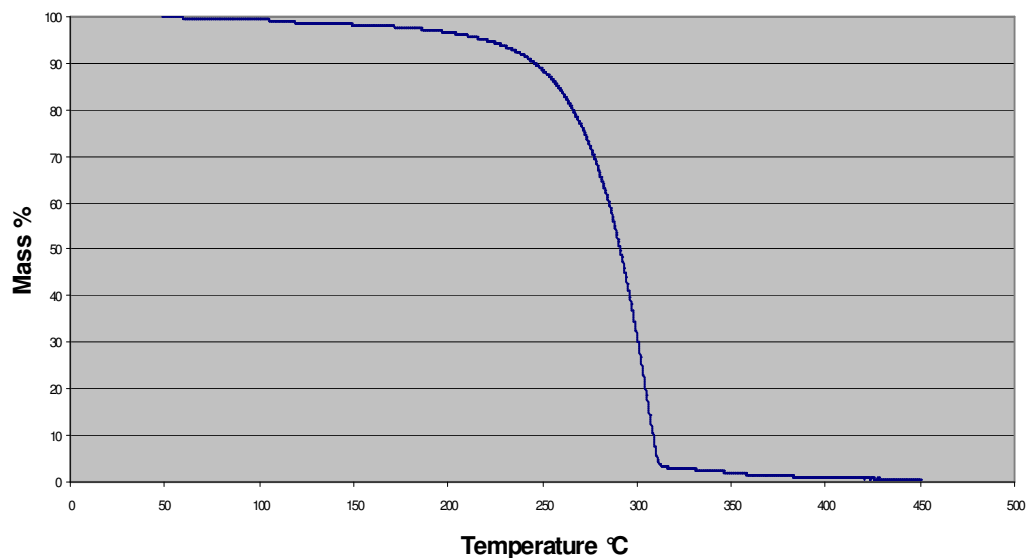

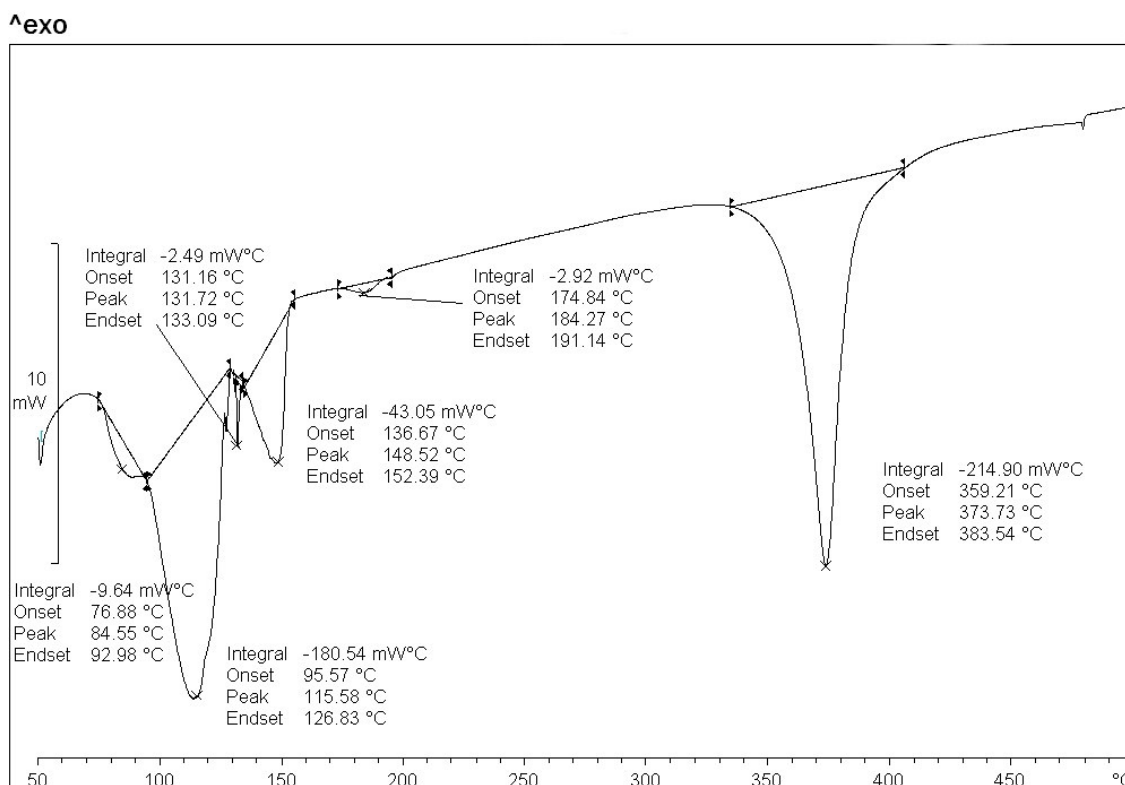**Fig. 4.7** *TGA thermogram for yttrium acetate*

Fig. 4.8 *DSC thermogram for 4.41 mg of yttrium acetate*

The DSC thermogram also shows a remarkably stable baseline, which indicates that heat capacity of the compound retains a constant value throughout decomposition, suggesting that heat capacity of this compound is independent of the coordinating carboxylate group. The following equation (equation 4) summarises the thermal decomposition of this compound, with enthalphy values obtained from DSC data:

$$2Y(CH_3COO) \cdot 4H_2O \quad \rightarrow \quad Y_2O_3 \quad \Delta H = -6.62 \text{ J. mg}^{-1} \quad \textbf{(4)}$$

4.124 Crystallographic data

Previous workers have reported this structure with an R index of 4.6 %,[13] and we now report a data collection and refinement of a structure which shows an improvement to 2.4%. The crystals obtained as described in the experimental section were white and semi transparent and had a cubic white appearance.

91

Figure 4.9 shows that yttrium(III) acetate forms a dimeric unit between two yttrium acetate molecules. This is a structure type that has also been reported for longer chain yttrium(III) carboxylates, specifically the hexanoate analogue.[4]
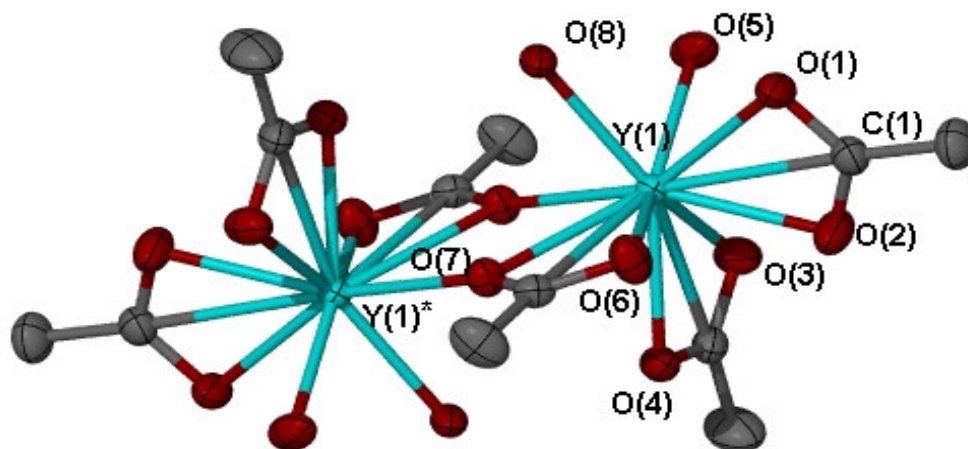

Fig. 4.9 *Dimeric structure of yttrium(III) acetate*

It is noticeable that the yttrium-yttrium distance remains relatively constant (4.16 Å, for both acetate and hexanoate) when comparing shorter and longer chain yttrium carboxylate dimers, suggesting that carboxylate chain length has little or no effect upon it. This distance between yttrium atoms in the complex is 0.60 Å greater than in elemental yttrium.

 The carboxylate group coordinates in a η^3-fashion, with the carboxylate angle (O-C-O), remaining almost undisturbed (0.60 ° difference, see Table 4.3) whether the carboxylate shares an oxygen or not. Two types of water molecules are present in the structure, one pair is coordinated another is uncoordinated to the central metal (displayed in Fig. 4.10). An yttrium-carbon distance of 2.892(2) Å indicates enough metal – carbon interaction to be considered a bond. Previous reports of yttrium-carbon bonding distances include values of up to 2.92 Á.[13]
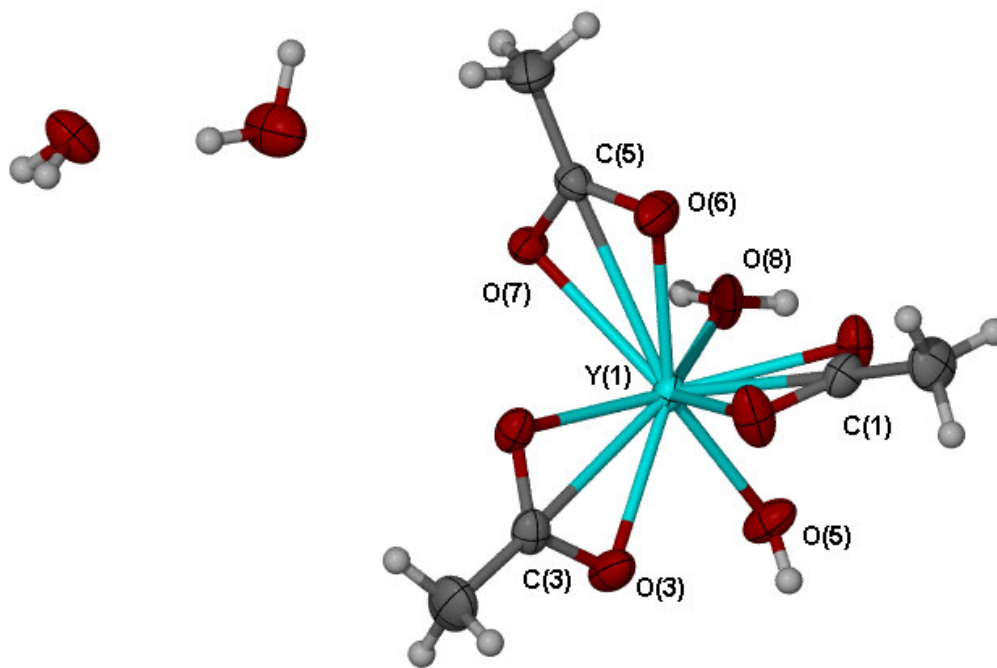
Fig. 4.10 *Single yttrium(III) acetate unit, showing enclatherated water*

In this dimeric form there are two types of chelating carboxylates. One type is coordinated to only one yttrium atom (Y(1)), while the other shares an oxygen with the neighbouring yttrium atom (Y(1)*)).

Table 4.3 *Selected angles, bond lengths and inter atom distances*

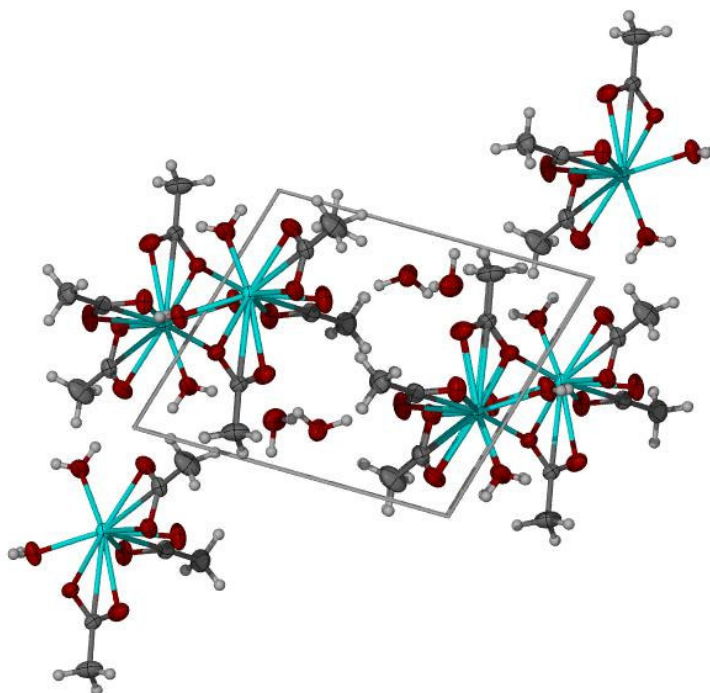| Distances (Å)		Angles (°)	
Y(1)…Y(1)*	4.16	Y(1)-O(7)-Y(1)*	115.84 (5)
Y(1)-O(2)	2.381 (2)	O(7)-Y(1)-O(7)*	64.16 (5)
Y(1)-O(3)	2.450 (2)	O(1)-C(1)-O(2)	118.95 (2)
Y(1)-O(6)	2.424 (2)	O(6)-C(1)-O(7)	118.31 (2)
Y(1)-O(7)	2.351 (1)		
Y(1)*-O(7)	2.351 (1)		
Y(1)-C(5)	2.892 (2)		

93

Fig. 4.11 *Crystal packing of yttrium(III) acetate as viewed along the a axis*

It is quite interesting to note that the distance between the oxygen and the neighboring yttrium (O(7)-Y(1)*) atom is exactly the same as the distance between the chelating oxygen and yttrium atom (O(7)-Y(1)), which makes the oxygen tri-valent. The packing diagram (Fig. 4.11) shows that only dimerisation takes place and polymerisation does not occur.

4.13 Yttrium(III) Propionate

4.131 Synthesis

Several different approaches were followed in the preparation of this compound in order to obtain a product suitable for single crystal diffraction. Reacting yttrium carbonate with the corresponding acid, as with the earlier carboxylates was the first method used (equation 5):

$$Y_2(CO_3)_3 \cdot xH_2O + 6CH_3CH_2COOH \rightarrow 2Y(CH_3CH_2COO)_3 + CO_2(g) + H_2O \quad \textbf{(5)}$$
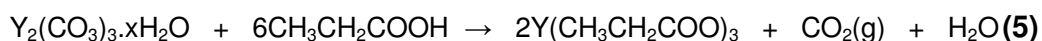
The sol-gel method was also attempted to obtain a suitable crystalline product. It has been reported that neutralizing nitric acid with ammonium hydroxide in a solution containing Y^{3+} ions and acetic acid produces a gel and allows growth of yttrium acetate over a period of two days.[14]

When this was attempted with propionic acid, however, gelation did not occur and the liquid solution produced crystals similar (but overgrown) in nature to those obtained with the earlier aqueous methods.

Once precipitated, the product only dissolved again in water upon prolonged and vigorous shaking.

4.132 Infrared Spectroscopy

Two distinct –OH stretches are observed here (see Fig. 4.12) and these are indicative of both coordinated and uncoordinated solvent water molecules contained in the compound. The calculated frequenct difference between the symmetric and asymmetric stretch of the carboxylate group is 172 cm^{-1} and according to Nakomto *et al.*[11] the ligand therefore most likely bridges two metal atoms.

Table 4.4 *Infrared band assignments*

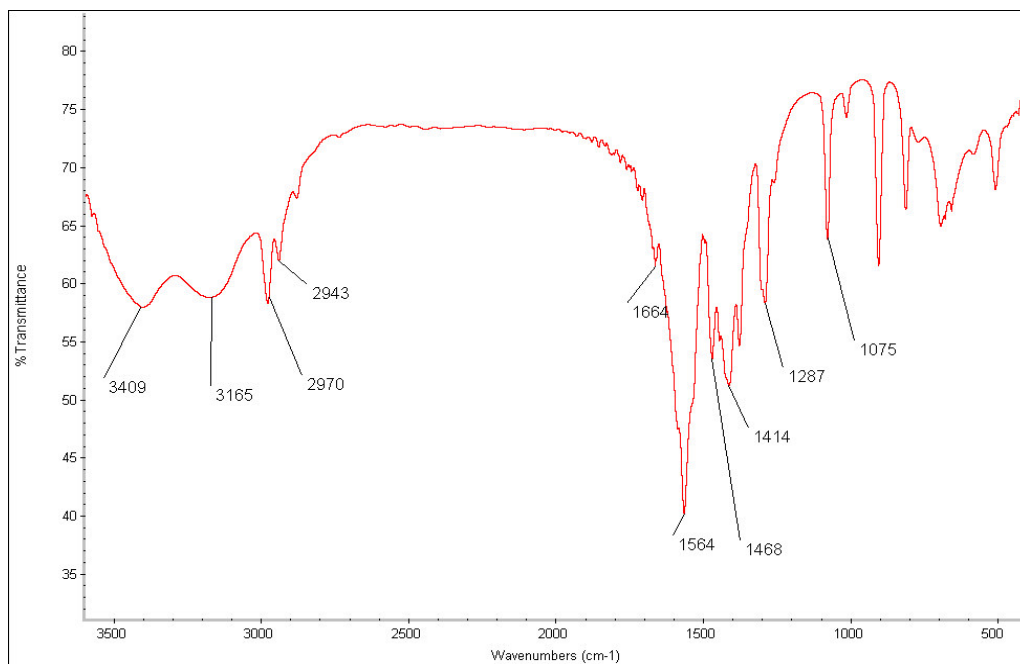| Band (cm^{-1})	Assignment
3429, 3155	Hydroxide absorptions
2970-2959	CH_3, CH_2 stretching frequencies
1551	Asymmetric carboxylate stretch
1448	Aliphatic bands
1372	Symmetric carboxylate stretch
1075	C-O stretches

Fig 4.12 *Infrared spectrum of yttrium(III) propionate*

4.133 Thermal Analysis

Mass losses observed using thermogravimetry (Fig. 4.13) correlate well to endotherms observed on the DSC plot in Fig. 4.14. The slight shoulder on the first endotherm indicates the stepwise release of water from the compound. This suggests that, like yttrium(III) acetate, two different types of water molecules exist in the structure.

The empirical weight of yttrium(III) propionate monohydrate is 326 and accordingly the initial mass loss of 6% shows the evaporation of the single molecule of coordinated water.
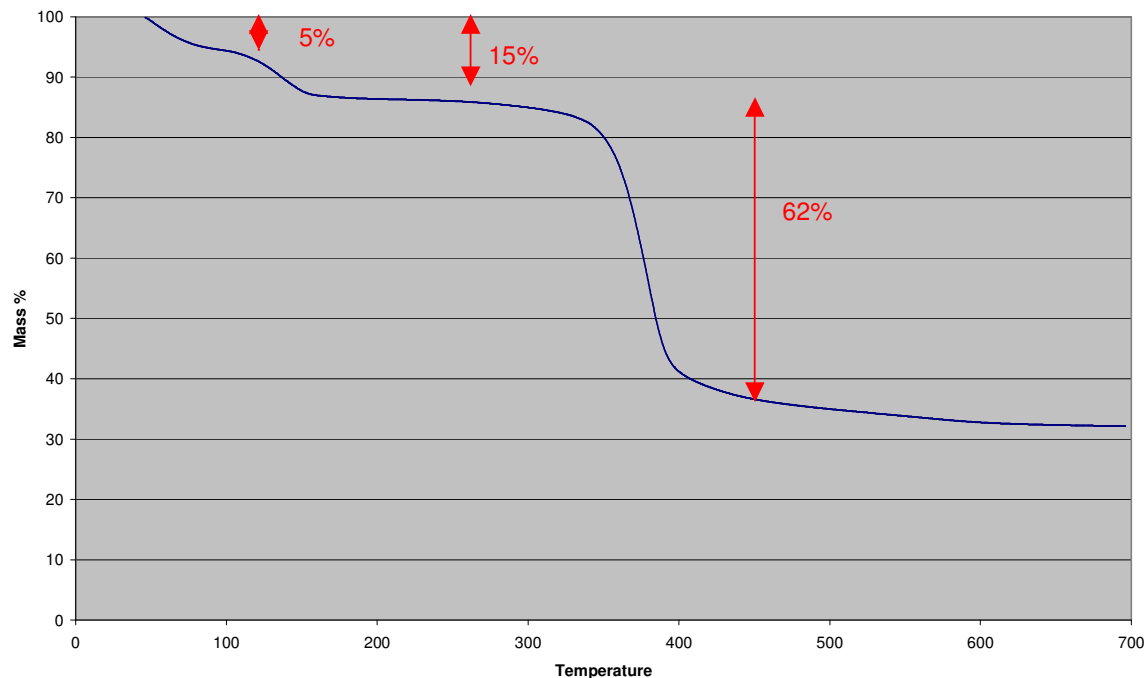
Fig. 4.13 *TGA thermogram of yttrium(III) propionate*

The onset of decomposition occurs at 320 ˚C and continues to just below 400 ˚C after which a stable mass is maintained. From gravimetric calculations the thermal decomposition product of the compound was to be yttrium oxide. The next equation shows the thermal decomposition of yttrium propionate as well as enthalpy data obtained from calorimetric studies:

$Y(CH_3CH_2COO)_3 \rightarrow Y_2O_3 +$ by products $\Delta H = -4.03$ J.mg^{-1} **(6)**

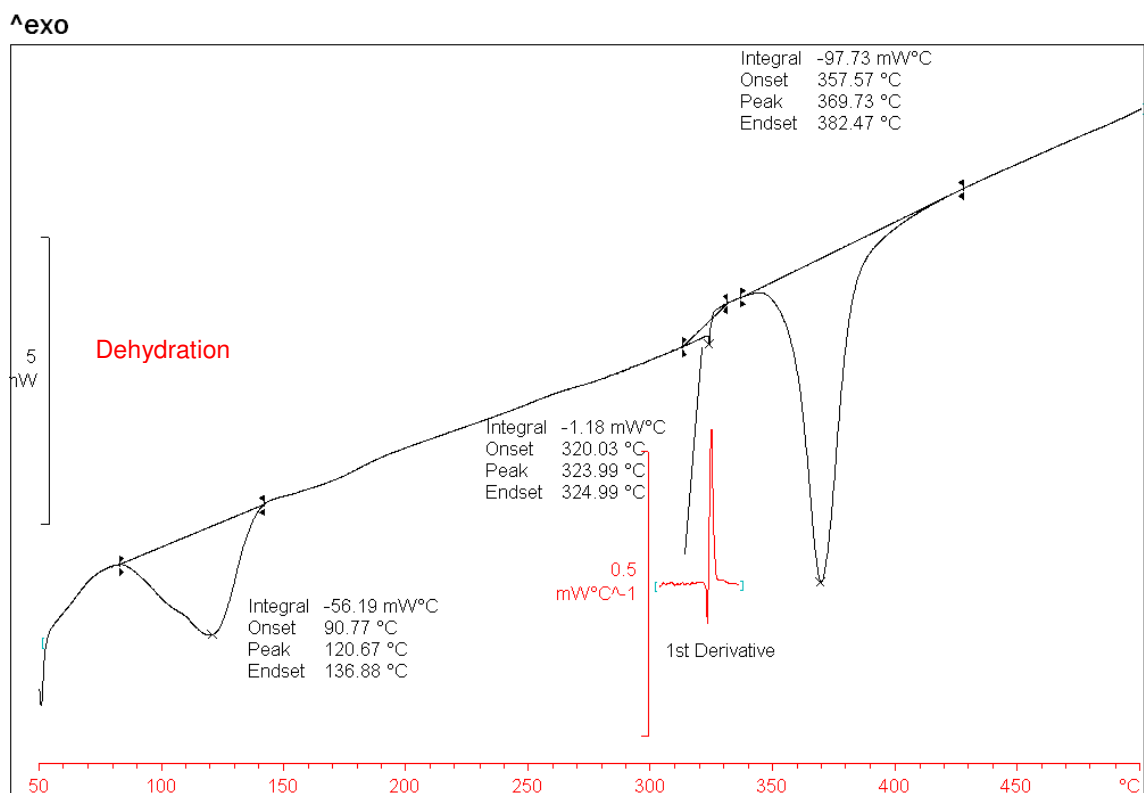**Fig 4.14** *DSC thermogram for 2.31 mg yttrium(III) propionate*

4.135 Powder Diffraction

Figure 4.15 shows the collected diffraction pattern for the compound with the vertical grey bars indicating literature matches with previously recorded patterns for yttrium propionate. At least 20 lines are matched and the compound can, therefore, now be unambiguously identified as hydrated yttrium(III) propionate.[17]
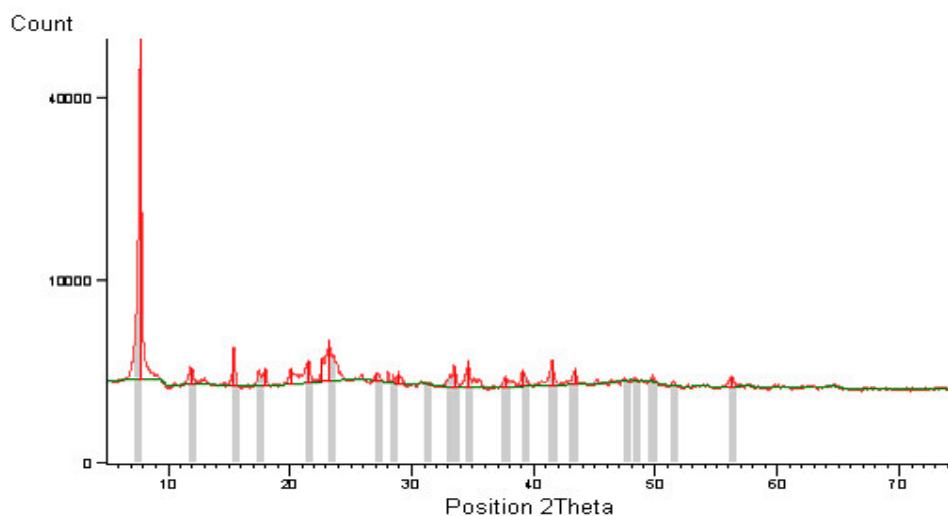
Fig 4.15 *Powder diffraction pattern and match for yttrium(III)*
propionate

Table 4.5 *Indexing data for yttrium(III) propionate*

Merit	Prog	Volume	a	b	c	alpha	beta	gamma
7	TR	718.66	7.89	8.33	11.63	93.77	99.24	106.55
7	TR	835.94	4.43	11.96	16.50	107.12	90.00	90.00
7	TR	835.94	4.43	11.96	16.50	107.12	90.00	90.00
7	TR	783.94	6.98	9.79	11.51	90.00	90.00	94.80
7	TR	810.14	5.90	11.69	12.02	102.32	90.00	90.00
7	TR	810.10	5.90	11.69	12.02	102.32	90.00	90.00
8	TR	720.67	7.87	8.36	11.65	93.88	99.44	106.20
10	TR	529.72	5.73	8.27	11.90	74.34	88.86	77.42
12	TR	885.07	4.80	8.06	22.92	94.06	90.00	90.00
15	TR	500.81	5.94	7.66	11.44	83.80	82.77	76.52

The pattern was indexed using the Crysfire[18] software package with Table 4.5
containing crystallographic data resulting from indexing and sorted according
to figures of merit, as defined by each indexing program used.

99

Twenty lines had accepted d-spacings and between 16 and 18 were successfully indexed for the given programs. The most favourable result (figure of merit 15, with 18 indexed lines) was obtained using the TREOR algorithm, which considers all symmetries when searching and indicates a triclinic structure and unit cell volume of 500.813 Å^3.

4.136 Computational Studies

Since no specimen suitable for single crystal diffraction could be crystallised we considered the computational alternative.

Noting the similarities between, the C2 and C6 yttrium(III) carboxylates, a closer inspection was made. Although these compounds crystallise in different space groups, the internal yttrium-oxygen core seems to form a parallelogram with very distinct measurements.

We then investigated if the length of the organic part of the carboxylate group, had any effect on the yttrium complex inner core.

A series of computational studies were run with Gaussian[18] - a computational software package - on yttrium aliphatic carboxylates considering both solvated and unsolvated metal centers. DFT calculations were completed on B-LYP level theory with frozen core yttrium atoms (LANL2dZ on Y). The results that follow allow the statement that the carbon chain length of the carboxylate group has little or no effect on a dimeric yttrium core. This statement is supported by data reported for known crystal structures.

While the only known modes of crystallisation for yttrium(III) formiate are those reported earlier in this chapter, this is not relevant to the current situation since data to be collected is limited to the effect of aliphatic carbon chain length on the central structure. Data to be collected by calculation are directed towards the extrapolation of a likely structure for yttrium(III) propionate.

Figure 4.16 shows the result for modelling an unsolvated yttrium(III) formiate (molecule A) dimeric molecule. The job took 32 minutes and 8 seconds of CPU time on a cluster of Pentium 4 computers working on a Linux platform to run to completion.
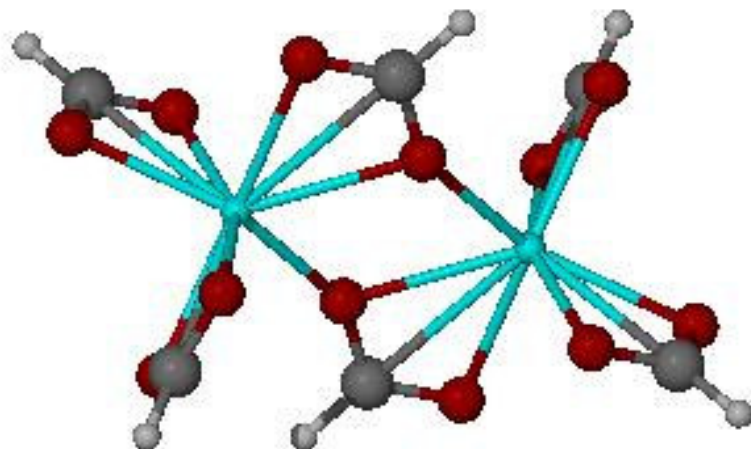

Fig. 4.16 *(A):* Yttrium(III) formiate from dimeric modelling

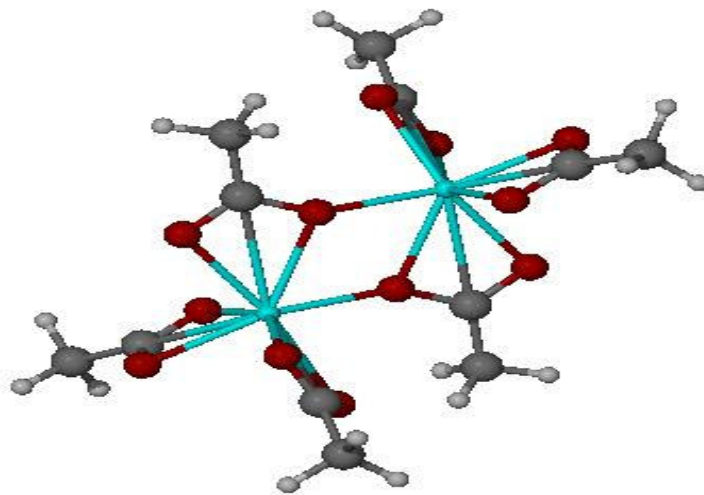Figure 4.17 shows the result for modelling the yttrium(III) acetate dimeric unit (molecule B).

Fig. 4.17 *(B):* Unsolvated yttrium(III) acetate from dimeric modelling
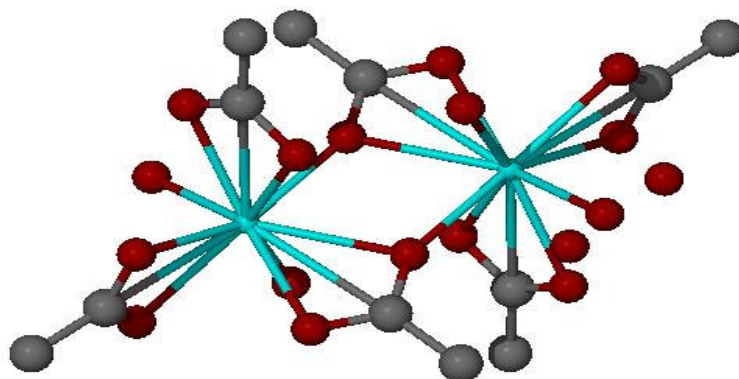
Fig. 4.18 (**C**): *Molecular structure yttrium acetate*

The collected crystal structure for yttrium(III) acetate (molecule C) is shown in Fig. 4.18 as has been reported earlier in this chapter. The similarities between this and the modelled compounds are obvious at first glance and comparison of angles and bond lengths (Table 4.6) is sufficient proof for the accuracy of the model.

Table 4.6 *Crystallographic comparison between known, collected and modelled compounds*

Molecule	Y-O-Y (°)	Y-O-C (°)	Y-Y (Å)	Spacegroup
A	112.67	91.53,90.5	3.980	Modelled
B	112.23	93 ,91.5	3.947	Modelled
C	115.83	92,94	4.164	P-1
D	114.02	94.1,94.5	4.087	P21/a

While no crystalline form of yttrium(III) pentanoate is known (and was not successfully obtained during the course of this project) yttrium(III) hexanoate[4] (molecule D) shows a similar structure to the molecules listed above even though crystallisation occurs in a different space group.

The powder diffraction studies carried out in section 4.32 suggest unit cell volumes between 500 and 800 cubic angstroms with most results lying in the 700 $Å^3$ region. This compares extremely well with the unit cell volume (660 $Å^3$) for the collected yttrium(III) acetate structure.

Taking into consideration all above mentioned data and experimental conditions for preparation of the compound the structure corresponding to Fig. 4.19 is proposed with Y-O bonds and O-C bonds not defined and inter atomic distances and bond angles similar to those listed in Table 4.6. The model represented in Fig. 4.19 was drawn and geometry optimisation achieved using ArgusLab 4.[20]
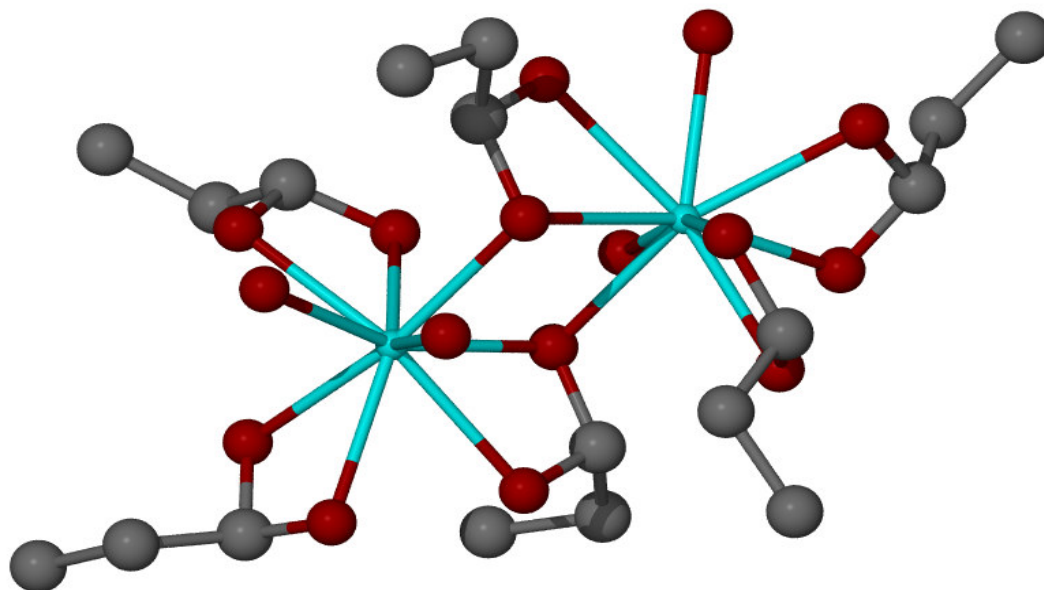

Fig 4.19 *Proposed structure for yttrium(III) propionate*

4.14 Yttrium(III) Butanoate

To date, very little analytical data has been published on the butyrate salt of yttrium with only a few passing references citing it as part of a larger study.

103

4.141 Synthesis

The acid base reaction between yttrium carbonate and butyric acid, forms a clear solution that precipitates to leave yttrium(III) butanoate. (equation 7)

$6CH_3CH_2CH_2COOH + Y_2CO_3 \rightarrow 2Y(CH_3(CH_2)_2COO)_3 + CO_2\uparrow + H_2O$
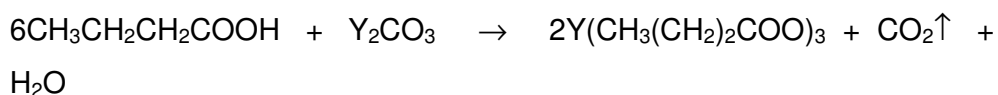
(7)

The resultant white powder seemed crystalline when viewed under a microscope and was weakly soluble in both ethanol and water after many hours of vigorous stirring and shaking. The compound didn't dissolve in any of the other organic solvents used. When the reaction was repeated using ethanol as solvent, only a non-crystalline product could be obtained.

4.142 Infrared Spectroscopy

The infrared spectrum of yttrium(III) butanoate is shown in Fig. 4.20. In this spectrum a hydration band is visible at 3421 cm^{-1}. The symmetric and asymmetric bends of the aliphatic chains appear next followed by the strong carboxylate carbonyl absorption at 1554 cm^{-1}.
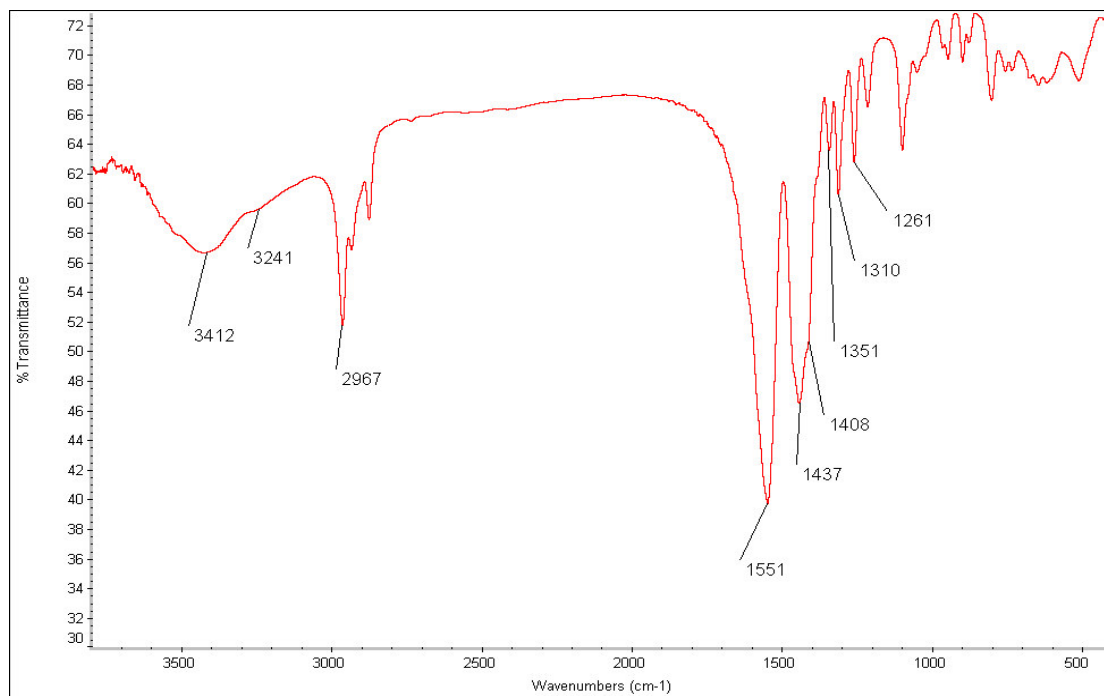

Fig. 4.20 *Infrared spectrum of yttrium(III) butanoate*

From the rules laid down by Nakamoto[9] and the difference in symmetric-asymmetric carboxylate stretching frequencies (143 cm^{-1}), a carboxylate bonding mode cannot be unambiguously identified, even though a bridging bonding mode seems most likely. A slight shoulder on the carbonyl band, in combination with the shoulder at 3241 cm^{-1} supports the suggested presence of water of crystallisation. An assigned list of absorption bands is compiled in Table 4.7.

Table 4.7 *Infrared band assignment for yttrium(III) butanoate*

Band (cm^{-1})	Assignment
3421, 3252	-OH stretches
2967-2872	CH$_2$, CH$_3$ symmetric and asymmetric stretching frequencies.
1554	Asymmetric carboxylate stretch
1442	Aliphatic bending bands
1351	Symmetric carboxylate stretch
1100	C-O bands

4.143 Thermal Analysis

Thermal analysis (TGA in Fig. 4.21 and DSC in Fig. 4.21) shows that all solvated molecules (water and organic solvents used) dissipate around 100 ˚C, due to the small percentage (<4%) it takes up of the total mass, this can be attributed to "wetness" of the sample and these solvent molecules should not be considered as part of the compound.

While the shape of the DSC (Fig. 4.22) occurrence at 200˚C is achingly similar to what happens when the temperature program is disrupted, repeated studies show that this artifact persists and first derivatives calculated in this area (Fig 4.23) show that two thermal events do take place in this region.
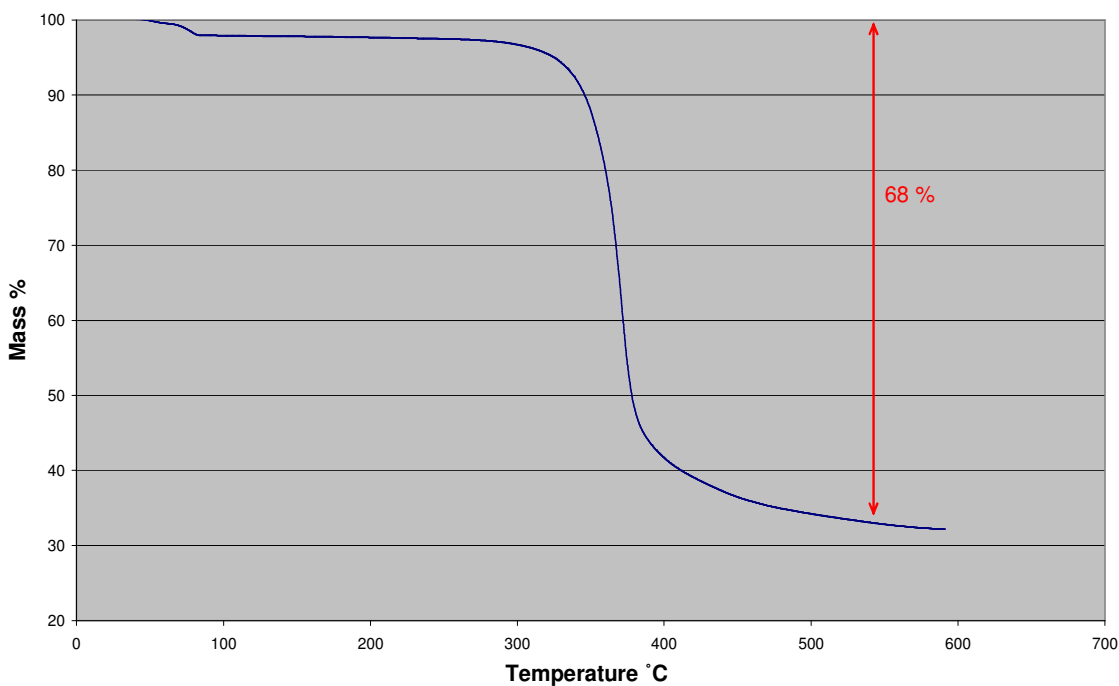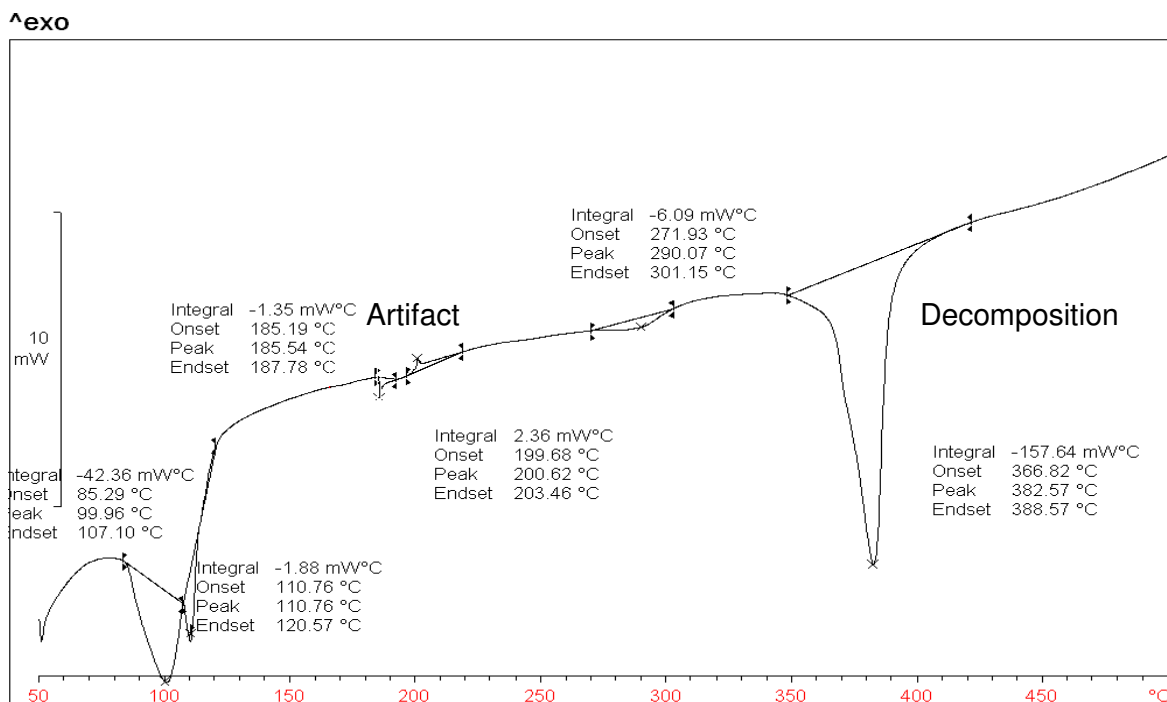
Fig. 4.21 *TGA thermogram for yttrium(III) butanoate*

Fig 4.22 *DSC thermogram for 4.48 mg yttrium(III) butanoate*

A slight endotherm at 300˚C does not correspond to any measurable mass loss. This is most likely a phase shift from crystalline to amorphous material this, however, has not been confirmed.
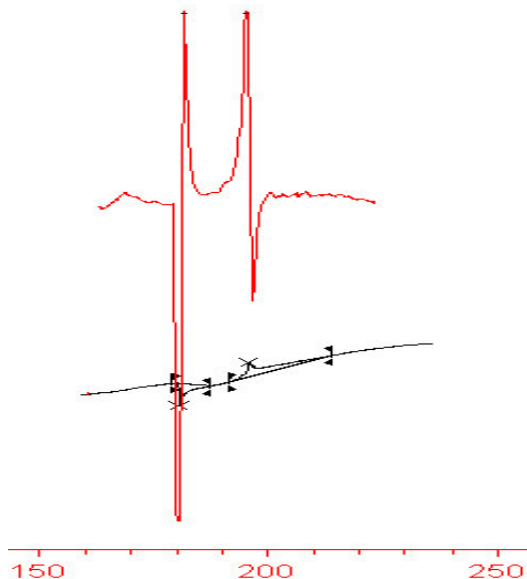

At 380 ˚C decomposition takes place as indicated by an intense endotherm on the DSC and 68 % mass loss on the TGA. The final mass percentage confirms the formation of yttrium(III) oxide when the compound is heated above 400 ˚C.

Fig 4.23 *First derivative and expansion over artifact region*

4.145 Powder diffraction

The powder pattern (Fig. 4.24) of the compound has been collected on a Phillips PW 1710 diffractometer with the collection program described in section 4.28. No match for this pattern was found in the database, which confirms that, up to date this pattern has not been collected and indicates a high probability of a unique compound.

The indexing data (Table 3.8) shows the most favourable indexing results (sorted according to figure of merit) for the compound, it should be noted that the unit cell volume for the most likely solution (figure of merit 21) is roughly 4 times greater than the propionate analogue discussed earlier.
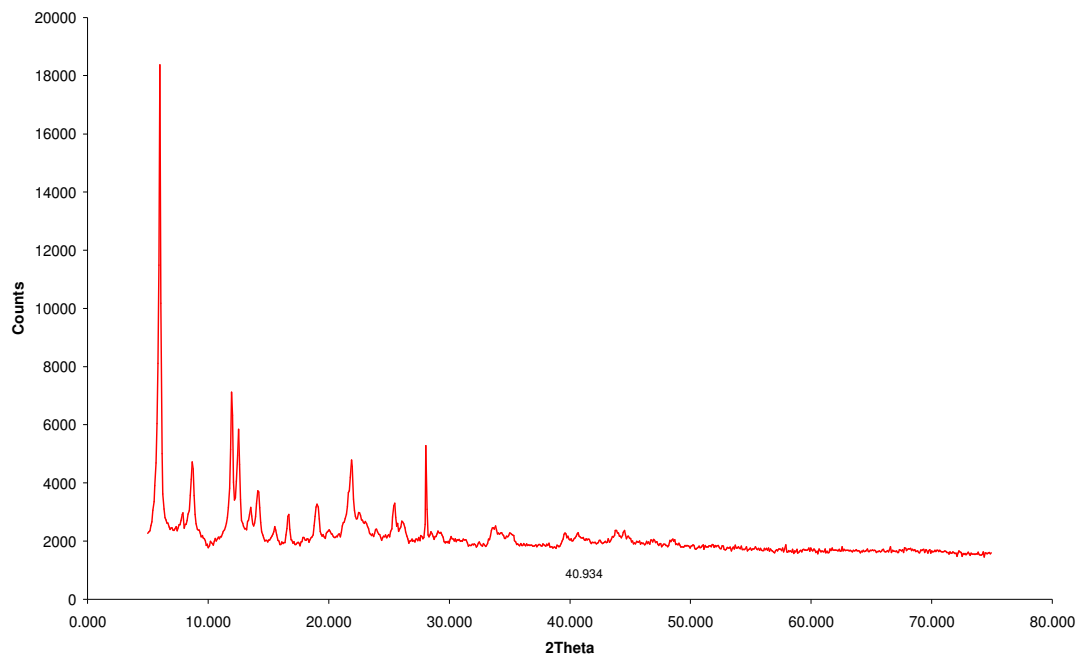
Fig. 4.24 *Powder diffraction pattern for yttrium(III) butanoate*

Table 4.8 *Indexing data for yttrium(III) butanoate sorted according to figures of merit*

| Merit	Prog	Volume	a	b	c	alpha	beta	gamma
10	TR	1292.052	6.201	14.045	14.836	90	90	90
10	TR	1292.052	6.201	14.045	14.836	90	90	90
10.6	DV	1686.792	8.191	13.948	14.798	90	93.828	90
10.6	DV	1686.785	8.191	13.948	14.797	90	93.828	90
10.6	DV	1686.776	8.191	13.948	14.797	90	93.828	90
11	TR	3843.788	14.886	16.069	16.069	90	90	90
11.5	DV	1821.831	8.867	13.969	14.955	90	100.395	90
11.5	DV	1821.831	8.867	13.969	14.955	90	100.395	90
16	TR	2089.022	6.837	15.036	20.321	90	90	90
21	TR	2070.858	6.849	14.892	20.305	90	90	90
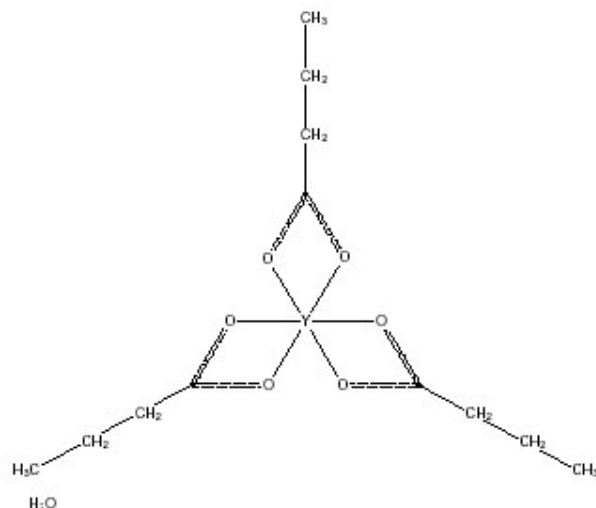
Fig. 4.25 *Molecular structure diagram of yttrium(III) butanoate.*[21]

Previously this compound has been prepared and reported not to have a dimeric structure. This compound is different from earlier carboxylates since despite having only a solvated monomeric unit in the unit cell, the volume that the unit cell encompasses is much greater than for dimeric units of shorter *and* longer chain analogues (acetate, hexanoate). No three dimensional data were available for this compound which excluded the possibility of a peak for peak match. On the basis of unit cell data, however, powder diffraction studies confirm that our prepared compound has the same structure as that reported for monomeric yttrium(III) butanoate displayed in Fig. 4.25.[21]

4.2 Experimental

All reagents were purchased from Sigma Aldrich with purities greater than 98% and used without further purification unless stated otherwise. Liquid reagents were weighed directly into the reaction vessel. To calculate mole quantities of $Y_2(CO_3)_3.xH_2O$, the molecular weight supplied by Sigma Aldrich (who supplied the compound) was used.

4.21 Preparation of Yttrium(III) Formiate

To provide the cation, 0.47 g (1.3 mmol) of $Y_2(CO_3)_3 \cdot xH_2O$ was used and reacted with 0.30g (7.9 mmol) of formic acid. A 0.2 ml formic acid excess was added.

The carbonate salt dissolves quickly in a 1M aqueous formic acid solution and to drive off any excess resulting carbon dioxide, the mixture was left to reflux for an hour to an open atmosphere. A powdery white precipitate was formed after roto vaporization and drying over night in an oven at 60˚C. Crystals suitable for single crystal diffraction appear in a dilute aqueous solution if the solvent is left to evaporate at room temperature. The reaction afforded a 92% yield upon repetition.

4.22 Preparation of Yttrium(III) Acetate

A 1.5 M aqueous solution of acetic acid (0.79 g, 2.2 mmol) was prepared and used to dissolve the yttrium carbonate(0.75 g, 13.3 mmol) salt, the reaction mixture was brought to reflux in an open atmosphere and all resulting CO_2 was driven off. The reaction mixture was evaporated at room temperature under vacuum to form a crystalline white precipitate. This precipitate proved soluble in water as well as ethanol and crystals suitable for single crystal diffraction were grown over a five day period at room temperature, from a dilute aqueous solution. The reaction afforded a 83% yield.

4.23 Preparation of Yttrium(III) Propionate

A stoichiometric amount of $Y_2(CO_3)_3 \cdot xH_2O$, (0.57 g, 1.6 mmol) was reacted with a 1M aqueous solution of propionic acid (0.71 g, 9.5 mmol). The carbonate salt dissolved quickly and the product precipitated upon evaporation of the water medium. If a dilute solution is left to evaporate at room temperature, very thin flat needles form, these needles are impossible to mount on the diffractometer due to their fragility. Repetition of this experiment with varied concentrations of reagents provided similar results.

110

4.24 Preparation of Yttrium(III) Butanoate

A 2M aqueous butyric acid (0.72 g, 8.2 mmol) solution was prepared and added to stoichiometric amount (0.47 g, 1.3   mmol) of yttrium(III) carbonate added. The mixture was heated to 50˚C, to promote solubility of the organic acid in water medium and allowed to stir for about 2 hours until all the carbonate was dissolved and no more gas (CO_2) was released.

The product was recrystallised from water and the dried first under vacuum at room temperature followed by over night drying in an oven at 60˚C. A yield of 92% was obtained.

4.25 Thermal Analysis

Thermogravimetry was carried out using a Perkin Elmer TGA 7 Thermogravimetric Analyser. The experiments were performed using a step size of $10˚C.min^{-1}$ and over temperature ranges as indicated on the graph, with data evaluation done with Microsoft Excel. Differential scanning calorimetry, was completed on a Mettler DSC 822^e, using the STARe software package to interpret and examine the data.

4.26 Infrared Spectroscopy

Infrared spectra were recorded using a Nicolet Thermstar IR spectrophotometer, dispersing the samples in KBr discs and using continuous dry nitrogen gas to purge the collection chamber. The collection range was 4000 cm^{-1} to 450 cm^{-1} at a resolution of 2cm^{-1}.

4.27 Structure determination of Yttrium(III) Acetate

A crystal of this complex was mounted on a glass fibre sample holder and set up on a Nonius Kappa CCD diffractometer.[23] Mo-Kα radiation, wavelength λ(0.17073Å) was used and compensation made for Lorentz and polarisation effects. Solution of the structure was completed using the X-Seed[22] crystallographic suite as interface, which calls the Shelx-97 program for solution and refinement.[21] The initial solution was obtained using direct methods. All other crystallographic data appears in Table 4.51.

4.28 X-Ray powder diffraction

X-ray powder diffraction patterns were measured using a Phillips PW 1710 diffractometer and Cu-Kα radiation. Samples were ground using an agate mortar and pestle and distributed on a glass sample holder lightly covered with high-vacuum grease. Collection commenced at 5° 2θ through to 75°2θ with a step size of 0.0170 and step time of 12 s. Patterns were indexed using the Crysfire[18].

Indexing was systematically achieved by eliminating (or finding) high symmetry solutions using the two exhaustive programs TAUP and DICVOL1. Followed by TREOR, a program that is tolerant of a measure of impurity lines and lastly DICVOL2 that considers exhaustively orthorhombic and monoclinic solutions.

We would like to repeat that the highest figure of merit, as described in Chapter 1, points at the most *likely* solution but doesn't exclude the possibility that one of the less likely solutions is the physical solution to the indexing problem.

Table 4.9 *Crystallographic data for yttrium acetate*

Empirical formula	$Y_2O_{20}C_{12}H_{34}$
Molar mass	676.21
Temperature (K)	300
Wavelength (Å)	0.71073
Crystal system, Space group	Triclinic, $P\bar{1}$
Cell Dimensions	
a (Å)	8.867(1)
b (Å)	9.251(10)
c (Å)	10.455(1)
α (°)	91.704(1)
β (°)	114.194(1)
γ (°)	117.790(1)
Volume (Å^3)	665.606(1)
Density (g.cm^{-3})	1.687
F(000)	344
Total Reflections	5501
Unique Reflections	2884
Goodness of fit	1.013
R index	0.0229

4.3 Conclusion

Even though all of the carboxylate complexes included in this and earlier chapters have carboxylate coordination modes that were accurately predicted using infrared spectroscopy, the spectrum of yttrium formiate (section 4.1) elucidates the fact that, at least for formiate compounds, Nakamoto's[11] guidelines cannot be blindly applied. The formiate compound shows a separation more than 50 cm^{-1} greater than expected for a bridging carboxylate

system. All prepared complexes crystallised in hydrated form and solvated water molecules are released from the system when a temperature higher than 100 ˚C is applied. After dehydration, yttrium aliphatic carboxylates are thermally stable up to at least 300 ˚C at which stage decomposition to yttrium oxide commences. The sloping DSC baseline for each of these complexes are expected due to the increase in heat capacity that occurs when compounds are heated. What is remarkable about this set of complexes is that even after decomposition, or dehydration, the slope of the DSC baseline remains constant. To explain this we suggest that the heat capacity of yttrium carboxylates, are independent of the ligand and only a function of temperature. Further studies to confirm this fact may be approached by studying the effects of different ligands - not only carboxylates - on the thermal properties of an yttrium complex.

4.4 References

1. AZoM™ - *Metals, Ceramics, Polymers, Composites, An Engineers Resource*, Copyright © 2004 by AZoM™.com Pty.Ltd

2. Y. Liu, Z. F. Zhang, J. Halloran and R.M Laine, *J. Am.Ceram. Soc.* (1998), **81**, 629

3. C. E. Housecroft, *Coord. Chem. Rev.*(1997), **162**, 241

4. N. G.Furmanova, Z.P.Razmanove, L.V.Soboleva,I.A.Maslyanitsin, G.Sigert, V.D.Shigorin and G.P.Shipulo, *Kristallografiya(Russ.) (Crystallogr.Rep.)* (1984) *,***29,** 476

5. A. S. Antsyshkina, M. A. Porai-Koshits, I. V.Archangelskii and L.A.Butman, *Koord.Khim.* (1976), **2,** 565

6. J. Ma, Z. Jin and J. Ni, *Acta Crystallogr. Sect. C:Cryst. Struct Commun.*(1994), **50**, 1010

7. Z. Delong, H. Chunhui, X. Guangxian, H. Cunheng, Z. Qitai and W. H. Xuebao(Chin.), *Chin.J.Inorg.Chem.* (1992)*,* **8,** 22

8. R. P. Turcotte, J. M Haschke, M. S. Jenkins and L. Eyring, *J. Solid State Chem.* (1970), **2**, 593

9. A. Pabst, *Canadian Mineralogist* (1978), **16**, 437

10. G. Rama Rao, K. C Patil and C.N.R Rao, *Inorg. Chim. Acta* (2001), **4**, 215

11. K. Nakamoto, F. Fujita, S. Tanaka and M and Kobayashi, *J. Am. Chem. Soc.* (1957), **79**, 4904

12. D.Stoilova and V. Vassileva, *Cryst. Res. Technol.*(1999), **34,** 397

13. G. B. Deacon, T. Feng, C. M Forsyth, A. Gitlits, D. C. R. Hockless, Q. Shen, B. W. Skelton and A. H. White, *J. Chem. Soc., Dalton Trans.* (2000), 961

14. F. Ribbot, P. Toledano and C. Sanchez, *Inorg. Chim. Acta*(1991), **185**, 239

15. M. F. Ramos Moita, M.T.S. Duarte and R. Fausto, *Spec. Lett.* (1994), **27**, 1421

16. G. A. M. Hussein, *Thermochim. Acta* (1994), **244**, 139

17. International Center for Diffraction Data (database)

18. R. Shirley (2000), The CRYSFIRE System for Automatic Powder Indexing: User's Manual, The Lattice Press, 41 Guildford Park Avenue, Guildford, Surrey GU2 7NL, England.

19. Gaussian 98, Revision A.11.3, M. J. Frisch, G. W. Trucks, H. B. Schlegel, G. E. Scuseria, M. A. Robb, J. R. Cheeseman, V. G. Zakrzewski, J. A. Montgomery, Jr., R. E. Stratmann, J. C. Burant, S. Dapprich, J. M. Millam, A. D. Daniels, K. N. Kudin, M. C. Strain, O. Farkas, J. Tomasi, V. Barone, M. Cossi, R. Cammi, B. Mennucci, C. Pomelli, C. Adamo, S. Clifford, J. Ochterski, G. A. Petersson, P. Y. Ayala, Q. Cui, K. Morokuma, N. Rega, P. Salvador, J. J. Dannenberg, D. K. Malick, A. D. Rabuck, K. Raghavachari, J. B. Foresman, J. Cioslowski, J. V. Ortiz, A. G. Baboul, B. B. Stefanov, G. Liu, A. Liashenko, P. Piskorz, I. Komaromi, R. Gomperts, R. L. Martin, D. J. Fox, T. Keith, M. A. Al-Laham, C. Y. Peng, A. Nanayakkara, M. Challacombe, P. M. W. Gill, B. Johnson, W. Chen, M. W. Wong, J. L. Andres, C. Gonzalez, M. Head-Gordon, E. S. Replogle and J. A. Pople, Gaussian, Inc., Pittsburgh PA, 2002

20. ArgusLab4.0, Mark A. Thompson, Planaria Software LLC, Seattle, WA, http://www.arguslab.com

21. M.A.Nabar and S.D.Barve (1984) *J.Appl.Crystallogr.,* **17,** 39

22. G.M Sheldrick, SHELXL-97, Program for Crystal Structure Analysis, University of Göttingen, Germany, 1997

23a. L. J. Barbour, *J. Supramol. Chem.* (2001), **1,** 189

23b. J.L. Atwood and L. J. Barbour, *Cryst. Growth Des.* (2003), **3**, 3

24. Nonius BV *COLLECT*, Data Collelction Software, Delft, The Netherlands

CHAPTER 5

LANTHANUM CARBOXYLATES

Research activity in the area of lanthanide coordination compounds has resulted from their wide applications in various fields of science and technology.[1] In the petrochemical industry the use of rare earth compounds has been studied as possible environmentally friendly anti-knock agents, where certain lanthanum carboxylates were shown to have the anti-knock properties required.[2]

Many structures of rare earth carboxylates have been recorded and today a rich diversity of structure types are known and published. Among these structures dimers bridged by two carboxylate centers, longer chain type compounds as well as mixtures of both are included. Lanthanide ions may assume coordination numbers between six and ten and when added to the wide variety coordination modes available to the carboxylate ion, it is clear that both solvated and unsolvated lanthanide carboxylates have many structural possibilities.[3]

Mayer *et al.*[5], has used powder diffraction to discriminate between samples of the same compound but different modes of hydration and also showed that anhydrous acetates show a broad range of thermal stability and can form basic carbonates ($Ln_2O_2.CO_3$) during decomposition. These basic carbonates are thermally stable up to 750 ˚C and later independent publications concur.[6]

Structural investigations of lanthanide metals with long alkyl chains, using powder diffraction, show that these compounds have a lamellar bi-layer structure. Jongen *et al.*[4] showed that lanthanum butyrate has this bi-layer structure and that the butyrate chains align themselves parallel to facilliate this. This layered structure of lanthanum butyrate is displayed in Fig. 5.1. In this chapter we investigate the structure of lanthanum propionate and see the effect of a shortened carbon chain on the crystallisation of the complex. In

117

addition to this we report and discuss several other physicochemical properties of lanthanum propionate, butyrate and pentanoate.
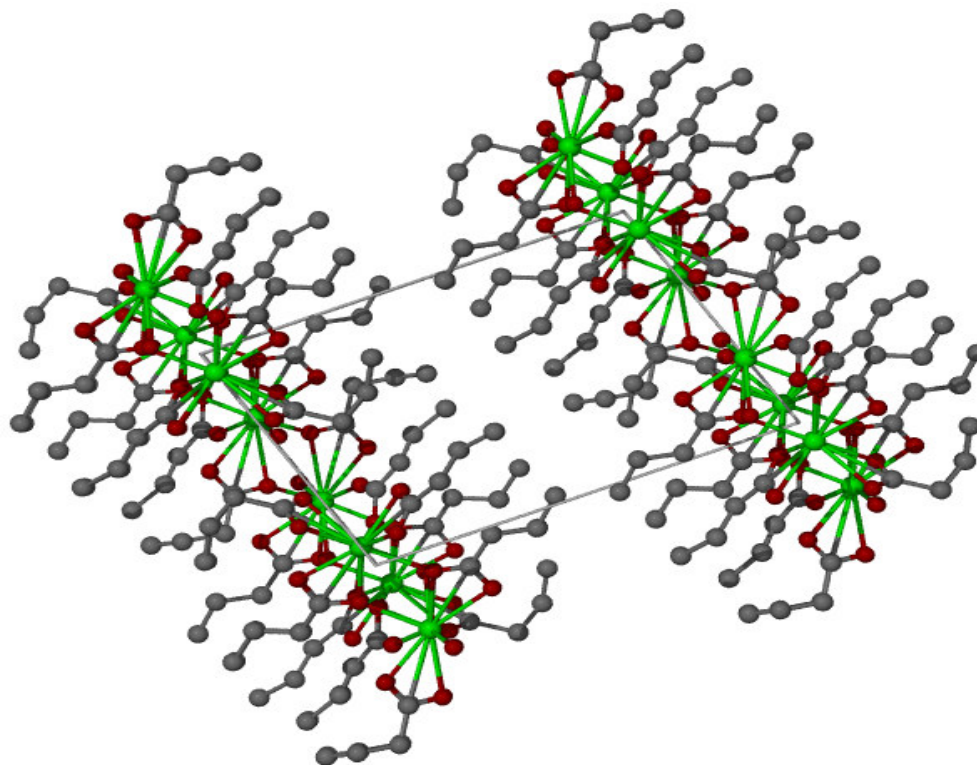

Fig 5.1 *Bi-layeral structure exhibited by lanthanum butanoate.[4]*

In a publication submitted by Ye *et al.*[7] lanthanum carboxylates and dipicolinates were used as structural model representations for different types of lanthanum complexes. We use lanthanum acetate, which is of known structure, as our choice of standard for crystallographic comparison.

While both lanthanum(III) formiate and acetate has been exhaustively investigated over the years, little is known of the propionate, butanoate and pentanoate analogues. It is these lesser known compounds that will be the focus of this chapter.

5.1 Results and Discussion

5.11 Lanthanum(III) Propionate

A previous thermal study of powdered lanthanum and nickel propionates, conducted by Kaddouri *et al.*[8]*.* produced DSC and thermogravimetric curves that mirrored our own even though our interpretation of the decomposition sequence differs. Kaddouri observed, like us, the formation of an intermediary carbonate product followed by decomposition to oxygen. He, however, only reported CO and CO_2 as gas phase products and not the formation of the symmetric ketone.

5.111 Synthesis

Using standard Schlenk techniques and degassed water as solvent to limit the amount of oxygen in the reaction, this preparation was facilitated using lanthanum carbonate and degassed propionic acid (equation 1).

$$La_2(CO_3)_3.xH_2O + 3CH_3CH_2COOH \rightarrow La(CH_3CH_2COO)_3 + (x+1)H_2O \qquad \textbf{(1)}$$
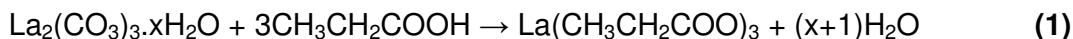
The product precipitated as small off-white crystals clinging to the side of the reaction vessel. After recrystallisation from a methanol solution suitable samples of the product were used for structural characterisation.

5.112 Infrared Spectroscopy

Figure 5.2 displays the infrared spectrum of lanthanum propionate. Two different –OH absorptions at appreciably different wavenumbers are listed in Table 5.1. One of these two bands are assigned to water coordinated to a lanthanum atom, which is supported by the weak band at 1640 cm^{-1} and the other to uncoordinated water present in the sample.

119

Table 5.1 *Infrared absorption bands for lanthanum(III) propionate*

Band(cm^{-1})	Assignment
3418, 3176	-OH stretches
2968-2865	CH_3, CH symmetric and asymmetric stretches
1563	Asymmetric carboxylate stretch
1411	Aliphatic bending bands
1300	Symmetric carboxylate stretch
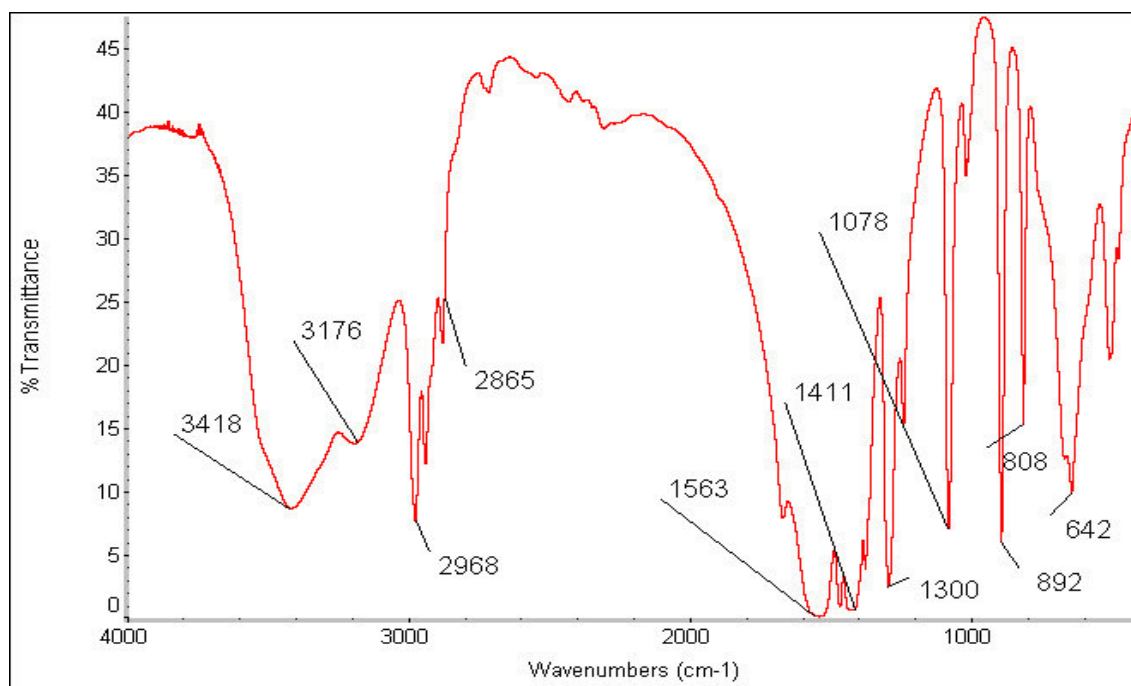
Fig. 5.2 *Infrared spectrum of lanthanum(III) propionate*

The characteristic aliphatic bands at 2968-2865 cm^{-1} and in the region of 1411 cm^{-1} confirm the presence of saturated organic chains in the compound. When the difference between symmetric and asymmetric carboxylate stretches is calculated, only a chelating carboxylate mode is identifiable by referring to results reported by earlier workers.[9] Even though the crystal structure (section 5.14) shows the presence of a bridging carboxylate ion, its symmetric absorption band is obscured by the absorption of chelating carboxylate symmetric stretches. These bands occur in the same region and

120

since the chelating stretches outnumber bridging stretches 2:1, the bands due solely to the presence of the bridging carboxylate ion, are difficult to identify.

5.113 Thermal Analysis

A mass decrease of five percent, occurs at 120˚C (Fig. 5.3) and is ascribed to the release of one water unit from the crystals. The DSC thermogram relayed in figure 5.4 shows a broad endotherm that peaks at 123 ˚C and corresponds to this thermal event. Two sharp endotherms at 260 ˚C and 394 ˚C mark further decomposition steps.
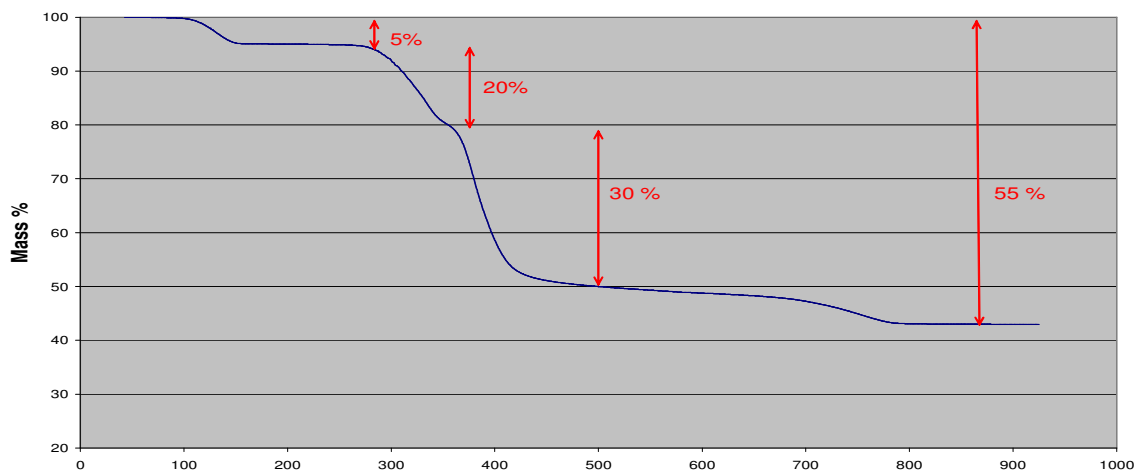

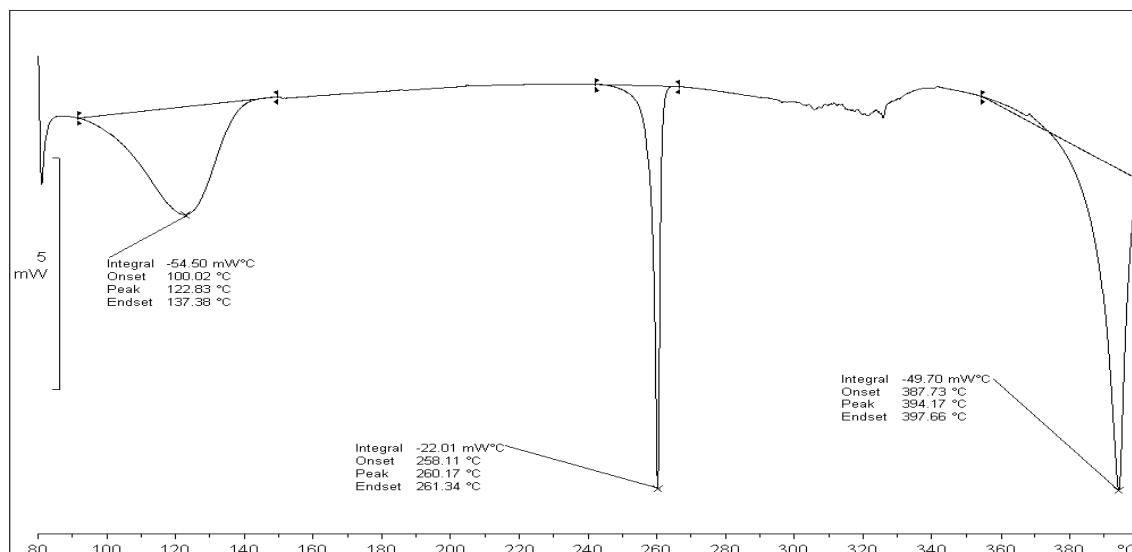**Fig 5.3** *TGA Thermogram of lanthanum(III) propionate*

Fig 5.4 *DSC Thermogram for 2.43 mg of lanthanum(III) propionate*
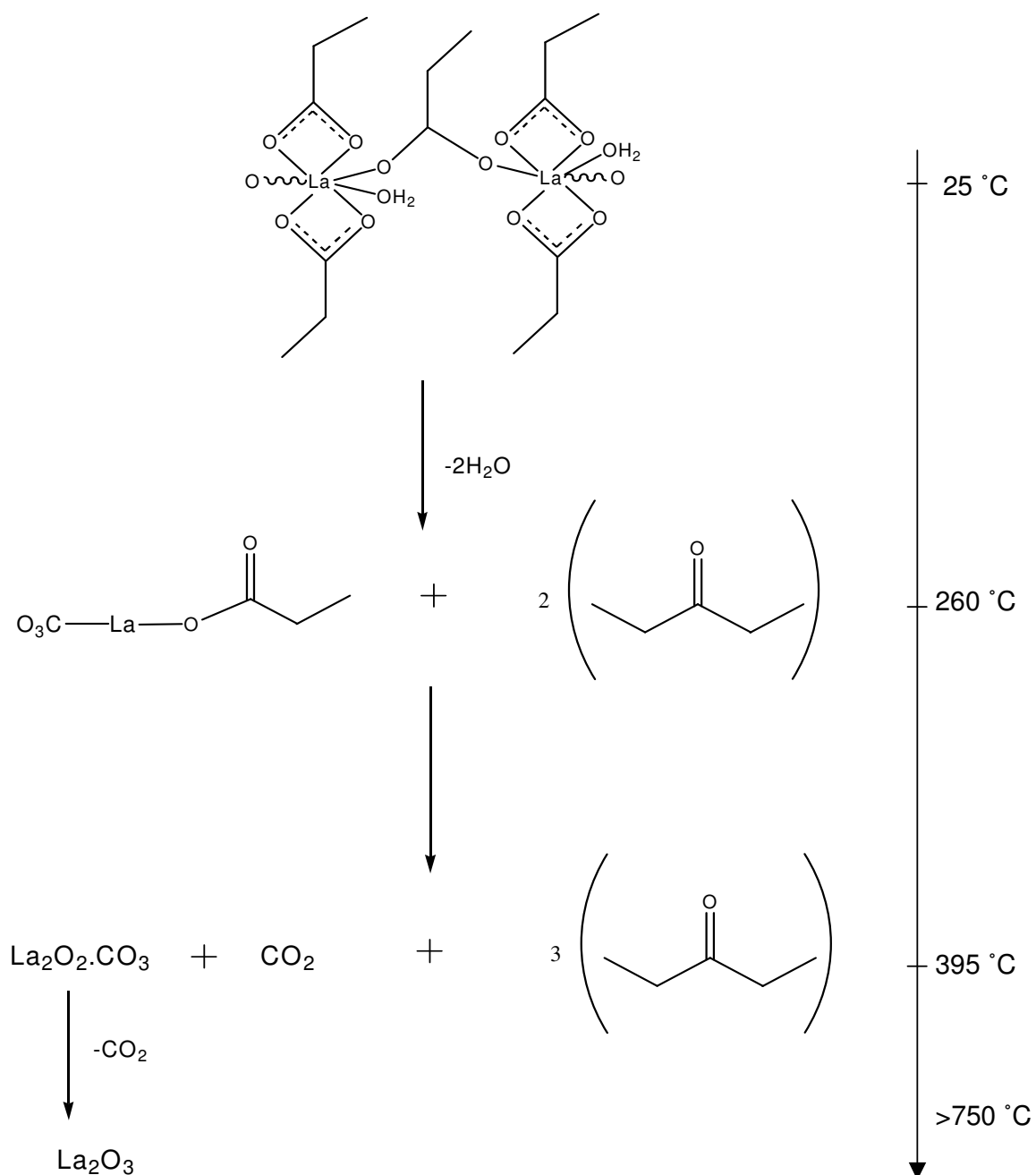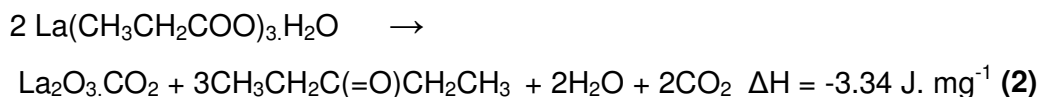
121

Fig. 5.5 *Thermal decomposition of lanthanum(III) propionate*

The successive mass-loss percentages (5%, 20%, 30%, 5%) indicate that after the release of the crystal water carbonato(propionato)lanthanum(III)

forms and a symmetric ketone is released. Lanthanum(III) oxide is then formed with a carbonate group still coordinated to the metal and, finally, the release of carbon dioxide occurs (see Fig. 5.5.) The reaction is summarised in equation 2 with the enthalpy value calculated from DSC data.

$2\ La(CH_3CH_2COO)_3.H_2O\ \longrightarrow$

$La_2O_3.CO_2 + 3CH_3CH_2C(=O)CH_2CH_3\ + 2H_2O + 2CO_2$ $\Delta H = -3.34\ J.\ mg^{-1}$ **(2)**

5.114 Crystallographic Studies

Lanthanum propionate crystallises in the triclinic space group $P\bar{1}$. In figure 5.14 the crystal structure of lanthanum propionate is given, with all lanthanum ions equivalent and in coordination mode 10. Each central lanthanum atom has one water molecule coordinated to it and is chelated in 0^3 fashion by two propionate ions while two other propionate ions are shared and bridging - Z,E-type bridging as defined by Ouchi *et al.*[10] - between neighbouring centers.

The distance between the carboxylate carbon atom and lanthanum center is slightly larger than average lanthanum-carbon single bond lengths, a bonding distance of this magnitude (2.993 Å) is not unprecedented. Carbon-lanthanum bonds of 2.992 Å and 2.931 Å have been reported and it is our feeling that due to electron delocalisation the carbon atom is at least partially coordinated to the lanthanum atom.[11, 12]

Even though 10 atoms are coordinated around the lanthanum center, lanthanum finds itself in a distorted pseudo octahedral environment with four oxygen atoms on its equatorial positions and carboxylate carbons at the apexes. The angles surrounding the lanthanum center range from 79.4˚ to 99.52˚ and are listed, along with other selected angles and bond lengths, in Table 5.2.
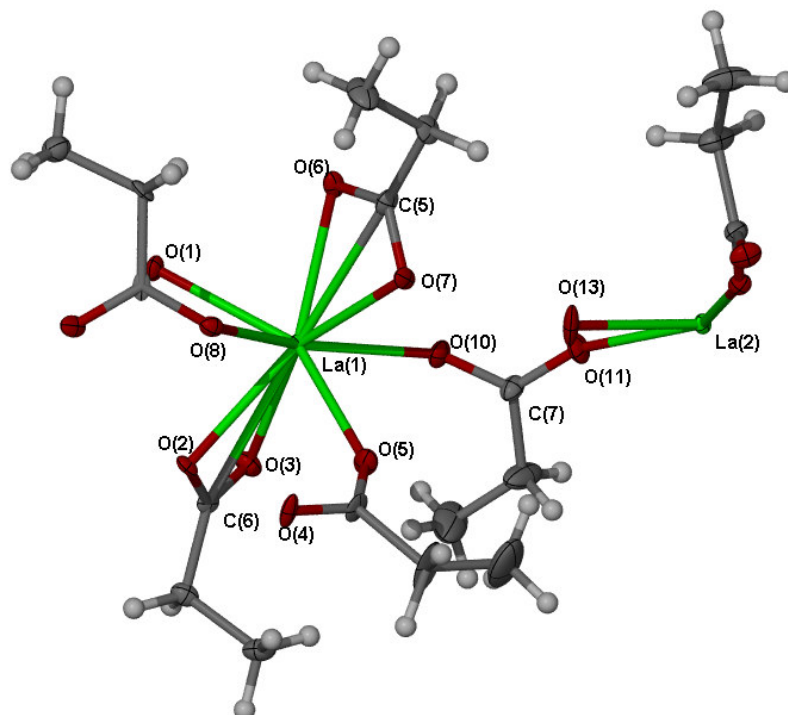
Fig 5.6 *Molecular structure of lanthanum(III) propionate*

Table 5.2 *Selected angles, bond lengths and inter atomic distances*

Bond Lengths (Å)		Bond Angles (°)	
La(1)-O(1)	2.623(5)	O(1)-La(1)-C(5)	99.5(2)
La(1)-O(2)	2.610(5)	O(1)-La(1)-O(10)	135.2(2)
La(1)-O(3)	2.575(6)	C(5)-La(1)-O(10)	79.4 (2)
La(1)-O(5)	2.451(5)	O(6)-C(5)-O(7)	120.3(8)
La(1)-O(8)	2.569(5)	O(10)-C(7)-O(11)	122.1(7)
La(1)-C(5)	2.993(9)	C(5)-La(1)-C(6)	165.8(2)

The packing diagram (Fig. 5.7) shows that molecules are arranged as independent – with no short interactions in between them - layers. Earlier workers have claimed that the length of the propionate chain is not long enough to force the molecules into parallel layer alignment and continued by stating that the butyrate group is the first in a series of lanthanide alkanoates which results in the "typical bilayer structure" of metal soaps.[4]
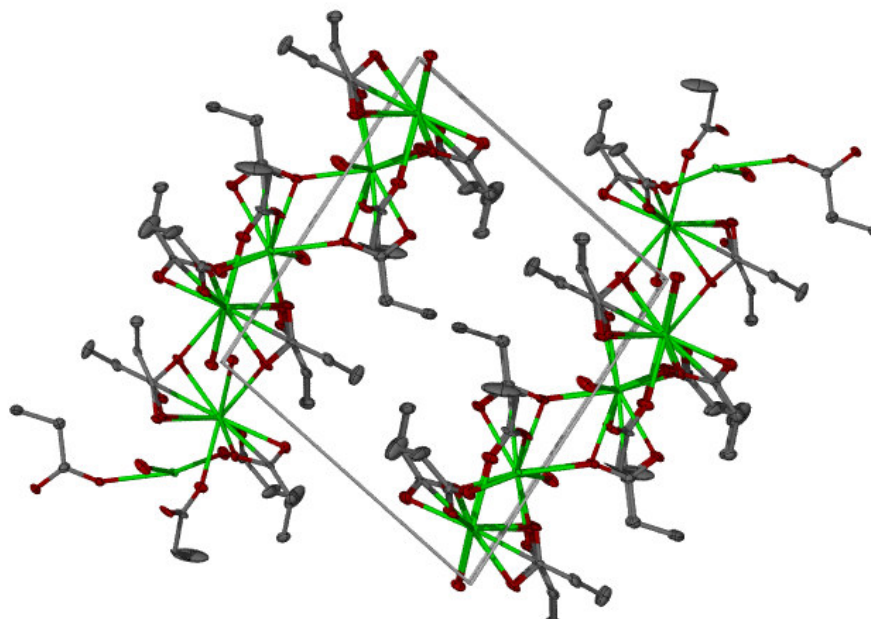
Fig 5.7 Lanthanum(III) propionate mono hydrate crystal packing along the b axis

The present structure solution has shown this assumption to be invalid. Even though the propionate chains do not align themselves parallel, this system also adopts a bi-layered form.

5.12 Lanthanum(III) Butyrate

Almost no publications, beyond the report of the molecular structure cited in this section, exist and a publication search of the CAS database using SciFinder scholar as interface, only yields three publications that mention this compound.

5.121 Synthesis

A micro crystalline powder was obtained after reacting lanthanum carbonate hydrate with butyric acid in a degassed aqueous medium using standard Schlenk techniques.

$$La_2(CO_3)_3 .xH_2O + 6CH_3CH_2CH_2COOH \rightarrow 2La(RCOO)_3.xH_2O + H_2O \qquad \textbf{(3)}$$

125
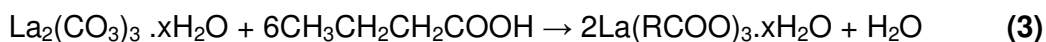
Using ICP analysis the amount of La in the compound was determined and confirmed to be as expected for lanthanum butyrate monohydrate $(La(C_3H_7COO)_3.H_2O)$.
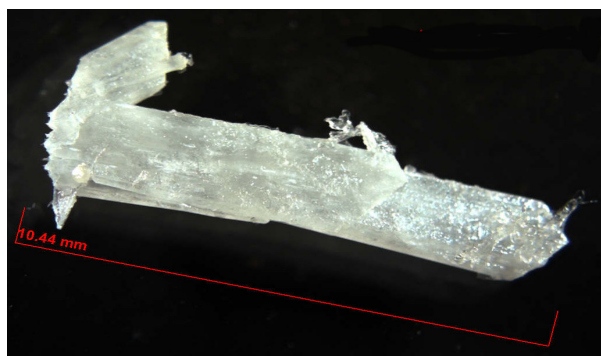

Fig. 5.8 *A lanthanum(III) butyrate crystal*

5.122 Infrared Spectroscopy

Strong aliphatic absorptions and carboxylate stretches are the predominant features of the infrared spectrum of lanthanum(III) butyrate. The spectrum, which is displayed in Fig. 5.9 also shows the hydration bands expected for a hydrated complex.
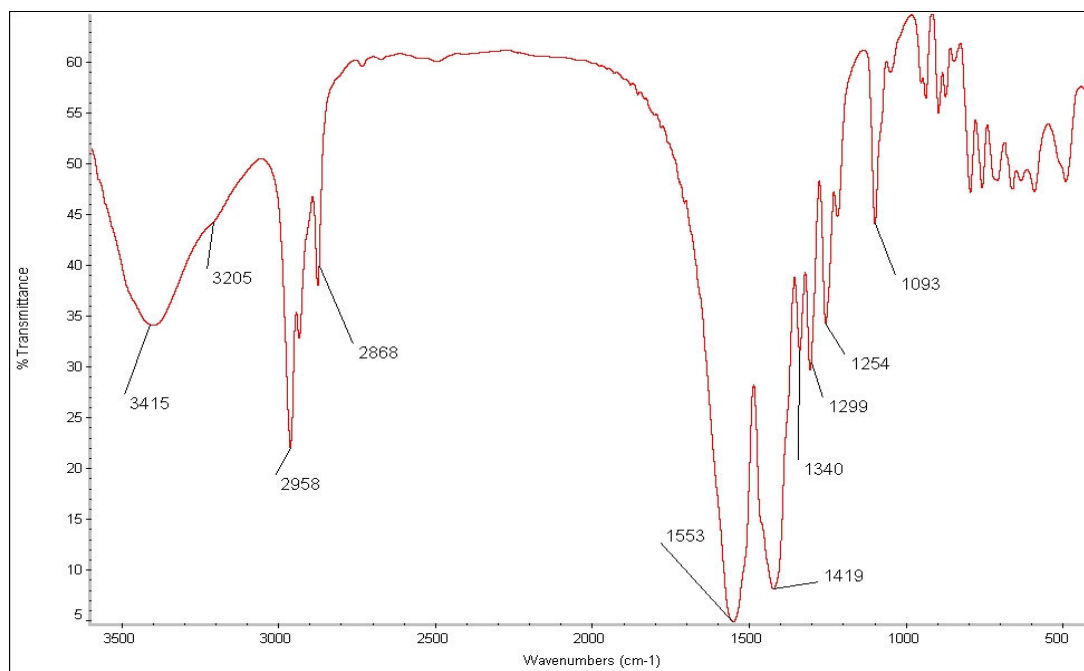

Fig. 5.9 *Infrared spectrum of lanthanum(III) butyrate*

126

The peak separation between the only identifiable symmetric and asymmetric carboxylate carbonyl stretches is 213 cm^{-1} which is large enough to be a result of a chelating carboxylate ion. Other assigned infrared absorption for this compound can be found in Table 5.21.

Table 5.3 *Infrared band assignments for lanthanum(III) butyrate*

Band (cm^{-1})	Assignment
3415, 3205	-OH band assignments
2958-2868	Aliphatic symmetric and asymmetric stretches
1553	Carboxylate asymmetric stretch
1419	Aliphatic bending modes
1340	Carboxylate symmetric stretch
1299	-CH$_2$ deformation vibration

5.123 Thermal Analysis

Thermal decomposition of the compound as illustrated by thermogravimetric data (see TGA thermogram, Fig. 5.10 supports the formation of pure lanthanum carbonate at temperatures in excess of 400˚C
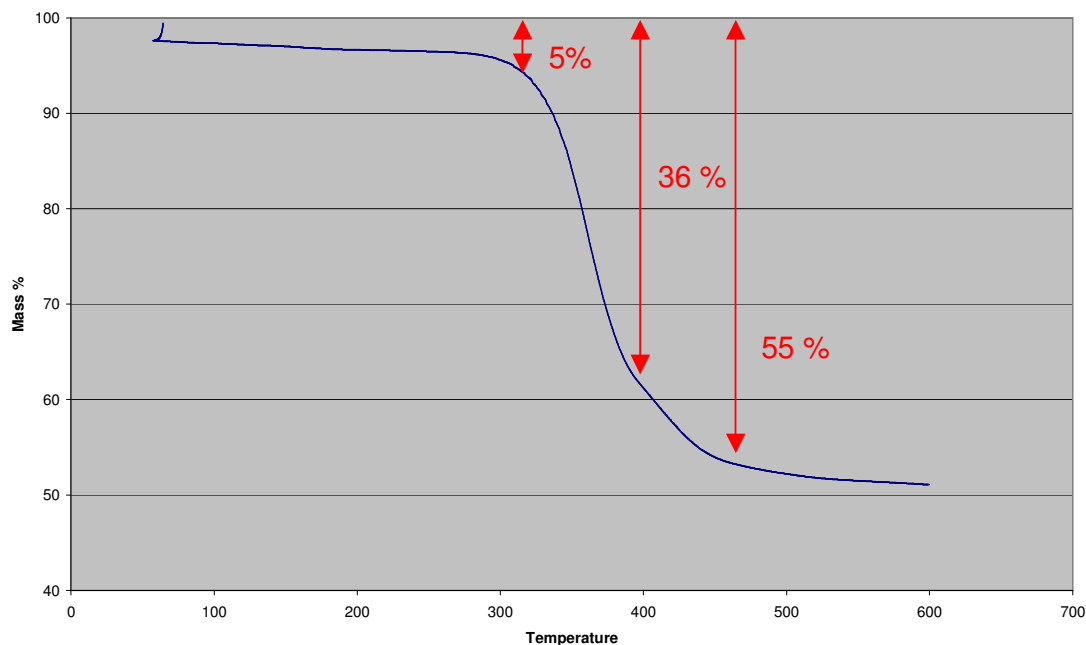

Fig. 5.10 *TGA thermogram of lanthanum(III) butyrate*

.

A endothermic peak, the first endothermic peak displayed at 187 ˚C on Fig. 5.11 corresponds to a phase transition since no decrease in sample mass is observable. A broad and ill defined peak at about 340 ˚C marks the onset of decomposition, which is followed by the strongly endothermic formation of lanthanum(III) carbonate.
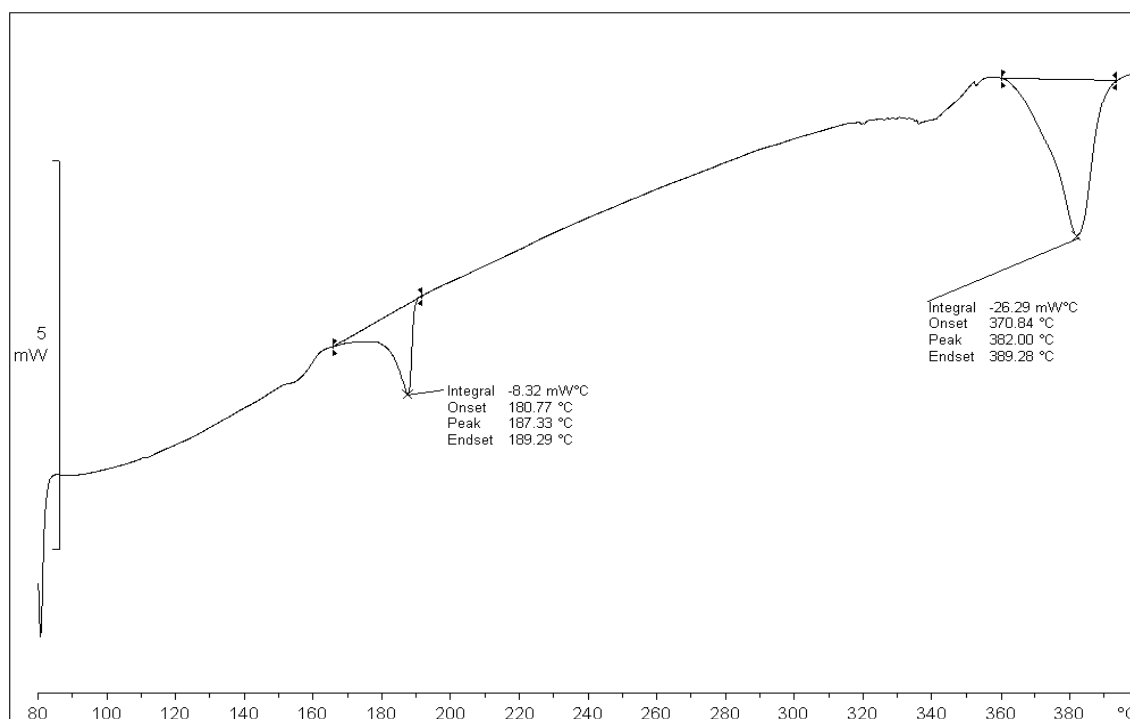

Fig. 5.11 *DSC thermogram for 2.25 mg of lanthanum(III) butyrate*

5.124 Crystallographic data

Jongen *et al.*[4] reported the crystal structure shown in Fig. 5.12 for lanthanum(III) butyrate. This structure is displayed using the X-Seed[14] software package and data obtained from the Cambridge Crystallographic Database. The hydration mode and coordination of the carboxylate ligand in this complex is as expected from spectroscopic and thermal data. Jongen described the coordination polyhedra for both crystallographic atoms in this complex as being mono capped anti prisms.

128

While not necessarily clear at first glance, this structure is dissimilar to the one discussed in section 5.11 for lanthanum(III) propionate and displays two crystallographically equivalent lanthanum atoms in the structure.

Though the anti symmetric unit is reminiscent of the structure of lanthanum(III) and yttrium(III) acetate (section 4.12) both of which also form dimeric a M-O-M-O center (M=Y, La), the important difference is that here, the metal atoms are crystallographically and chemically inequivalent.

One of the metal centers is di-hydrated and the other is anhydrous. The anhydrous center thus has coordination sites available for polymerisation to occur. Polymerisation of this compound is depicted in the packing diagram (Fig. 5.13).
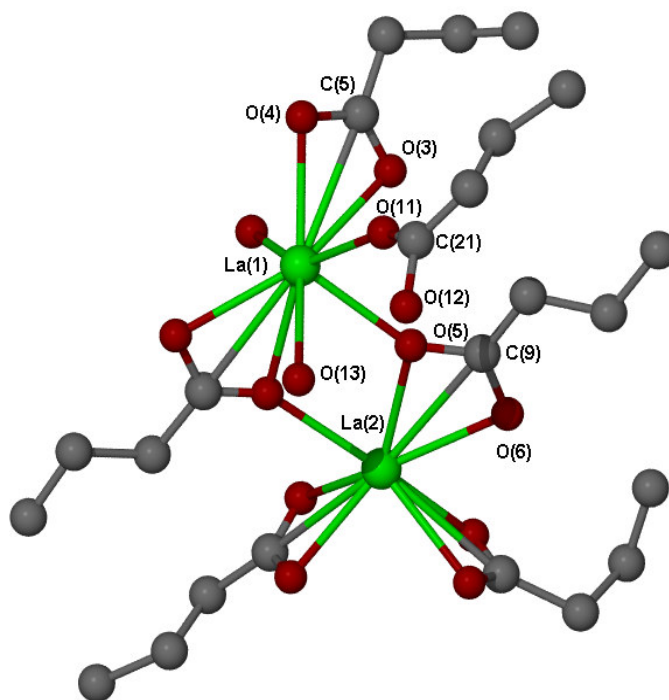

Fig. 5.12 *Molecular structure of lanthanum(III) butyrate mono hydrate, with hydrogen atoms omitted for clarity.*[5]
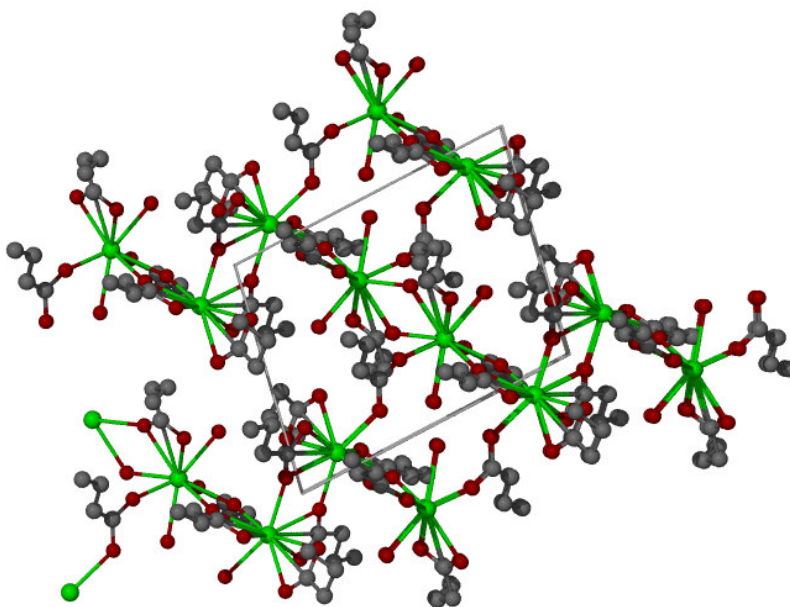
Fig. 5.13 *Packing diagram of lanthanum(III) butyrate*

Since both metal atoms in yttrium and lanthanum acetate are di-hydrated, no open coordination sites are available for polymerization and only a single dimer forms.

5.13 Lanthanum(III) Pentanoate

In paper published by Jongen *et al.*[13] it was concluded that saturated non-cyclic lanthanum(III) carboxylates, including lanthanum(III) pentanoate, show at least one smectic mesophase on heating and cooling. Our investigation, which was completed under similar conditions, concurs with the first two phase transitions Jongen observed for lanthanum(III) pentanoate, but we could not identify the third phase –a transition to isotropic liquid- that was reported.

5.131 Synthesis

This preparation was achieved, *via* the reaction between valeric acid and lanthanum carbonate. Carbon dioxide gas immediately started developing after the addition of the carbonate salt to a hot aqueous acid solution. Once formed, the product does not dissolve in polar organic solvents such as hexane but solvents such as ethanol, proved ideal.

130

5.132 Infrared Spectroscopy

The IR spectum contains a very clear and shouldered, hydration band at 3400 cm^{-1}. Another shoulder (1665 cm^{-1}) on the asymmetric carboxylate stretch at 1538 cm^{-1} suggests the presence of two structurally different carboxylate ions, even though one is clearly more abundant.
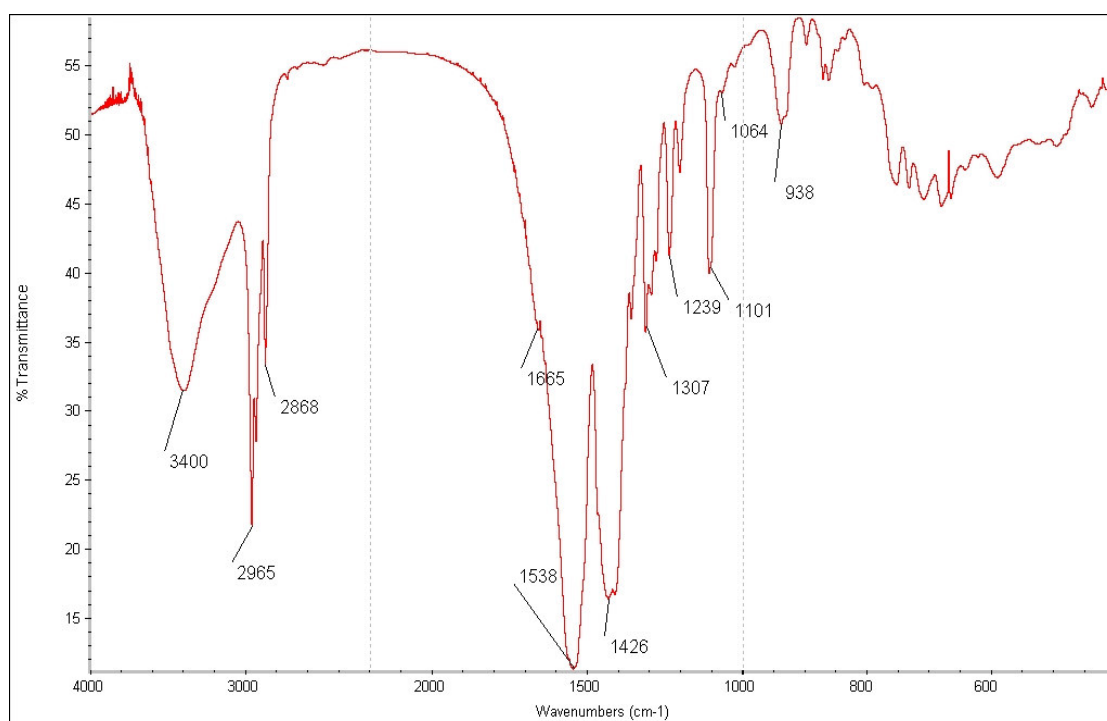
Fig. 5.14 *Infrared spectrum of lanthanum(III) pentanoate*

The respective differences between the asymmetric stretching frequencies and the symmetric (which are found at 1307 cm^{-1} for both carboxylate groups) stretching frequencies, are 339 cm^{-1} and 221 cm^{-1} respectively.

The very large difference between stretching frequencies for the first anion, strongly indicates that this is loosely coordinated carboxylic acid and that the acid oxygen – carbon bond possesses mostly single bond character. The

131

retention of some unreacted valeric acid in the structure also justifies the strong hydroxide absorption observed.

A complete list of assigned absorption bands are assembled in Table 5.41.

Table 5.4 *Infrared absorption bands for lanthanum pentanoate*

Band (cm^{-1})	Assignment
±3400	-OH absorption band
2975-28	CH$_3$, CH symmetric and asymmetric stretches
1665	Carbonyl stretch of loosely coordinated carboxylic acid
1528	Asymmetric carboxylate absorption
1411	Aliphatic bending bands
1307	Symmetric carboxylate absorption

5.133 Thermal Analysis

Analysis of this compound shows only endothermic events occurring between 80 ˚C and 400 ˚C. The first two these, observed at 107 ˚C and 127 ˚C, occur in an area that correspond to a gradual mass decrease on the TGA thermogram (Fig. 5.15). Since the observed mass-decrease is gradual, it cannot, on the basis of collected data, be assigned to either of the two endotherms observed on the DSC (Fig. 5.16).

Only a slight - less than 4 % - mass decrease is observed before 370 ˚C at which point the sample mass diminishes by 45 % followed by another 5 %. An area of thermal stability, after retaining only 47 % of the original mass, is then entered until the compound decomposes completely to form lanthanum(III) oxide at 750 ˚C.
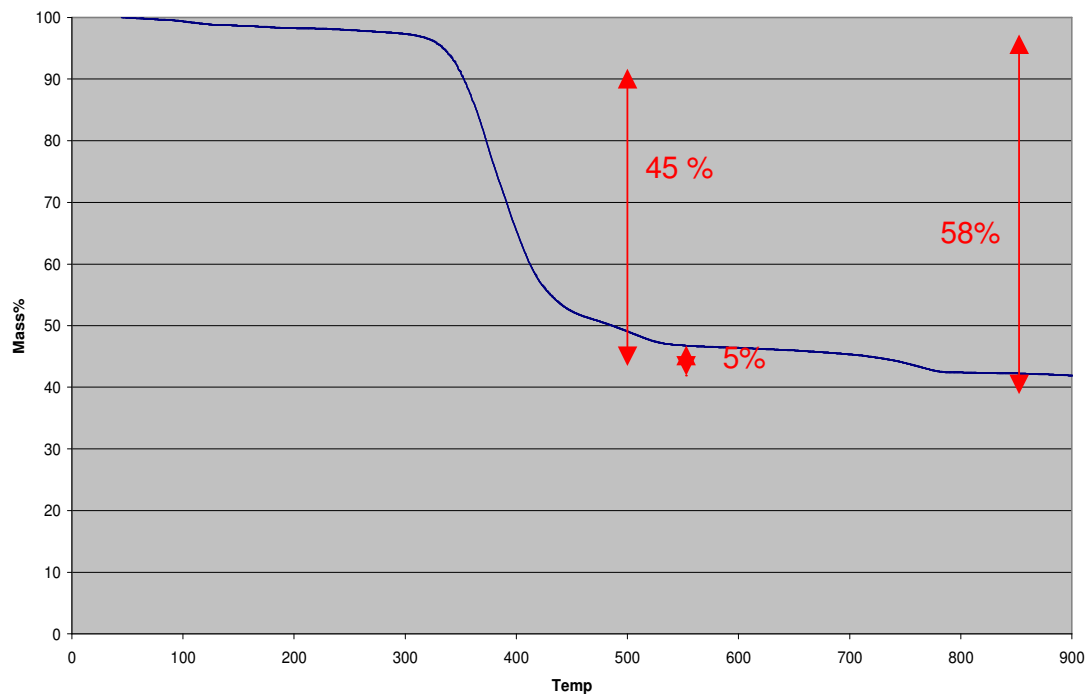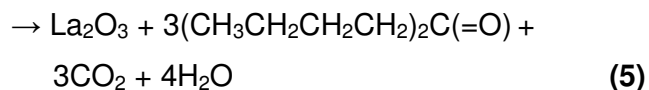
Fig. 5.15 *TGA thermogram for lanthanum(III) pentanoate*

The stepwise decomposition pattern observed here is as expected for the now gravimetrically confirmed molecular formula of $La(CH_3CH_2CH_2COO)_3.2H_2O$, the weight stable area - after 500 ˚C - suggests the intermediary formation of the normal carbonate (equation 4) as mentioned in the opening passages of this chapter. The total decomposition reaction is summarised in equation 5.

$$2La(CH_3(CH_2)_3COO)_3.2H_2O \rightarrow La_2O_2.CO_3 + 3(CH_3CH_2CH_2CH_2)_2C(=O) +$$
$$CO_2 + 4H_2O \qquad \textbf{(4)}$$
$$\rightarrow La_2O_3 + 3(CH_3CH_2CH_2CH_2)_2C(=O) +$$
$$3CO_2 + 4H_2O \qquad \textbf{(5)}$$

133
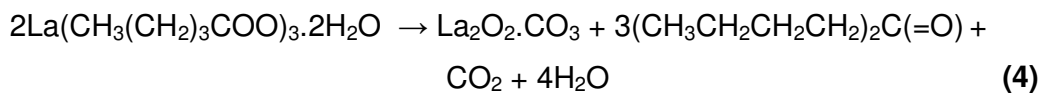
Fig. 5.16 *DSC thermogram for 3.12 mg lanthanum(III) pentanoate*

5.134 Powder Diffraction

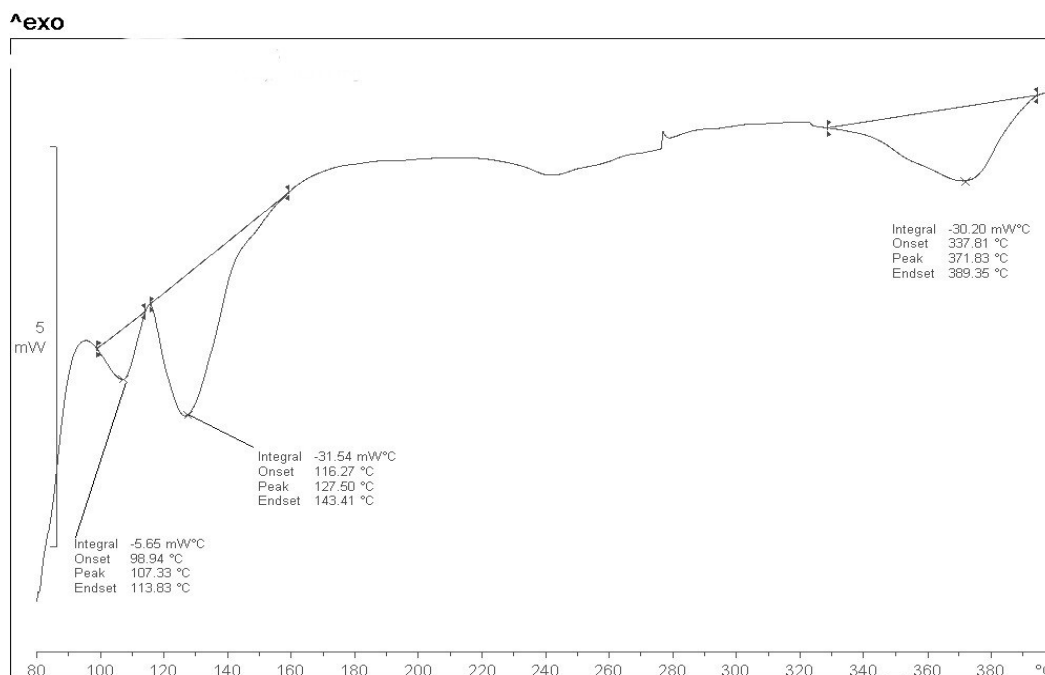The diffraction pattern of this compound (Fig. 5.17) has a very dominant peak at an early two-theta value which indicates that all the crystallites in this sample have a clear preferred orientation. Such a strong preference for a certain orientation, is usually indicative of sheet or needle like crystals. Despite the presence of such a strong peak, it was easy to identify 19 additional peaks that could be used for indexing.

Probable indexing solutions are summarised in Table 5.5. Even though some results which had more favourable figures of merit were also obtained during indexing, they were not included in Table 5.5. These results were discredited according to factors that resulted in them being an unsuitable solution. For instance, one of the solutions had a b-axis value smaller than 2.5 Å which isn't large enough to accommodate even a single butyrate chain. Such results,

134

while mathematically possible, are chemically nonsensical and do not merit further discussion.

These set of accepted indexing solutions suggest a probable unit cell volume between 1116 and 1525.26 $Å^3$. The diffraction pattern of this compound has not previously been reported and no single crystal data has been determined. All indexing sets listed in Table 5.6 should be considered a probable solution.
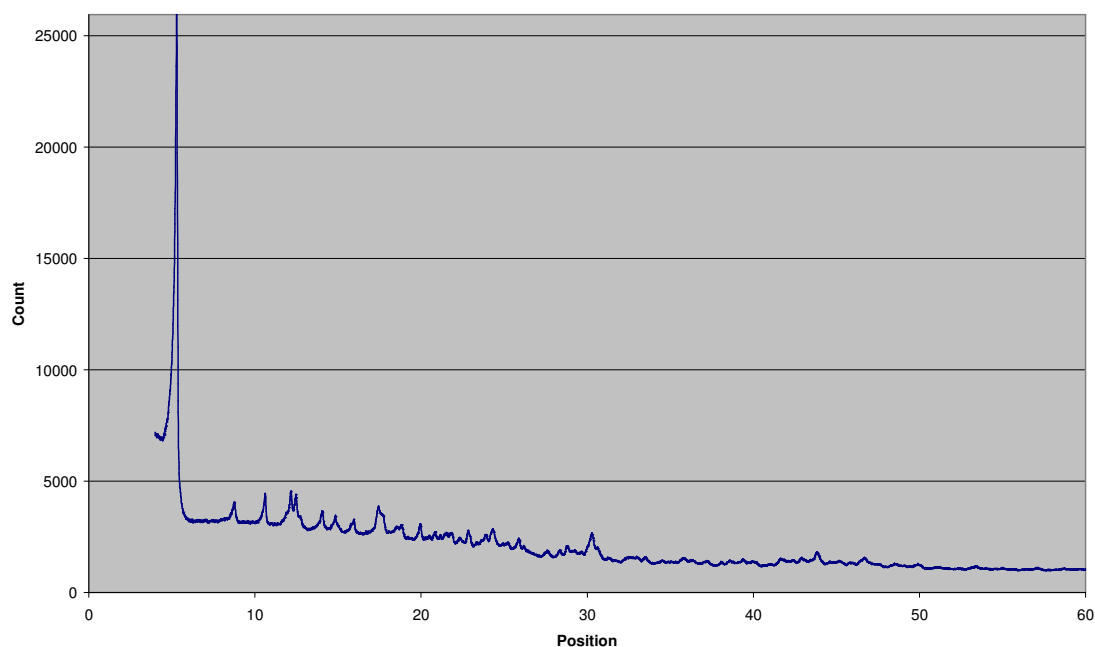

Fig. 5.17 *Powder diffraction pattern of lanthanum(III) pentanoate*

Table 5.6 *Indexing results for lanthanum(III) pentanoate*

Merit	Volume	Prog	a	b	c	alpha	beta	gamma
5.2	4869.04	DV	50.098	22.142	4.389	90	90	90
8	1399.33	TR	8.278	16.972	19.301	42.92	69.12	96.38
7	1525.26	TR	16.800	12.594	7.316	90	99.81	90
7	1525.26	TR	17.143	12.594	7.316	90	105.06	90
7	1525.26	TR	16.800	12.594	7.316	90	99.81	90
7	1116.74	TR	6.601	17.307	18.872	33.03	72.22	77.15
6	1522.12	TR	20.277	12.600	7.318	90	125.48	90
6	1218.49	TR	7.214	17.973	18.654	32.54	75.38	69.91
4.9	1402.60	IT	11.649	12.871	10.185	96.28	95.29	111.03

5.2 Experimental

5.21 Preparation of Lanthanum(III) Propionate

Lanthanum(III) carbonate (0.73 g, 1.6 mmol), was used to deprotonate propionic acid (0.71 g, 9.59 mmol). The reaction was completed in 20ml of degassed water and standard Schlenk techniques were used too keep the reaction mixture in an inert atmosphere. A 96% yield was obtained and upon recrystallisation from a methanol solution, a crystal suitable for a single crystal structure investigation could be isolated.

5.22 Preparation of Lanthanum(III) Butyrate

This reaction was completed in an open atmosphere by adding 0.23 g (0.75 mmol) of lanthanum(III) carbonate to a hot (approx. 65 ˚C) water (20 ml) and butyric acid (0.40 g, 4.6 mmol) solution. Precipitation of the product resulted on evaporation of the solvent.

5.23 Preparation of Lanthanum(III) Pentanoate

The same methodology was followed as described in 5.52, but 0.23 g (0.50 mmol) of lanthanum(III) carbonate and 0.25 g (0.41 mmol) valeric acid were used.

5.24 Infrared Spectroscopy

Infrared spectra were recorded on a Nicolet Thermstar IR spectrophotometer, with the samples dispersed in KBr discs and using continuous dry nitrogen gas to purge the collection chamber. The collection range was 4000 cm^{-1} to 450 cm^{-1} at a resolution of 2 cm^{-1}.

136

5.25 Thermal Analysis

Thermogravimetry was carried out using a Perkin Elmer TGA 7 Thermogravimetric Analyser. The experiments were performed using a step size of $10°C.min^{-1}$ and over temperature ranges as indicated on the respective graphs, with data evaluation done using Microsoft Excel.

Differential scanning calorimetry, was completed on a Mettler DSC 822^e, using the STARe software package to interpret and examine the data. Aluminium (40 µml) sample pans, pressed and vented by piercing the sample pan lid, were used during collection.

5.26 Powder Diffraction

Powder X-ray diffraction patterns were recorded using a Huber Imaging Plate Guinier Camera 670 using nickel-filtered CuKα_1 radiation (λ = 1.5405981 Å) produced at 40 kV and 20 mA by a Philips PW1120/00 generator fitted with a Huber long fine-focus tube PW2273/20 and a Huber Guinier Monochromator Series 611/15. A 2θ range of 4 - 100.0° was used with a step size of 0.005° 2θ.

5.27 Structure Solution

A crystal of this complex was cut to size and mounted on a glass fiber sample holder and set up on a Bruker SMART Apex diffractometer.[14] Mo-Kα radiation, wavelength λ(0.17073 Å) was used and compensation made for Lorentz and polarisation effects. Solution of the structure was completed using the X-Seed[15] crystallographic suite as interface, which uses the Shelx-97 program for solution and refinement.[16] The initial solution was obtained using direct methods. Crystallographic experimental data appear in Table 5.51.

Table 5.51 Crystallographic data for lanthanum(III) propionate

Empirical formula	$La_1O_7C_9H_{15}$
Molar mass	374.12
Temperature (K)	100
Wavelength (Å)	0.71073
Crystal system, Space group	Triclinic, $P\bar{1}$
Cell Dimensions	
a (Å)	9.505(3)
b (Å)	11.680(3)
c (Å)	12.236(3)
α (˚)	98.339(4)
β (˚)	91.245(4)
γ (˚)	106.230(4)
Volume (Å^3)	1287.7(6)
Density	1.930
F(000)	728
Total Reflections	6379
Unique Reflections	2812
Goodness of fit	0.819
R index	0.0490

5.3 Conclusion

In this chapter the layer-like structure of a novel lanthanum(III) carboxylate – lanthanum(III) propionate - is recorded and disclosed. This shows that even without the parallel alignment of alkyl chains required by Jongen (introductory passages of this chapter and section 5.114) lanthanum carboxylates may still adopt a bi-layeral structure.

The similarities as well as contrarieties between lanthanum(III) and yttrium(III) acetate and propionate carboxylate modes of crystallisation were illuminated.

We have shown the formation of stable lanthanum(III) carbonate intermediates for all prepared carboxylates upon thermal decomposition and accentuated the reliability of infrared spectroscopy as structural analysis tool for this type of compound.

The lanthanum(III) carboxylates investigated have no melting point since decomposition sets in too early. Unlike the series of yttrium(III) compounds (chapter 4), heat capacities of the lanthanum complexes are dependent on which species surrounds the metal atoms. Even though both lanthanum (III) butyrate and pentanoate are stable up to at least 350 ˚C, lanthanum(III) propionate starts it's decomposition at only 260 ˚C.

5.4 References

1. C. Hammond, *The Basics of Crystallography and Diffraction*, Oxford University Press Inc. (1997)

2. R.L. Rardin, W. B. Tolman and S.J Lippard, *New, J. Chem.* (1991), **15**, 417

3. D. G. Karraker, *J .Inorg. Nucl. Chem.* (1969), **31**, 2815

4. L. Jongen, G. Meyer and K. Binnemans, *J. Alloys and Comp.* (2001)*,* **323**, 142

5. I. Mayer and F. Kassierer*, J. Inorg. Nucl. Chem.* (1966)*,* **28**, 2430

6. D. A. Edwards and R. N. Hayward, *Can. J. Chem.*(1968), **46**, 3443

7. B. Ye, X. Li, I. D. Williams and X. Chen, *Inorg. Chem* (2002), **41,** 6426

8. A. Kaddouri and C. Mazzocchia, *J. of Anal. And Appl. Pyr.* (2002), **65**, 253

9. K. Nakamoto, F. Fujita, S. Tanaka and M, Kobayashi, *J. Am. Chem. Soc.*(1957), **79**, 4904

10. A. Ouchi, Y. Suzuki, Y. Okhi and Y. Koizumi, *Coord. Chem. Rev.* (1988), **92**, 29

11. W. J. Evans, R. Anwander, R. J. Doedens and J. W. Ziller, *Angew. Chem., Int. Ed., Engl.*(1994), **33**,1641

12. J. Scholz, A. Scholz, R. Weimann, C.Janiak and H. Schmann, *Angew. Chem., Int. Ed., Engl.*(1994), **33**,1171

13. L. Jongen and K. Binnemans, *Liq. Cryst.* (2001)*,* **28**, 1727

14. SMART, Data reduction software, Bruker AXS Inc., WI, 2003

15a. L. J. Barbour, *J. Supramol. Chem.* (2001), **1,** 189

15b. J. L. Atwood and L. J. Barbour, *Cryst. Growth Des.* (2003), **3**, 3

16. G. M. Sheldrick, Shelxl-97, University of Göttingen, Germany, 1997

APPENDIX A

SUPPLEMENTARY DATA

DSC calibration

Calibration of the instrument was performed against an indium standard and temperature measurements were well within expected limits but a slight deviation from literature energy values, as included in the instrument documentation, was observed. Calibration yielded the following results:

Measured melting point enthalpy (J.g^{-1}): -26.7 ± 0.6 after 23 measurements
Literature melting point enthalpy (J.g^{-1}): -28.62

Measured melting temperature (˚C)   : 157.0 ± 0.2 after 6 measurements
Literature melting point temperature(˚C): 156.6

Accordingly a correction factor of :
$$k = \frac{-28.62}{-26.7}$$
$$= 1.072$$

Integrals over DSC peaks yields values with a unit of mW.˚C, this can be converted into J.g^{-1} using the following method

$$\Delta H.mass = \frac{Integral[mW^{o}C]}{Heating\ rate[^{o}C.min^{-1}]}$$
$$= Energy\,[mW.min]$$
$$= Energy * 0.06\ [W.s]$$
$$= Energy * 0.06\,[J]$$
$$\Delta H = \frac{Energy}{sample\ mass} * 0.06[J.g^{-1}]$$